CHARACTERIZATION OF SUBGLACIAL TILL FROM ROBERTSON GLACIER, ALBERTA, CANADA: IMPLICATIONS FOR BIOGEOCHEMICAL WEATHERING

by

Russell Kelly Griggs

A thesis submitted in partial fulfillment
of the requirements for the degree

of

Master of Science

in

Earth Sciences

MONTANA STATE UNIVERSITY
Bozeman, Montana

April 2013

APPROVAL

of a thesis submitted by

Russell Kelly Griggs

This thesis has been read by each member of the thesis committee and has been found to be satisfactory regarding content, English usage, format, citation, bibliographic style, and consistency and is ready for submission to The Graduate School.

Mark L. Skidmore

Approved for the Department of Earth Sciences

David W. Mogk

Approved for The Graduate School

Dr. Ronald W. Larsen

STATEMENT OF PERMISSION TO USE

In presenting this thesis in partial fulfillment of the requirements for a master's degree at Montana State University, I agree that the Library shall make it available to borrowers under rules of the Library.

If I have indicated my intention to copyright this thesis by including a copyright notice page, copying is allowable only for scholarly purposes, consistent with "fair use" as prescribed in the U.S. Copyright Law. Requests for permission for extended quotation from or reproduction of this thesis in whole or in parts may be granted only by the copyright holder.

Russell Kelly Griggs

April 2013

ACKNOWLEDGEMENTS

I would like to thank my graduate advisor, Dr. Mark Skidmore, for his guidance and patience over the course of my degree completion. I also thank my committee members, Drs. David Mogk and Jim Schmitt, for assistance and guidance throughout the process. Many thanks also go out to my friends and family for providing support during the more difficult periods and for providing outlets to celebrate during more successful times. Partial financial support for field/laboratory work and five semesters of my time at MSU were provided by NASA Exobiology Grant NNX10AT31 to Dr. Mark Skidmore.

TABLE OF CONTENTS

TABLE OF CONTENTS – CONTINUED

LIST OF TABLES

LIST OF TABLES – CONTINUED

Table Page

LIST OF FIGURES

Figure Page

LIST OF FIGURES – CONTINUED

Figure Page

LIST OF FIGURES – CONTINUED

Figure Page

LIST OF FIGURES – CONTINUED

Figure Page

ABSTRACT

Physical and biogeochemical weathering occurring during transport in the subglacial traction zone impacts the lithology and petrology of sediment in tills. Grain size distribution, particulate organic carbon (POC) content, and bulk/clay mineralogy of recently exposed tills from the terminus of Robertson Glacier, Alberta, Canada were characterized via sieving, laser diffractometry, loss-on-ignition, and X-ray diffraction/scanning electron microscopy (SEM) in order to describe physical and mineralogical properties of these tills. The matrix material of all tills exhibit a grain size distribution biased toward medium to coarse sand-sized particles and the dominant minerals are calcite, dolomite, quartz, and K-feldspar with lesser muscovite, pyrite, phlogopite, and chlorite. POC abundance ranges from 1.1 to 3.5 weight percent and is negatively correlated with grain size for grains from 125 - 2000 μm. POC abundance is also positively correlated with calcite abundance, especially for grains from 125 - 2000 μm. Pyrite is present at < 1% bulk abundance, with a significant portion of the pyrite observed via SEM as ~5-15 μm grains. The modal particle size of the till matrix of medium to coarse sand is consistent with limited physical weathering due to the short (< 3 km) subglacial transport distance and is comparable to that from a metasedimentary glaciated catchment in the Swiss Alps. The small grain size of pyrite produces a large reactive surface area, which supports its potential importance as a key chemical energy source for microbially-mediated chemical weathering.

CHAPTER 1: INTRODUCTION AND LITERATURE REVIEW

1.1. Introduction

Glacially-produced ("glacigenic") sediments, particularly those formerly known as boulder-clays or drift, have been studied since the early- to mid-1800's. However, the term "till" first emerged into prominence in the late 1800's with the definition as an "unstratified conglomeration of boulders and gravel in a matrix of stiff clay" in relation to observations of glacigenic sediments in Scotland by Geikie (1863). More recently, sediments deposited in glacial environments have been classified as primary or secondary deposits, depending on whether their deposition is a result of solely glacial processes or have also undergone reworking by non-glacial processes respectively, with tills fitting into the former (Benn and Evans, 2010). Till is most often generally defined as "sediment that has been transported and deposited by or from glacier ice, with little or no sorting by water" (Dreimanis, 1988) or more restrictively as "sediment deposited directly by glacier ice [that] has not undergone subsequent disaggregation and resedimentation" (Lawson, 1981).

Supraglacial and englacial debris generally retains the same grain size distribution as the source bedrock, but the process of active transport in the subglacial traction zone produces a distribution much different from that of its parent material, generally producing a polymodal distribution ranging from clay/silt to boulders (Benn and Evans, 2010). Till granulometry, especially grain-size distribution, is one of the most common parameters used in macroscopic description and classification of till lithology

(Dreimanis, 1971). The mineral content of till is also often studied in order to characterize the composition and texture of the grains at the microscopic scale, or its petrology. Of particular importance are minerals contributing to chemical weathering to a greater degree than expected based solely on bulk abundance, for example trace pyrite (Tranter, 2003). Pyrite oxidation in glacial environments is likely microbially-mediated (Skidmore et al, 2005) and enhances chemical weathering of other minerals due to production of H^+ (Tranter, 2003). Organic carbon content is another compositional characteristic studied in tills due to its importance in the subglacial environment as a potential substrate for heterotrophic respiration by microbial populations, which has implications for carbon cycling on a range of scales from local to continental (Sharp et al, 1999; Skidmore et al, 2000).

Relatively few studies of till properties have taken place directly on contemporary subglacial tills, due to the difficulty of accessing the subglacial environment (e.g., Hooke and Iverson, 1995; Tulaczyk et al, 1998). The most commonly studied close analog to collecting subglacial till from beneath the interior of glaciers has been tills recently unearthed at the glacial terminus (e.g., Sharp et al, 2002; Montross, 2007; Boyd et al, 2010) or debris-rich basal ice along the glacial terminus (e.g., Sharp et al, 1999). Further, the majority of previous studies on till lithology/petrology have focused on selected size classes or on bulk properties for determination of sediment provenance or mineral exploration (e.g., Tarvainen, 1995; Kjær, 1997; Akselsson et al, 2006). The focus on sediment provenance and mineral exploration has also led to a significant body of work examining tills deposited by former ice sheets, such as the Laurentide Ice Sheet in the

case of many North American tills (e.g., Wilding et al, 1971; Taylor and Faure, 1979; Szabo, 2006).

Chemical weathering occurs contemporaneously to physical weathering, as evidenced by influences on the geochemistry of proglacial streams fed by water flowing through the subglacial environment (Figure 1). Study of solute flux from glaciers has demonstrated several patterns in subglacial chemical weathering, namely: *a)* products of carbonate dissolution tend to dominate solute fluxes, *b)* sulfide oxidation reactions are often a significant contributor to solute fluxes, and *c)* only limited evidence for silicate weathering reaction products is present in solute fluxes from alpine glacial systems (Tranter, 2003).

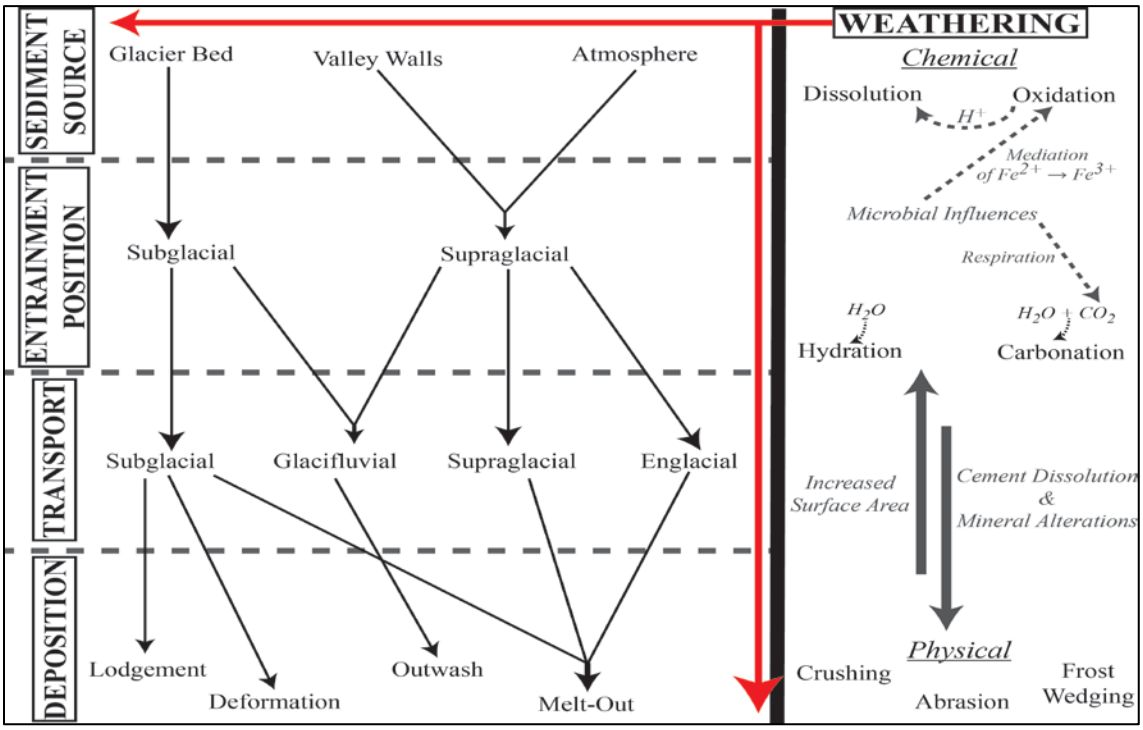

Figure 1. Concept diagram for glacial erosion and weathering. Gray text and arrows indicate physicochemical feedbacks. Red arrow represents occurrence of weathering across all stages of erosion.

1.2. Literature Review

1.2.1. Classification of Till

The definition and classification of tills has been an ongoing and constantly changing field since the first scientific observation of tills during the mid-1800's (Geikie, 1863). Although there have been many different variations, most historic till classification schemes have centered on differentiating tills based on the processes by which they were deposited. For instance, prior to the year 2000 the most widely-accepted till classification scheme split tills into lodgement, melt-out, and deformation end members (Dreimanis, 1988; Benn and Evans, 1996). A more recent, revised classification of tills subdivides primary glacigenic deposits into the categories of glacitectonite, subglacial traction till, or melt-out till based on contrasting the transport and depositional processes with level of deformation (Evans et al, 2006). In this scheme, glacitectonite encompasses sediments that were partially deformed during subglacial transport but still retain some of the structural characteristics of their parent material (Benn and Evans, 1996; Evans et al, 2006). Subglacial traction till is sediment transported via lodgement and deformation occurring in the subglacial traction zone during the sliding of the glacier sole over its bed, with the sediment being deposited via pressure melting and homogenized by shearing (Evans et al, 2006). In contrast to glacitectonite, subglacial traction till generally exhibits near complete deformation and retains almost none of the structural characteristics of its parent material. The third primary type of till in the above classification scheme, melt-out till, is distinguished by a relative lack of subglacial traction features. Melt-out till

includes sediment directly deposited, without subsequent transport or deformation in the traction zone, during the melting of debris-rich ice (Evans et al, 2006).

Alternative modern classification terms applied to tills also include diamicton and tectomict (Flint et al, 1960; Menzies et al, 2006). The term diamicton is used to describe sediment deposits without reference to method or environment of deposition, instead just representing a poorly sorted sediment containing a wide range of particle sizes (Flint et al, 1960). In order to separate tills from non-glacial sediments of similar size distribution and lack of sorting, tills are more specifically labeled as glacial diamicts (Harland et al, 1966). An alternative description of till as structural rather than depositional sediment, thus making it a “tectomict”, has also been proposed due to the observed role of deformation in the production of most tills (van der Meer et al, 2003; Menzies et al, 2006).

1.2.2. Lithology and Petrology of Tills

One of earliest descriptions of grain size distribution and mineralogy in tills was conducted by Crosby (1892) in a study of drumlins near Boston in order to compare volumes and mineralogy of till size classes to those from the resulting outwash bodies. Since that time it has been demonstrated that basal till has a bimodal particle-size distribution split between a clast-size mode of rock fragments and a matrix of mineral fragments, assuming that the source rock is monomineralic or is composed of minerals with similar physical properties (Dreimanis and Vagners, 1971). If the source rock is composed of minerals with differing physical properties a set of modes will develop for each group of physically-similar minerals (Dreimanis and Vagners, 1971). Haldorsen

(1981) attributed polymodal distributions to the combination of crushing (breakage of interlocking grains) and abrasion (removing small fragments from grains sliding past each other). In experiments replicating subglacial particle interactions using rock fragments and tumbling steel balls in the drum of a ball mill it was found that crushing and abrasion produce similar distribution modes to those found in natural tills, with crushing producing particles of ~0.016-2 mm and abrasion creating particles of ~0.002-0.063 mm (Haldorsen, 1981). The mode of the clast and matrix within a till varies with distance from bedrock source, with the clast mode representing a larger percentage of the total till in close proximity and steadily decreasing with distance due to the cumulative effects of comminution (Dreimanis and Vagners, 1971). However, there is also a lower size limit known as the "terminal grade" for the matrix beyond which no further comminution occurs due to a lack of sufficient energy to cause further fracture (Dreimanis and Vagners, 1971). The terminal grade of the matrix is determined by bedrock lithology and the relative resistance of each mineral component to comminution during glacial transport (Dreimanis and Vagners, 1971).

1.2.3. Previous Research on Till at Robertson Glacier

Robertson Glacier is underlain by Late Devonian impure limestone, dolostone, and dolomitic limestone, with interbeds of shale, siltstone, and sandstone (McMechan, 1988). Previous work at Robertson Glacier analyzed the bulk mineralogy of one till sample from the till plain in front of the Robertson Glacier (RG) terminus and 13 bedrock samples representative of the major lithologies from proglacial and valley wall outcrops (Sharp et al, 2002). Mineral identification was conducted via X-ray diffraction (XRD) on all

samples, while whole rock geochemical elemental analysis was conducted on a subset of 7 bedrock powders via instrumental neutron activation analysis (INAA). Based on these analyses, Sharp et al (2002) concluded that the primary mineral phases in the bedrock are calcite and dolomite with lower amounts of quartz, K-feldspar, and muscovite. Illite [$(K,H_3O)(Al,Mg,Fe)_2(Si,Al)_4O_{10}\{(OH)_2(H_2O)\}$] and bassanite [$2CaSO_4 \cdot H_2O$] were also present in till samples and pyrite was observed in bedrock samples. Results from INAA confirmed the presence of significant K-silicates and that Na is present at much lower levels than K in bedrock, in addition to producing K/Rb ratios suggesting that the K-silicate fraction is dominated by K-feldspar rather than muscovite (Sharp et al, 2002). More recently, Doxsey-Whitfield (2012) analyzed the bulk mineralogy and partial grain size distribution of four sites along a till chronosequence extending ~1.6 km (~10 to 160 years since deglaciation based on the space-for-time substitution applied) down valley from the summer 2010 RG terminus with regard to potential controls on microbial nitrate production. Major minerals found via XRD were calcite, dolomite, quartz, and albite [$NaAlSi_3O_8$], along with phlogopite [$KMg_3AlSi_3O_{10}(F,OH)_2$] at the sampling site closest (~15 m) to the terminus. Mean content of clay-sized grains in till ~15 m from the July 2010 RG terminus was ~30%, decreasing to ~19-20% at 660 and 1190 m down valley, and then increasing slightly to 22% at the site farthest down valley along the till chronosequence (Doxsey-Whitfield, 2012).

1.2.4. Till Characteristics in Other Carbonate-Dominated Glaciated Catchments

Studies of other carbonate-dominated glaciated catchments have also been conducted elsewhere in North America. The grain size distribution of several predominantly limestone and dolostone tills of southeast Manitoba were studied by Fenton (1974) in order to attempt stratigraphic correlations of these Laurentide Ice Sheet (LIS)-derived tills. The tills were found to contain ~30-60% sands, 30-50% silt, and ~15% clay, with the mineralogy of the coarse (1-2 mm) sand fraction being predominantly (35-60%) dolostone and limestone in a 1.3:1 ratio (Fenton, 1974). Furthermore, the mineralogy of the silt/clay fraction was 30-50% carbonate, with a 2:1 ratio of dolomite to calcite (Fenton, 1974). Mineralogical content and grain size distribution has also been studied for LIS-derived Late Wisconsin till from the Powell-Union City Moraine, Ohio (Taylor and Faure, 1979). Taylor and Faure (1979) found a bimodal grain size distribution with the <63 μm size fraction accounting for >75 weight % and the >1 mm size fraction accounting for ~11% of the total. Furthermore, carbonate mineral content was highest (~50%) in the coarse sand (0.5-1 mm) size fraction and then decreased with decreasing grain size to ~25% until a slight rise to ~30% for the <63 μm size fraction. Illite also showed a bimodal distribution with greatest concentrations observed in the <63 μm (~25%) and >250 μm (~20%) size fractions (Taylor and Faure, 1979). Kaolinite and chlorite were most prevalent (~30%) in the >250 μm size fraction, while quartz was concentrated in fine-medium sands (125-500 μm, ~20% average) and feldspar in the fine sand (125-250 μm, ~30% maximum) size fraction (Taylor and Faure, 1979). The size distribution of these minerals was used to infer that carbonates, illite, and

kaolinite/chlorite were likely derived from grinding of local bedrock clasts due to their predominance in larger size fractions, while quartz and feldspar were derived from more distant sources on the Canadian Precambrian Shield due to their predominance in smaller size fractions (Taylor and Faure, 1979).

1.2.5. Basal Ice Sediment Characteristics

Basal ice, the debris-rich ice in direct contact with or close proximity to the glacier bed, transports a portion of the sediment that ultimately will be deposited as till. Thus, characterization of sediments from basal ice is important in tracing the path from bedrock to comminuted till. Basal ice can be classified into facies based on sediment content and its arrangement, generally as stratified layers or as massive unlithified sediment conglomerations. Sediments from basal stratified laminated ice facies of the 20-km long Variegated Glacier in the St. Elias Mountains of southeastern Alaska have been found to exhibit a grain size distribution centered around modes in fine silt (11 μm), fine sand (125 μm), and fine pebbles (2.82 mm) (Sharp et al, 1994). The grain size for the massive basal ice facies of a series of 11 alpine glaciers in the Swiss Alps was found to be an average of 0.8±0.4 mm (Hubbard and Sharp, 1995).

1.2.6. Suspended Sediments in Proglacial Streams

Silt and sand-sized particles have been found to dominate grain size distributions of suspended sediments in proglacial streams of many alpine glacial environments, including Glacier de Tsidjiore Nouve in the Swiss Alps (Fenn and Gomez, 1989) and Taikot/Chungphar Glaciers in the western Himalaya (Owen et al, 2003). For comparison,

analysis of suspended sediments in non-glacial fluvial settings has found that alpine streams predominantly carry sand and gravel with much less silt and clay-sized particles than observed in proglacial streams (Gomi and Sidle, 2003; Mao and Lenzi, 2007).

1.2.7. Particulate Organic Carbon

Particulate organic carbon (POC) in subglacial sediments is generally derived from bedrock (Durand, 1980) or soils overridden by the glacier and surface inwash (Sharp et al, 1999; Skidmore et al, 2000). Glacial sediment POC content is generally fairly low, ranging from ~0.3 weight % for supraglacial debris (Sharp et al, 1999) to 0.3-4.1 weight % for proglacial or ice marginal zones (Skidmore et al, 2000). Previous work on subglacial sediments from RG has measured ~1.6 to 2.5 weight percent POC (Boyd et al, 2010; Doxsey-Whitfield, 2012).

1.2.8. Biogeochemical Weathering

Study of solute flux from glaciers has demonstrated several patterns in subglacial chemical weathering, namely: *a)* products of carbonate dissolution tend to dominate solute fluxes, *b)* sulfide oxidation reactions are often a significant contributor to solute fluxes, and *c)* only limited evidence for silicate weathering reaction products is present in solute fluxes from alpine glacial systems (Tranter, 2003). Furthermore, additional products of sulfide oxidation, such as nanoparticles and surface coatings of Fe-oxyhydroxides, have been observed in several glacial environments (Mitchell et al, 2001; Raiswell et al, 2009). The dominance of carbonate dissolution on glacial solute flux may be linked to the approximately five orders of magnitude difference in chemical

weathering rate constants between silicate and carbonate minerals (Anderson, 2007). Calcite dissolution is also less sensitive to temperature effects than silicates due to an activation energy ~2-6 times lower than for silicate minerals (Morse and Arvidson, 2002; White et al, 1999). Carbonate dissolution also acts to partially buffer acid production from sulfide oxidation (Tranter, 2003).

Subglacial environments harbor active endogenous microbial ecosystems with greater diversity and evenness than glacial surface environments (Hamilton et al, 2013). These subglacial bacteria have previously been proposed to have a role in mediating subglacial chemical weathering, modifying it to biogeochemical weathering (Montross, 2007, 2013; Foght et al, 2004; Sharp et al, 1999; Skidmore et al, 2005; Skidmore et al, 2000; Tranter et al, 2002; Tranter et al, 2005). For instance, the concentration of sulfate produced from sulfide oxidation can exceed the amount predicted based on dissolved oxygen concentrations (Tranter et al, 2002). It has been proposed that microbial populations at glacier beds may mediate this reaction by utilizing Fe^{3+} as an oxidizing agent under anoxic conditions (Bottrell and Tranter, 2002; Skidmore et al, 2005). Oxidation of ferrous iron (Fe^{2+}) to ferric (Fe^{3+}) iron is often the rate limiting step in sulfide oxidation, but microbial activity can increase this rate by as much as 10^6 and thus increase the rate of sulfide oxidation (Singer and Stumm, 1970). Sulfide oxidation rates have also been shown to be directly correlated to available surface area, with a first-order linear relationship having previously been demonstrated in carbonate-buffered solutions of ~20% pyrite (215, 108, or 54 μm grain diameter) and a 79.9/0.1% quartz/calcite sand (Nicholson et al, 1988). Furthermore, pyrite has been shown to be the dominant

mineralogical control on subglacial bacterial community structure and composition at Robertson Glacier (Mitchell et al, in press). The composition of subglacial microbial populations at two glaciers characterized with 16S rRNA gene clone libraries also showed a correlation between the metabolic pathways employed by phylogenetic groups and runoff geochemistry (Skidmore et al, 2005), which suggests that microbes control some glacial weathering fluxes. Furthermore, laboratory experiments examining chemical weathering of glacial sediments and meltwater have shown an up to eightfold increase in dissolved major cations in biotic relative to abiotic experiments (Montross et al, 2013).

1.3. Study Purpose

The aim of this research was to characterize melt-out till for a setting in which bedrock mineralogy and proglacial stream geochemistry have already been characterized so as to improve the understanding of an intermediate stage in the weathering process in this system. Of particular focus as potentially important substrates for chemical and biological weathering are pyrite and POC. Robertson Glacier, a temperate glacier located in Peter Lougheed Provincial Park, Kananaskis Country, Alberta, Canada was the study site for this research. Robertson Glacier (RG) is approximately 3 km long and spans an elevation range of 2370 to 2900 m, terminating on a flat till plain with glacially smoothed bedrock surfaces exposed along the glacier margins (Sharp et al, 2002).

During the summer of 2011, four recently exposed tills from three locations along the RG terminus were sampled for subsequent lithologic and mineralogic analyses (Table 1).

Table 1. Description of sediment sampling locations and nomenclature used for reference.

Sampling Location:	*Sediment Description:*	*Nomenclature Used in Thesis:*	*Sample Weight (kg):*
1	Basal melt-out till from sediment bank of an ice cave	Basal Melt-Out Till	1.5
2	Finer-grained lag deposit from floor of the ice cave, basal melt-out till with minor fluvial reworking	Reworked Basal Melt-Out Till	0.75
3	Melt-out till from basal and supraglacial material	Basal/Supraglacial Melt-Out Till	0.3
4	Proglacial stream deposit, melt-out till with minor fluvial reworking	Reworked Melt-Out Till	0.3

Specific objectives of this study were to characterize: 1) the grain size distribution of these tills and 2) several specific parameters for each major grain size class, including i) organic carbon content, ii) carbonate (specifically calcite and dolomite) content, iii) bulk mineralogy, and iv) clay mineralogy. This data was used to answer the following research questions:

Research Question #1: Does the relatively short subglacial transport distance for tills cause a bias in the grain size distribution toward larger grains?

Research Question #2: What is the abundance of POC and the geochemically reactive trace mineral pyrite in till?

Research Question #3: Are abundances of POC and pyrite linked to: *a)* size distribution and/or *b*) specific minerals?

CHAPTER 2: METHODS

2.1. Study Site Description

Robertson Glacier (50° 44’ N, 115° 20’ W) is a temperate valley glacier that drains the north flank of the Haig Icefield in Peter Lougheed Provincial Park, Kananaskis Country, Alberta, Canada (Figure 2.1A). The valley containing Robertson Glacier is oriented SSE to NNW, with the glacier located in the north-facing col at the SE end (Figure 2.1B). Robertson Glacier (RG) is approximately 3 km long and spans an elevation range of 2338 to 2852 m, terminating on a flat till plain with glacially smoothed bedrock surfaces exposed along the glacier margins (Sharp et al., 2002). The local bedrock underlying Robertson Glacier is Late Devonian in age (Mount Hawk, Palliser, and Sassenach Formations) and consists of impure limestone, dolostone, and dolomitic limestone, with interbeds of shale, siltstone, and sandstone (McMechan, 1988). A single major stream, Robertson West (RW), drains the terminus of Robertson Glacier , merging ~200 m downstream with a formerly active but now largely absent smaller stream, Robertson East (RE), to form the larger proglacial stream flowing the remaining length of the valley containing Robertson Glacier (Figure 2.1C).

Sediments for this work were collected from three locations along the RG terminus in August and September 2011 (Figures 2.1C and 2.2). Detailed description of the sediment samples was presented earlier in Table 1.

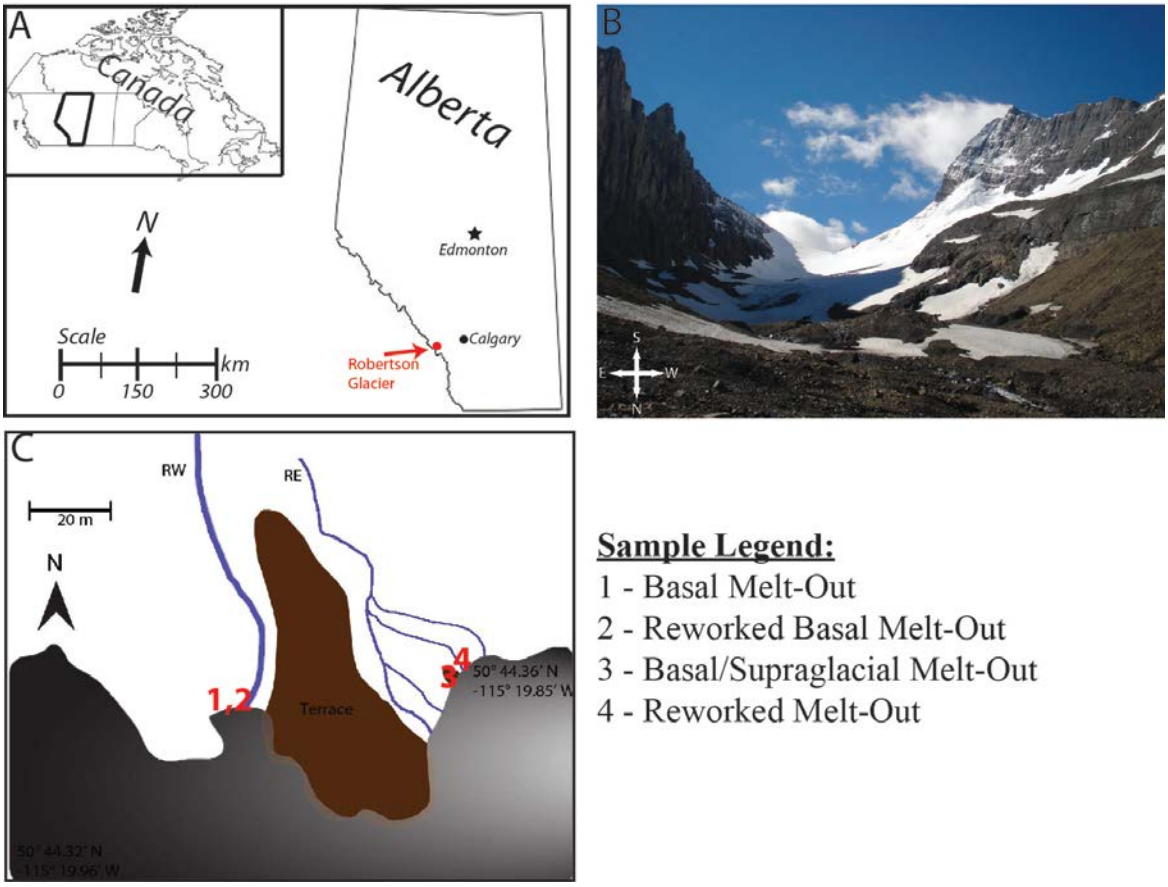

Figure 2.1. Location map for Robertson Glacier (*a)*, Robertson Glacier looking upvalley (*b*), and diagram (*c*) of terminus during September 2011 with locations of sample sites (as described in Table 1). Panel *c* modified from figure by Terra Spotts, with data derived from September 2011 GPS survey of ice front by John Dore.

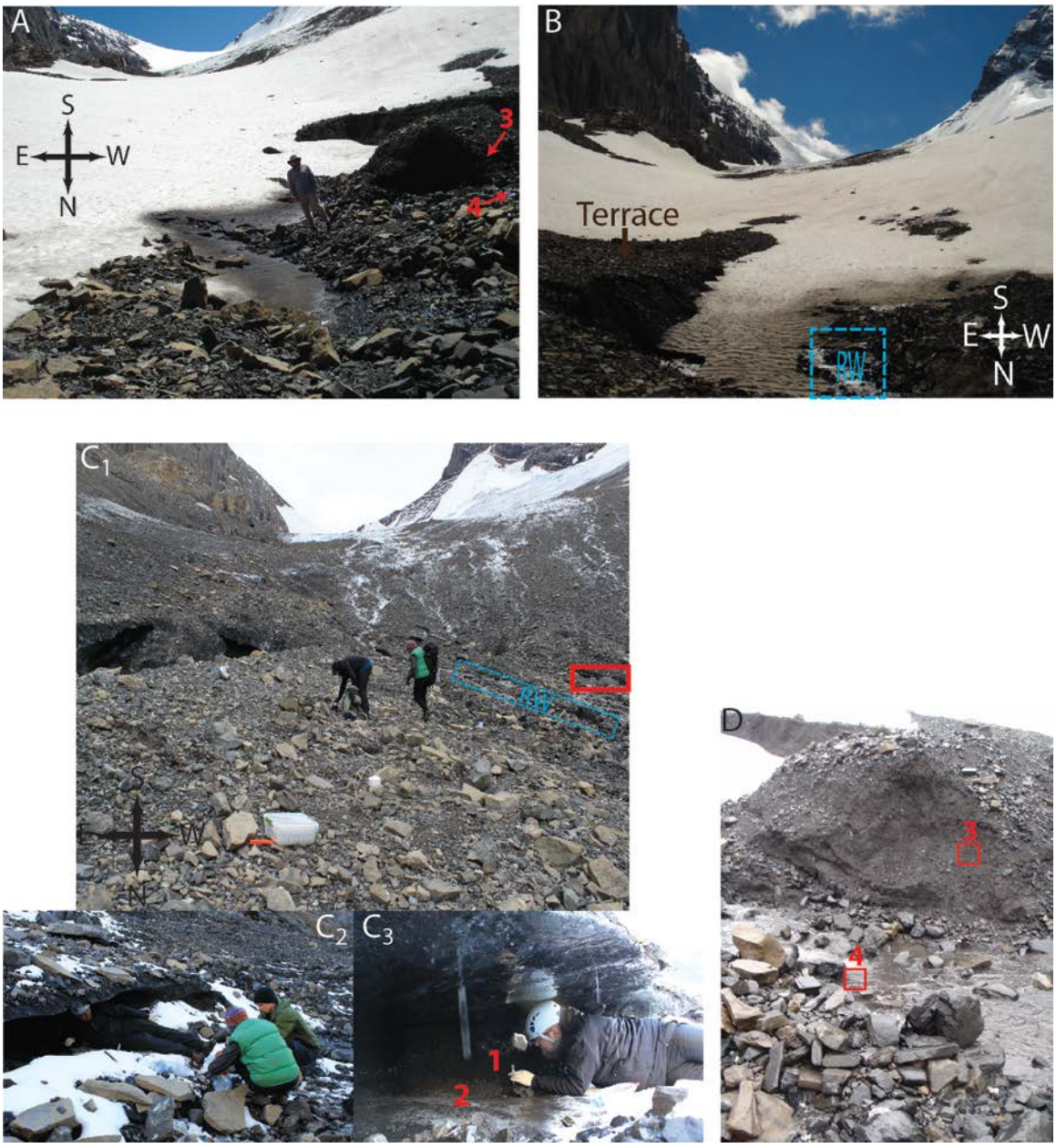

Figure 2.2. Eastern (a) and western (b) glacier margins as of August 2011, during sampling of sites #3-4. Glacier terminus in September 2011 with ice cave sample site (#1/2) shown in panel *c*. Panel $c_{2\text{-}3}$ show sampling of sites #1/2 during September 2011. Panel *d* shows detailed location of sampling sites #3 and 4.

2.2. Labware Preparation

All labware utilized was thoroughly cleaned and sterilized prior to use. Glassware was washed with soap and water, rinsed with distilled H_2O, soaked in 1 M HNO_3 for one hour, rinsed again with distilled H_2O, re-rinsed with 18.2 MΩ ultrapure H_2O, dried in a laminar flow hood, and finally furnaced (550°C, 4 hours) with foil caps. Plasticware was washed identically and then autoclaved (121°C, 20 minutes). Metal utensils were washed in a similar manner with the exception of the nitric acid-wash and then autoclaved in foil wrappers.

2.3. Sediment Preparation

Basal melt-out and reworked basal melt-out till sediments consisted of ~1.5 kg and ~0.75 kg samples, respectively (Table 1). Basal/supraglacial melt-out and reworked melt-out till sediments consisted of ~0.3 kg samples pooled from triplicate 50-mL conical tubes. Sediments were removed from -80°C storage and thawed overnight at room temperature (~24°C) in their original sealed collection vessels. Once fully thawed, sediments were aseptically transferred to 9 x 13” sterile borosilicate glass baking dishes in a laminar flow hood. Sediments were spread into as thin of a layer as possible using sterile metal utensils and then allowed to dry overnight in the laminar flow hood. All sediment samples were subjected to identical analyses of grain size distribution, POC content, carbonate content, X-ray diffraction, and scanning electron microscopy.

2.4. Determination of Grain Size Distribution via Sieve Analysis

Dried sediments were added to a pre-weighed, sterile sieve stack (U.S. Standard #10 / 2000µm, U.S. Standard #35 / 500µm, U.S. Standard #60 / 250µm, U.S. Standard #120 / 125µm, U.S. Standard #230 / 63µm, and catch pan; all 8" diameter) in a laminar flow hood. The sieve stack was then double-wrapped in plastic bags to minimize contamination during the mechanical sieving process. The sieve stack was mechanically shaken (~275 oscillations and ~150 taps per minute) for 10 minutes using a Ro-Tap® RX-29 mechanical sieve shaker. Following sieving, the sieve stack was returned to the laminar flow hood, unbagged, and sediments aseptically transferred to pre-weighed sterile 16-oz plastic jars. The collection jars and sieves were re-weighed following sediment transfer to determine the weight of sediment per size class and the weight of untransferred embedded residue in each sieve's mesh, respectively. Due to the large (~58%) amount of sediment with >2 mm grain size from the basal melt-out till sample, the >2 mm size class was resieved in an identical manner as above using the following sieves atop a catch pan: U.S. Standard #$^{5}/_{16}$ / 8mm, U.S. Standard #5 / 4mm, and U.S. Standard #10 / 2mm. Graphic mean (M), inclusive graphic standard deviation (D), inclusive graphic skewness (S), and graphic kurtosis (K) were calculated from graphs of cumulative probability versus grain size using formulae from Folk and Ward (1957).

2.5. Calculation of Surface Area Distribution

Grains were assumed to be perfect spheres with radii equal to one-half the mean of top and bottom size class limits, which was applied to calculate the volume and surface area of such spheres for each size class, along with the number of spheres that would fill 1 cm^3. Sediment mass measured during grain size distribution analysis was converted into sediment volume using a calculated density, and then multiplied by the number of spheres per cm^3 and the calculated surface area of said sphere to calculate the total surface area of each size class. Distribution (i.e., % of total) of surface area was calculated by summing total surface area of all size classes and dividing surface area of each size class by this total. For the >8 mm size class of unsorted basal melt-out till sediments and the >2 mm size class of all other sediments, average radius was assumed to be 4 mm or 1 mm, respectively, because based on a visual survey the majority of grains recovered barely exceeded the minimum size for the size class. For the <63 μm size class of all sediments the radius was calculated to be 31.5 μm based on an upper size limit of 63 μm. A calculated mean density of 2.7 g/cm^3 (based on an average of values for calcite, dolomite, quartz, K-feldspar, and muscovite from Perkins, 2010) was used for conversion of measured dry sediment weights into sediment volumes.

2.6. Determination of Residual Water and Particulate Organic Carbon Content

2 x 10 g aliquots of basal melt-out till and reworked basal melt-out till sediment per size class were transferred to pre-weighed sterile 250-mL glass beakers. A single 5 g aliquot of basal/supraglacial melt-out till and reworked melt-out till sediments per size class was transferred to pre-weighed sterile 250-mL glass beakers. The beakers and sediment were dried at 105°C overnight and then re-weighed to determine weight loss upon evaporation of residual water that was not removed during initial drying at room temperature. Dried sediment classes were subsequently combusted at 550°C for 8 hours and re-weighed to determine the amount of particulate organic carbon via loss-on-ignition (Heiri et al, 2001). POC abundances reported here may potentially include weight loss due to removal of structural water from hydrated clays and thus represent an upper limit.

2.7. Determination of Carbonate Content via Sequential Acid Leaches

Calcite and dolomite were selectively leached from sediments via sequential treatment with acetic acid following Sharp et al (2002). All sediments utilized had POC removed via loss-on ignition prior to acid dissolution. Calcite was dissolved from sediments by treatment of two ~2 g aliquots per size class with 1.7 N acetic acid (1:20 ratio of sediment to acid) at room temperature for 10 minutes. The mixture of acid and sediment was then centrifuged (10,000 x g, 5 minutes) and supernatant discarded after measuring pH to confirm that acid was in excess. Remaining sediment was then washed

twice with ~10 mL 18.2 MΩ ultrapure H_2O, dried overnight at 50°C, and re-weighed to determine the mass of calcite dissolved.

Dolomite was subsequently dissolved from the above sediments by treatment with 1.7 N acetic acid (1:20 ratio of sediment to acid) at room temperature for 120 minutes. As described above, the mixture was centrifuged and supernatant discarded following pH measurement. Remaining sediment was then washed twice with ~10 mL 18.2 MΩ ultrapure H_2O, dried overnight at 50°C, and re-weighed to determine the mass of dolomite dissolved.

2.8. Calculation of Statistical Significances

Fisher's Least Significant Difference (LSD) Test was applied to determine the minimum difference between means to satisfy a certain level of statistical probability of difference (Williams and Abdi, 2010). Fisher's LSD Test is an ad-hoc test applied following one-way ANOVA in order to compare individual group means, carrying on the square root of the residual mean square from the one-way ANOVA as the pooled standard deviation. If the difference between any two means for different size classes for a given parameter are greater than the LSD they are considered to be significantly different at the stated statistical probability. LSD is calculated using the following formula where *t* represents the student's t-test statistic for a given *df* (degrees of freedom) and α (level of significance), *rMS* represents the residual mean square calculated from a single-factor ANOVA of all possible samples, and *n* represents the number of sample groups being compared (i.e., size classes).

$$LSD = t_{df,\alpha}\sqrt{\frac{2 * rMS}{n}}$$

For example, the LSD for particulate organic carbon values was calculated to be 1.17 weight % for basal melt-out till sediments as shown below in Tables 2.1-2 and Figure 2.3. Thus, since none of the average POC abundance values in Table 2.1 are separated from another by at least 1.17 weight %, none of the means are statistically different at a significance of p=0.05.

Table 2.1. POC data from basal melt-out till, for use in worked example of LSD statistic.

Size Fraction:	*Weight % POC, Replicate #1*	*Weight % POC, Replicate #2*	*Weight % POC, Average*
>2 mm	0.99	1.97	1.48
0.5-2 mm	1.12	2.44	1.78
250-500 µm	1.37	2.34	1.86
125-250 µm	1.54	2.99	2.26
63-125 µm	1.07	2.03	1.55
<63 µm	1.78	2.65	2.21

Table 2.2. Output from single-factor ANOVA analysis of basal melt-out till POC data, for use in example of LSD statistic. Residual mean square (*rMS*) value for input into LSD calculations is highlighted.

Groups	*Count*	*Sum*	*Average*	*Variance*
>2 mm	2	2.96	1.48	0.48
0.5-2 mm	2	3.56	1.78	0.87
250-500 µm	2	3.71	1.86	0.47
125-250 µm	2	4.53	2.26	1.06
63-125 µm	2	3.10	1.55	0.46
<63 µm	2	4.43	2.21	0.38

Source of Variation	*Variance, Sum of Squares*	*df*	*Variance, Mean Square*	*F, Test*	*Significance (p=)*	*F, Critical*
Between Size Fractions	1.07	5	0.214	0.34	0.87	4.39
Within Size Fractions ("Residual")	3.72	6	0.619	n/a		

$$LSD = t_{df,\alpha}\sqrt{\frac{2 * rMS}{n}}$$

$$= 2.57\sqrt{\frac{2 * rMS}{n}}$$

Student's t-statistic for 5 degrees of freedom (*df*) and p=0.05 level of significance (α). Degrees of freedom were calculated as *n*-1, where *n*=sample size (i.e., 6).

$$= 2.57\sqrt{\frac{2 * rMS}{6}}$$

Sample size (*n*) = 6.

$$= 2.57\sqrt{\frac{2 * 0.62}{6}}$$

Residual mean square (*rMS*) calculated from single-factor ANOVA equals 0.62.

$$= 2.57\sqrt{\frac{1.24}{6}}$$

$$= 2.57\sqrt{0.207}$$

$$= 2.57 * 0.45$$

$$= 1.17$$

Figure 2.3. Example of LSD statistic calculations for basal melt-out POC data.

2.9. X-Ray Diffraction (XRD)

Sediments were ground into a disaggregated homogeneous powder with a mortar and pestle to homogenize the mixture and then sieved through a 270-mesh (53 μm) sieve. Sediments were mounted in an unoriented fashion for XRD analysis by preparing an ethanol slurry that was pipetted onto glass microscope slides and allowed to dry at room temperature. XRD analysis was conducted using a Scintag XGen-4000 X-ray Powder Diffraction Spectrometer with a Cu x-ray source at 40 kV beam voltage and 45 mA beam current. X-ray spectra were generated across a 2θ range of 5-70° in 0.02° steps with a scan rate of 2°/minute for an initial survey and across regions of prominent peaks at

0.5°/minute for greater detail. X-ray spectra were analyzed using the Scintag Diffraction Management System for NT (DMSNT) computer software package to determine peak positions and relative intensities and subsequently compared to the International Centre for Diffraction Data (ICDD) powder diffraction file catalog for identification of crystalline minerals.

XRD analysis was conducted on both native and acetic-acid-leached sediments from basal melt-out till to better identify non-carbonate minerals. Given mineralogical data from Sharp et al (2002) and preliminary work on basal melt-out till, XRD analysis was conducted solely on acetic-acid-leached aliquots of reworked basal melt-out, basal/supraglacial melt-out, and reworked melt-out tills to better identify non-carbonate minerals.

XRD analysis of clay minerals was conducted following the standardized methodology of USGS Open-File Report 01-041 (Poppe et al, 2001). Sediments used for this analysis consisted of the acid-leached <63 μm size classes previously obtained during grain size distribution analysis. Silt-sized (2-63 μm) grains were removed from these samples by addition of 5% sodium hexametaphosphate as a dispersant/deflocculant (2:1 ratio of liquid to sediment) followed by centrifugation-assisted settling of grains >2 μm from suspension following Jackson (1979). Following removal of grains >2 μm, the remaining suspended clay size class were filtered onto methyl-ester of cellulose membrane filters, mounted in an oriented fashion by transferring membrane filters with solid filtrate side down onto glass microscope slides, rolling over the backside of filters with glass 10-mL vials to transfer clay minerals onto slides, and allowed to air-dry. These

mounts were sequentially analyzed under the following three treatment conditions: 1) air-drying, 2) ethylene glycol saturation overnight at 65°C, and 3) baking at 400°C overnight followed by cooling to ~150°C prior to analysis. X-ray spectra were generated across a 2θ range of 3-18° in 0.02° steps with a scan rate of 0.5°/minute. Spectra were analyzed as above, with the addition of a clay mineral identification flow diagram associated with the methodology from USGS Open-File Report 01-041. XRD peak resolution (i.e., full width half maximum / FWHM) was measured in order to differentiate muscovite and illite based on the illite crystallinity method utilizing the Scherrer equation's inverse relationship between peak resolution and crystallite size (Scherrer, 1918; Kübler and Jaboyedoff, 2000). Ordered structures and their narrow range of d-spacing produce small FWHM, while more poorly ordered or interstratified structures produce wider, diffuse peaks with larger FWHM (Moore and Reynolds, 1997). Lower (<0.4 °2θ) IC values were interpreted to represent ordered muscovite, while higher (> ~1 °2θ) IC values were interpreted as interstratified illite, based on XRD results from Verdel et al (2011) representing mixtures of varying % muscovite and illite.

2.10. Scanning Electron Microscopy (SEM)

SEM imaging and energy dispersive spectrometry was conducted using a JEOL 6100 Scanning Electron Microscope with a LaB_6 electron source. Secondary electron (SEI) and back-scattered electron (BSE) images and energy-dispersive spectrometry (EDS) spectra were generated with a beam voltage of 20 keV and a working distance of 39 mm. Sediments were mounted for SEM analysis by sprinkling sediment grains onto carbon

stick-dots and then sputter-coating with Ir (45 seconds at 20 mA) to reduce charging. Sediment grains larger than 2 mm were also directly connected to the SEM mount with a painted strip of colloidal graphite around the perimeter to enhance charge dissipation. SEI/BSE images were collected for representative size classes at a variety of magnifications for comparison of grain morphologies, while EDS was utilized to determine the elemental composition of sediment grains.

In order to characterize both carbonate and silicate minerals present in basal melt-out till, an initial EDS survey of 200 grains per size class less than 2 mm and 40 points from 5 separate grains for >2 mm size classes was completed. In order to better characterize quantities of silicates and other lower quantity minerals, 125 grains from each size class <2 mm previously treated via the sequential acid leach protocol were also analyzed via EDS for all tills sampled.

SEM imaging of native sediments demonstrated that all sediments sampled contained primary grains covered by much smaller (~5-15 μm) fragments that complicated analysis of individual grain mineralogy due to composite SEM-EDS elemental spectra that represented a mix of primary and fragmental secondary grain compositions (Figure 2.4). However, mineral abundance point counts corresponding to primary and secondary mineral grains were weighted equally in determination of percentage composition for each mineral. SEM imaging of sediments treated via the sequential acid leaching protocol for carbonate dissolution also revealed coverage by small mineral fragments, but SEM-EDS elemental spectra represented single minerals (Figure 2.5), likely due to washing off of the majority of easily detached secondary grains during the acid washing protocol. It is

also possible that the secondary grains were subglacial $CaCO_3$ precipitates formed from supersaturation on the lee side of bedrock protrusions over which Robertson Glacier passed, as observed in the forefront of other carbonate-dominated glacial systems in the northern Rocky Mountains (Hallet, 1976).

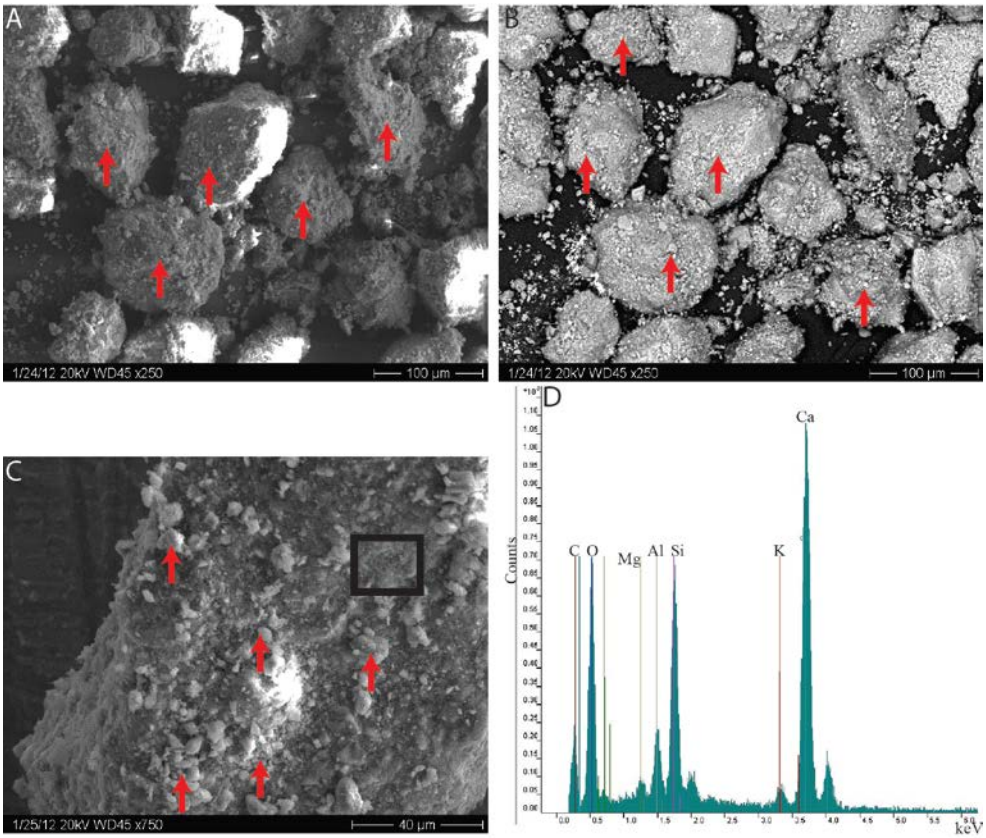

Figure 2.4. Secondary electron (*a* & *c*) / backscattered electron (*b*) images and corresponding SEM-EDS spectrum (*d*) of native grains from the 63 – 125 µm size class of basal melt-out till sediments. Note coverage of significant portions of primary grain surface area with grain fragments as highlighted by red arrows in panels *a*, *b*, and *c*. Black box in panel *c* notes approximate location of the spot EDS analysis. Primary mineral in composite spectrum interpreted as calcite due to predominance of Ca, with the smaller secondary mineral grains identified as phlogopite based on presence of Si >> Al / O > K and limited Mg.

See Appendix C for additional images of other grain size classes.
See Appendices E/F for additional EDS spectra and interpretations representing other mineral combinations.

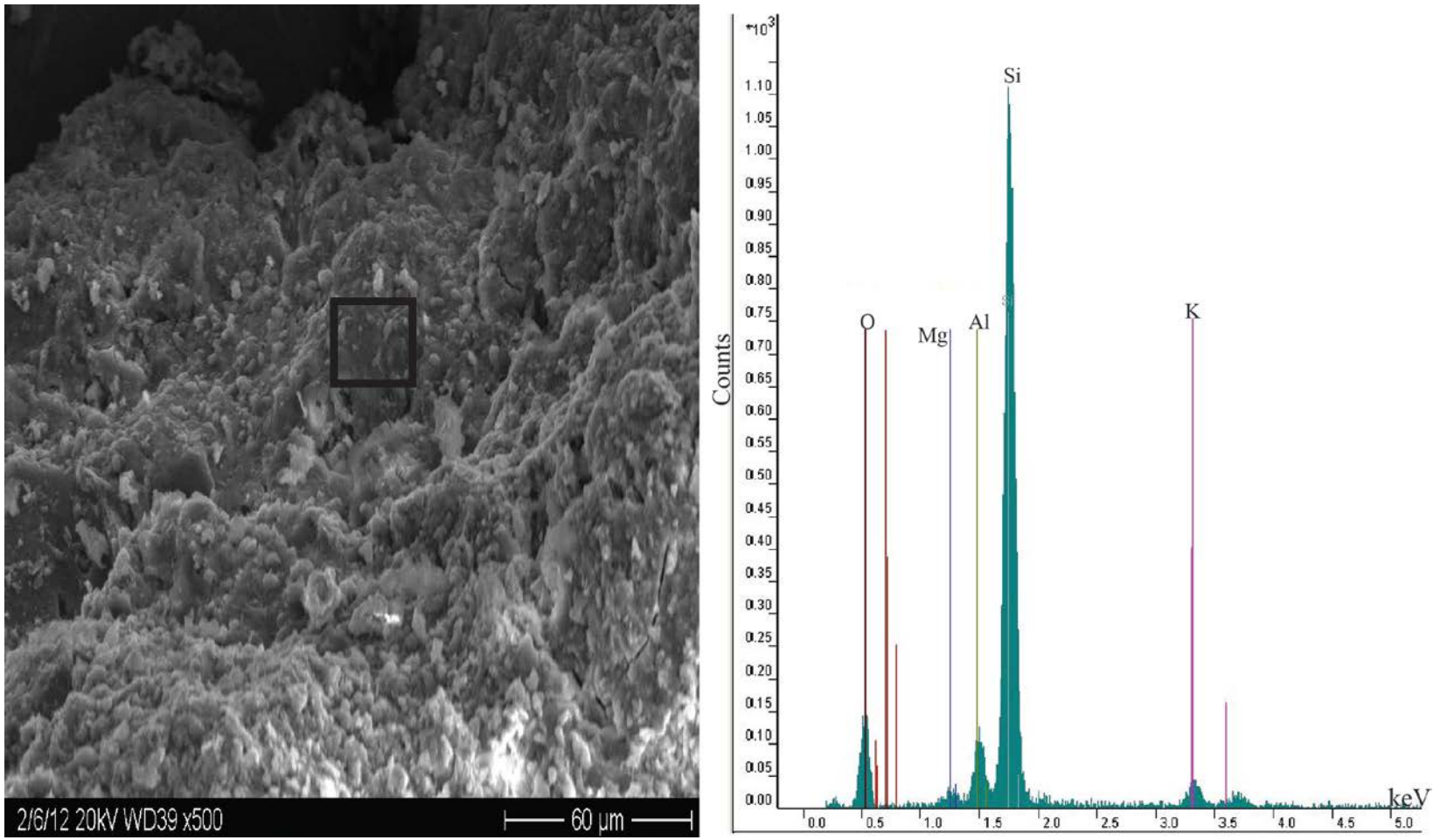

Figure 2.5. Secondary-electron image (*a*) and corresponding SEM-EDS spectrum (*b*) of grain surface from the 250 – 500 µm size class of basal melt-out till sediments, post sequential acetic acid leaches. Black box on SEI image notes approximate location of spot EDS analysis. Note that grain surface is still covered with grain fragments following acid leaches, but that EDS spectrum represents nearly pure quartz (i.e., Si/O peaks) with just minor phlogopite peaks (i.e., Si >> K/Mg/Al).

2.11. Determination of <63 μm Size Class Grain Size Distribution via Laser Diffractometry

Laser diffractometry was conducted with a Malvern Instruments Mastersizer 3000 laser diffractometer with a red 4 mW He-Ne laser (λ=632.8 nm) / blue 10 mW LED (λ=470 nm) light sources and a Hydro LV automated wet dispersion unit. Diffracted light is measured by 63 sensors (0.015-144° range relative to light sources) and was accumulated into 100 size class bins, with data being compiled via Malvern's Mastersizer 3000 software version 2.01. Each measurement was set to run for 30 seconds per light source (~10,000 reads/second, ~300,000 reads total), with the data reported here reflecting the average of five successive runs. Mie scattering theory was utilized to convert measured light scattering to grain size, with the data reported here as volume percentage for each size bin. The simpler Fraunhofer diffraction approximation model, which does not account for refraction, was not utilized due to inaccuracy for particles smaller than 10λ (~6 μm for the Mastersizer 3000), where λ is laser wavelength (Bayvel and Jones, 1981). Refractive index for the sediments analyzed was calculated to be 1.557 via a weighted average based on the percent abundance of minerals measured during SEM-EDS, while absorption was set at 1.0 based on results of Sperazza et al (2004) regarding effects of altering parameters in Mie scattering theory calculations. Graphic mean (M), inclusive graphic standard deviation (D), inclusive graphic skewness (S), and graphic kurtosis (K) were calculated from graphs of cumulative probability versus grain size using formulae from Folk and Ward (1957).

Samples for laser diffraction granulometry consisted of the <63 μm size class of each till sample, both native and following loss-on-ignition (LOI) for all but basal melt-out till for which only post-LOI was available in sufficient quantity. Approximately 0.5-0.8 g of sediment was transferred to a 50-mL conical tube containing 25 mL of 5.5 g/L sodium hexametaphosphate as a dispersant/deflocculant and then shaken at 300 rpm for 12 hours on a platform shaker at room temperature (~23°C). Prior to analysis of samples on the Mastersizer 3000 the Hydro LV automated wet dispersion unit's 600-mL dispersant tank was flushed and refilled three times with distilled H_2O and then baseline/background data was collected for 30 seconds per light source with the stirrer running at 2000 rpm. Samples were then vigorously shaken for ~60 seconds and added via pipette until obscuration was ~15%, after which the dispersant/sample was subjected to 60 seconds of ultrasonication at 100% power (40W, 40 kHz). Between each sample the Hydro LV automated wet dispersion unit's dispersant tank was again flushed/refilled three times prior to beginning baseline/background measurement for the next sample.

2.12. Calculation of Pyrite Specific Surface Area and Oxidation Rates

Pyrite grains were assumed to be cuboidal with side length of 5, 10, or 15 μm, which was applied to calculate the volume and surface area of such cubes, along with the number of cubes that would fill 1 cm^3. Percentage abundance for pyrite from SEM-EDS analysis was converted to sediment mass by assuming a 1 g sample and then converted into sediment volume using a density of 5.01 g/cm^3. Calculated pyrite volume per 1 g sediment was then multiplied by the number of 5/10/15 μm cubes per cm^3 and the

calculated surface area of individual cubes to calculate the total specific surface area of each size class.

Theoretical potential pyrite oxidation rates for Robertson Glacier were calculated by applying a linear first-order relationship between inverse particle diameter and pyrite oxidation rates from Nicholson et al (1988). Nicholson et al (1988) used inverse particle diameter (1/d) as a proxy for surface area, but their stated 20% pyrite abundance and pyrite grain size (215, 108, or 54 μm) were applied using the same methodology as above to calculate specific surface areas that could be used to derive a linear first-order relationship between pyrite specific surface area and oxidation rate. Rates of pyrite oxidation were converted from moles FeS_2/g/day to moles SO_4/g/day by multiplying by two as indicated by the stoichiometry of the following balanced reaction, $FeS_{2\,(s)} + {}^{15}/_{4}\ O_2 + {}^{7}/_{2}\ H_2O \rightarrow Fe(OH)_{3\,(s)} + 2\ SO_4^{2-} + 4\ H^+$.

Pyrite oxidation rates were also derived for Haut Glacier d'Arolla and Bodalsbreen using data from Montross et al (2013). Montross et al (2013) reported SO_4 normality, incubation time, and sediment mass as related to laboratory sediment slurry experiments examining subglacial biogeochemical weathering. SO_4 normality was converted to molarity, for ease of comparison to other pyrite oxidation data, by multiplying by two as indicated by the stoichiometry of H_2SO_4 dissolution into $2\ H^+ + SO_4^{2-}$ and the resulting normality : molarity ratio of 2:1. Pyrite oxidation rates were then calculated by dividing SO_4^{2-} molarity by sediment mass and experiment length.

CHAPTER 3: RESULTS

3.1. Quantitative Physical Lithological and Mineralogical Analyses

Composite profiles of grain size distribution, POC abundance, and carbonate content data were created and analyzed to compare trends across the four different sub-environments sampled. As can be seen in Figures 3.1-4, all samples exhibit the same broad trends across all grain size classes with respect to grain size distribution, POC abundance, and carbonate content. The composite grain size distribution demonstrates mean grain sizes of medium to coarse sands with strong positive skewness toward negative phi values and leptokurtic to platykurtic distributions (Figure 3.1). POC and calcite content exhibit visual trends of an approximately normal distribution centered on the 125-250 μm size class, with POC exhibiting a lower amplitude distribution and calcite a higher amplitude (Figures 3.2-3). Dolomite content exhibits a visual trend of positive correlation with grain size (Figure 3.4).

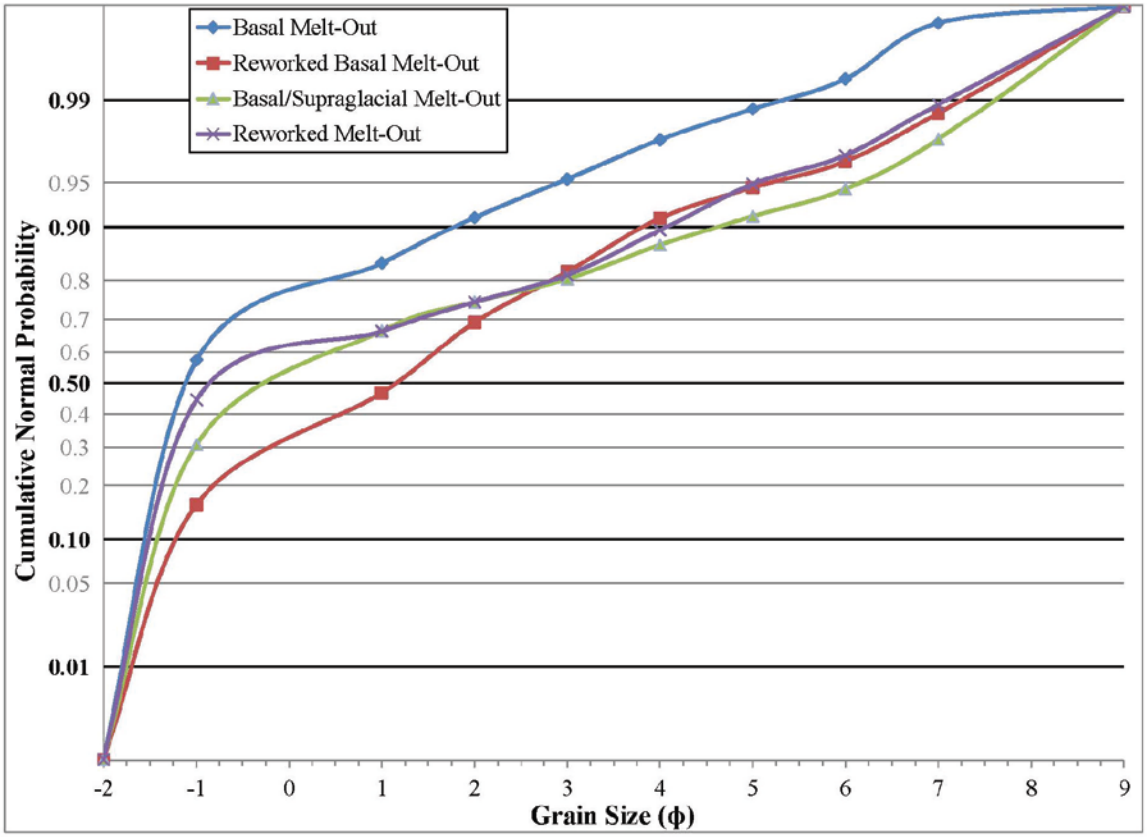

Sample:	*Mean, M (ϕ):*	*Standard Deviation, D (ϕ):*	*Skewness, S:*	*Kurtosis, K:*
Basal Melt-Out	-0.5	0.1	0.7	1.8
Reworked Basal Melt-Out	1.1	1.1	0.1	0.9
Basal/Supraglacial Melt-Out	0.6	1.2	0.6	1.0
Reworked Melt-Out	0.4	0.9	0.8	0.7

Figure 3.1. Cumulative probability curves for all sediments, compiled from sieving and laser diffraction grain size distribution analyses. All samples have mean grain size centered on medium to very coarse sands ($-1 \leq M \leq 2$) and range from poorly ($1 \leq D \leq 2$) to moderately ($0.7 \leq D \leq 1$) or very well sorted ($D \leq 0.4$). Reworked basal melt-out till is nearly symmetrical ($-0.1 \leq S \leq 0.1$), while all other samples are strongly positively skewed toward negative-phi values ($0.3 \leq S \leq 1$). Basal melt-out till is highly leptokurtic ($1.5 \leq K \leq 3$) and basal/supraglacial melt-out till is mesokurtic ($0.9 \leq K \leq 1.1$). Reworked basal melt-out and reworked melt-out till are platykurtic ($0.7 \leq K \leq 0.9$).

See Figures A.5-6 for separate cumulative probability curves from sieving and laser diffractometry analyses of grain size distribution.

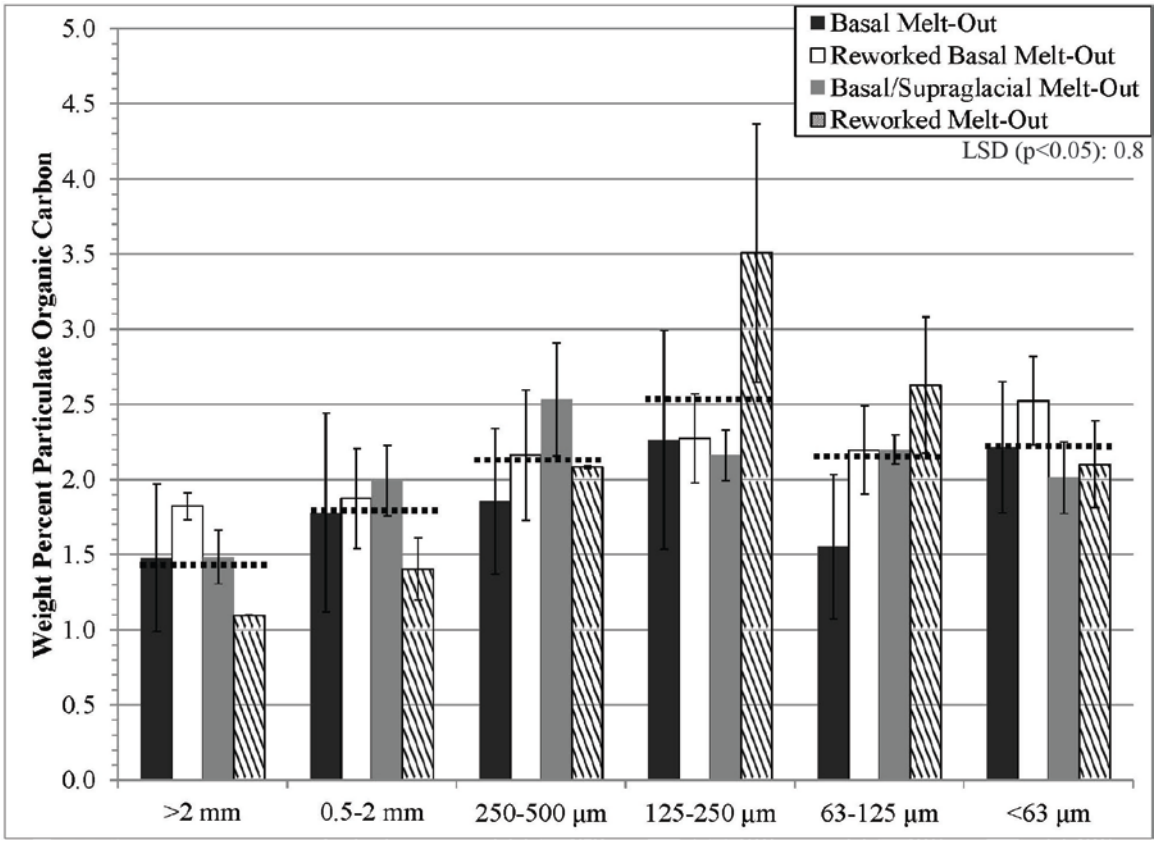

Figure 3.2. Comparison of POC content for all sediment samples across spectrum of grain size classes surveyed in this study. Black dotted lines represent average value for each grain size class. Error bars indicate standard deviation between duplicate samples. Least significant difference (LSD) value represents minimum difference between means to satisfy $p<0.05$ statistical probability of similarity. Sole significantly different means are >2 mm vs 125-250 µm size classes.

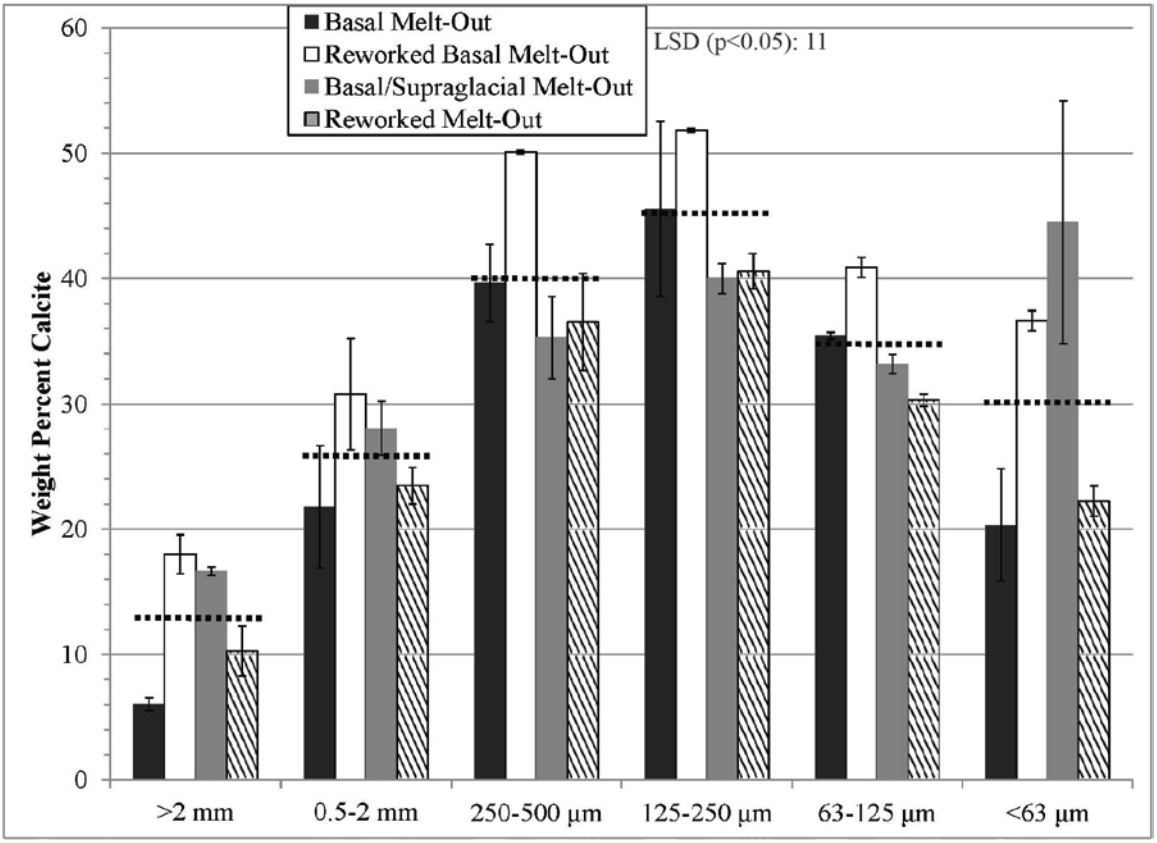

Figure 3.3. Comparison of calcite content for all sediment samples across spectrum of grain size classes surveyed in this study. Black dotted lines represent average value for each grain size class. Error bars indicate standard deviation between duplicate samples. Least significant difference (LSD) value represents minimum difference between means to satisfy $p<0.05$ statistical probability of similarity. Significantly different means are >2 mm vs all other size classes, 0.5-2 mm vs 250-500 / 125-250 µm size classes, and 125-250 µm vs <63 µm size classes.

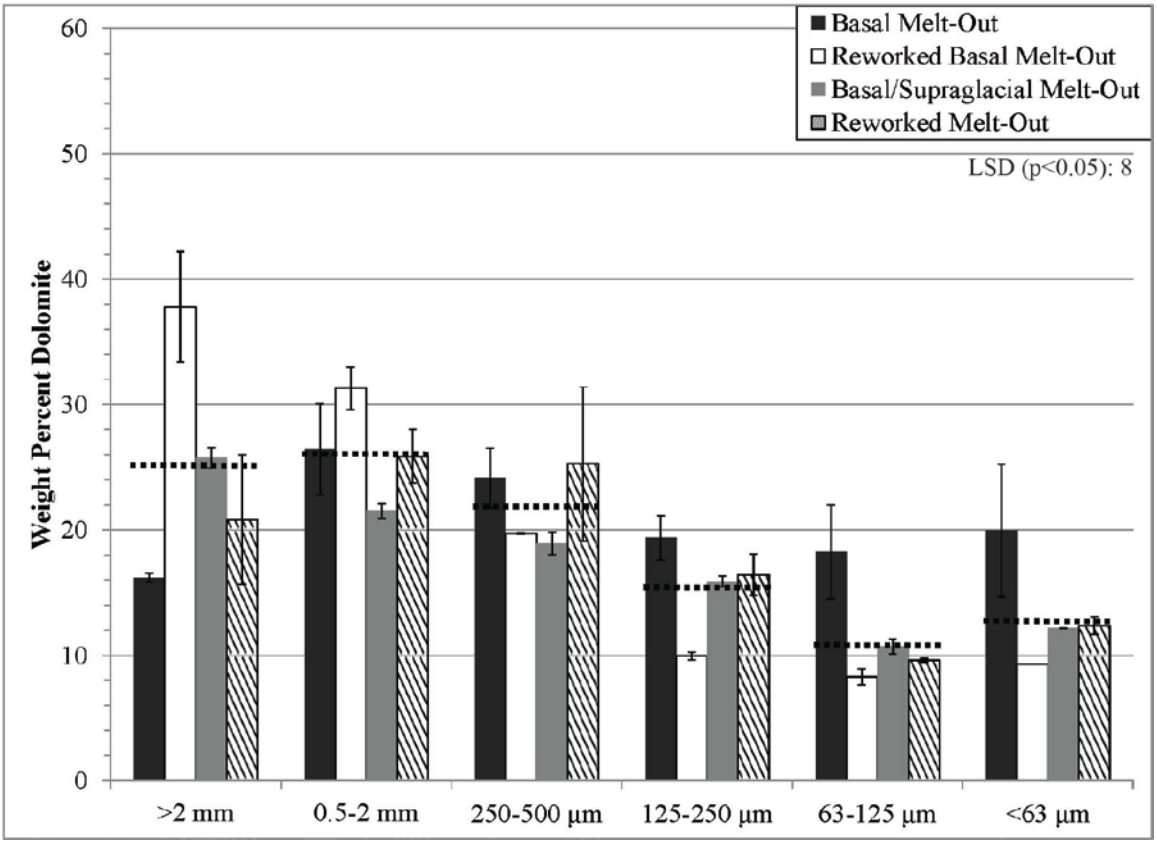

Figure 3.4. Comparison of dolomite content for all sediment samples across spectrum of grain size classes surveyed in this study. Black dotted lines represent average value for each grain size class. Error bars indicate standard deviation between duplicate samples. Least significant difference (LSD) value represents minimum difference between means to satisfy $p<0.05$ statistical probability of similarity. Significantly different means are >2 mm vs 125-250 / 63-125 / <63 µm, 0.5-2 mm vs 125-250 / 63-125 / <63 µm, and 250-500 µm vs 63-125 / <63 µm size classes.

3.1.1. Statistical Quantification of Physical Lithological and Mineralogical Trends

Grain size class frequency is positively correlated with grain size for the composite profile (R^2=0.70, p<0.01). However, this positive correlation is not entirely representative, with the standard deviation from mean values for >2 mm and 0.5-2 mm size classes overlapping (p=0.41), a significant decrease in % of total sediment mass between the 0.5-2 mm and 250-500 µm size classes (p=0.01), overlap between standard deviations from mean values for the 250-500 and 125-250 µm size classes (p=0.33), and then statistically identical (p=0.50-0.84) values for the 125-250 µm, 63-125 µm, and <63 µm size classes. Furthermore, the positive correlation between composite grain size class frequency and grain size continues across the silt/clay-sized (<63 µm) class when analyzed separately (R^2=0.75, p<0.01).

Visually there is a normal distribution of weight % POC versus grain size for the composite profile, with an apparent negative correlation between grain size and weight % POC until 125 µm and then a potential positive correlation for grains < 125 µm (Figure 3.2), but only the trend for grain size >125 µm is statistically significant (R^2=0.33/p<0.01 and R^2=0.01/p=0.78, respectively).

When calcite and dolomite abundance data are separately pooled from all samples to create composite profiles there are several statistically-significant correlations with grain size. Across all size classes, % calcite is negatively correlated (R^2=0.52, p<0.01) with grain size and % dolomite is potentially positively correlated (R^2=0.38, p<0.01) with grain size. Although visually % calcite appears to be positively correlated with grain size for grains <125 µm (Figure 3.3), when split into sub-categories of >125µm / <125 µm %

calcite becomes more negatively correlated (R^2=0.83, p<0.01) with grain size for grains >125 μm and only slightly positively correlated for grains < 125 μm (R^2=0.35, p<0.01). When compared across all grain sizes, dolomite is only moderately positively correlated (R^2=0.38, p<0.01) with grain size due to significant differences between grain size class means only occurring for the 0.5-2 mm / 250-500 μm (p=0.08) and 250-500 / 125-250 μm (p<0.01) size classes (Figure 3.4).

3.2. Mineralogy

XRD and SEM analysis indicates that all melt-out tills sampled for this study are composed primarily of calcite, dolomite, quartz, orthoclase K-feldspar, and much smaller amounts of muscovite (Figures 3.5-10, Tables 3.1-5). Lower abundance minerals also observed were pyrite and phlogopite in SEM (Figures E.1 and E.5) and chlorite and muscovite in clay mineral XRD (Table 3.1, Figure 3.11). Pyrite was solely observed in SEM-EDS analysis of native basal melt-out till sediments, likely due to its observed presence as small (~5-15 μm) secondary grains on the surface of primary mineral grains and washing off during the acid-leach process. Calculated specific surface area for cuboidal pyrite grains of 15, 10, or 5 μm side length ranges from 719 to 2156 $mm^2\ g^{-1}$, which equates to calculated theoretical potential FeS_2 oxidation rates of 0.7-2.2 μmol $SO_4^{2-}\ g^{-1}\ d^{-1}$ (Table 3.6).

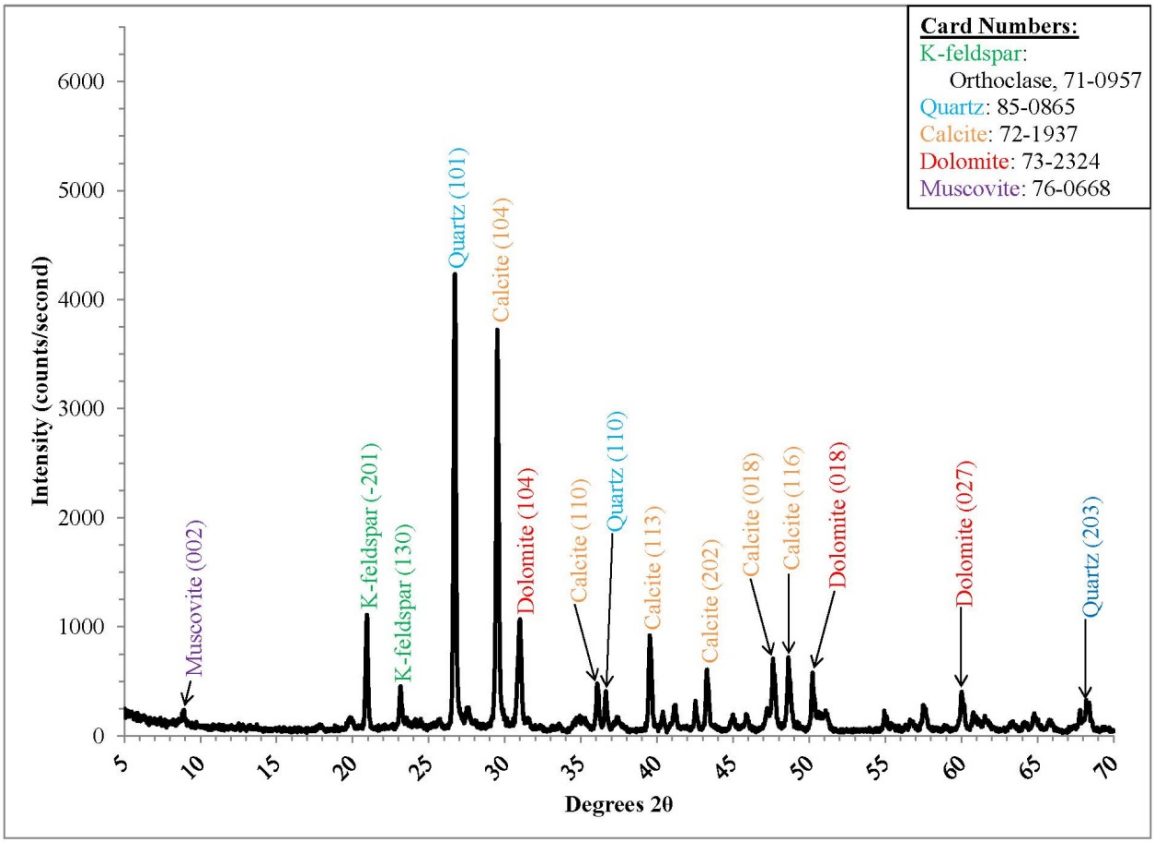

Figure 3.5. Representative X-ray spectrum for basal melt-out till sediments from 0.5 – 2 mm size class.

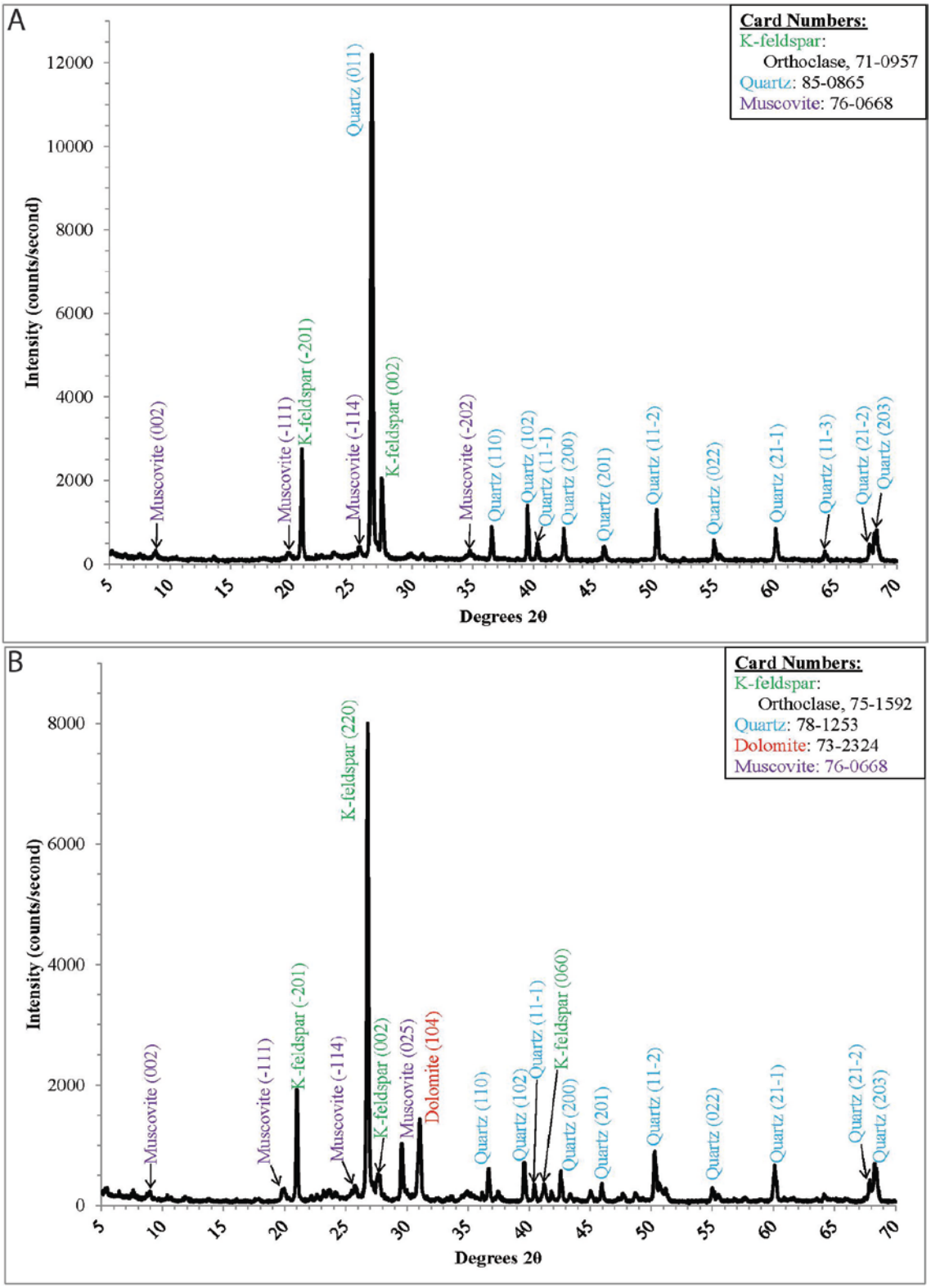

Figure 3.6. Representative X-ray spectra for acid-leached basal melt-out till sediments, from 63-125 µm (*a*) and 2-4 mm (*b*) size classes.

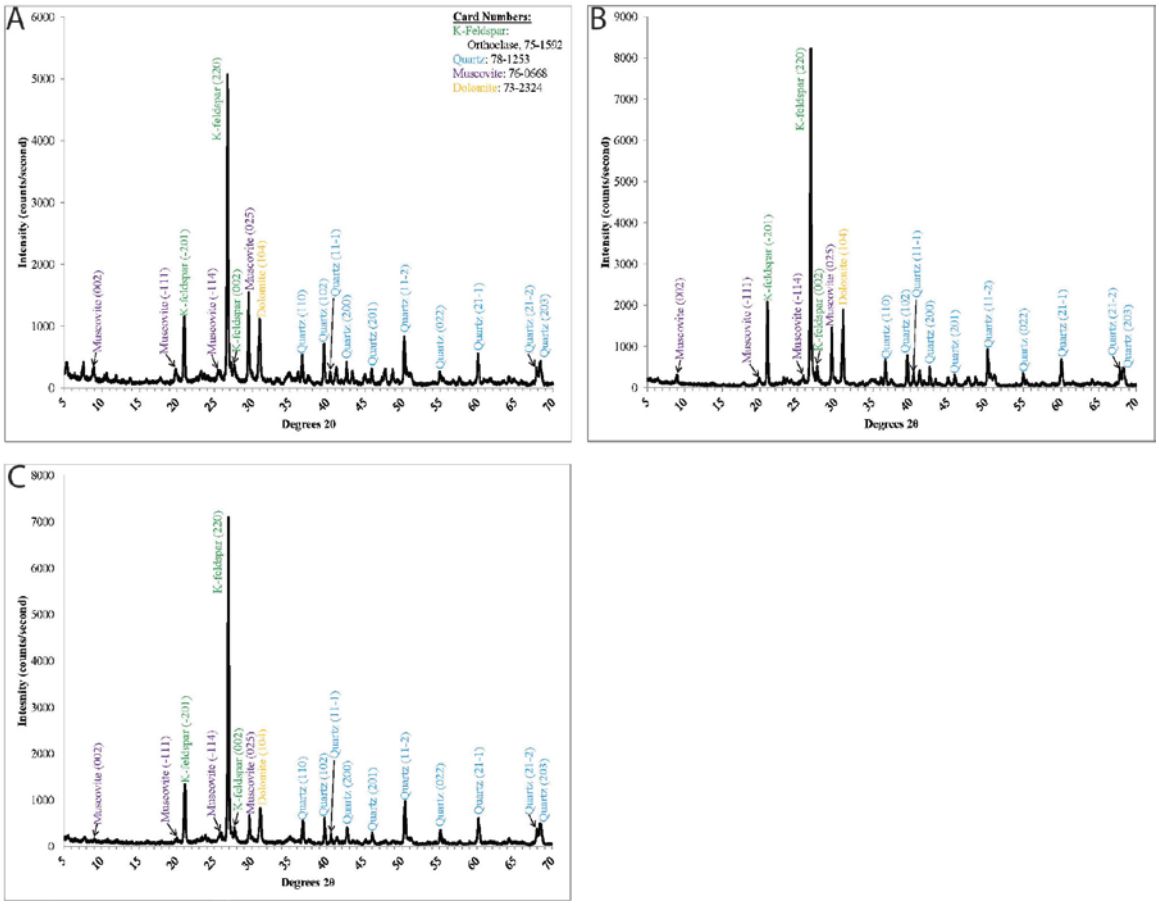

Figure 3.7. Representative X-ray spectra for acid-leached reworked basal melt-out till (*a*), reworked melt-out till (*b*), and basal/supraglacial melt-out till (*c*) sediments, from >2 mm size classes.

Table 3.1. Mineralogy by size class derived from SEM-EDS point-counts (n=200) on native basal melt-out till sediments. *See Tables D.1-2 for full data.*

Size Fraction:	*# Grains:*	*% Calcite:*	*% Dolomite:*	*% Quartz:*	*% K-Feldspar:*	*% Muscovite:*	*% Pyrite:*
>2 mm	*200*	14.0	12.6	23.3	48.7	1.1	0.3
0.5-2 mm	*200*	20.5	16.5	22.0	40.5	0.5	0
250-500 μm	*200*	41.5	14.5	20.0	20.0	3.0	1.0
125-250 μm	*200*	38.0	13.0	17.5	29.0	1.5	1.0
63-125 μm	*200*	38.0	15.0	21.5	24.5	1.0	0
<63 μm	*200*	24.0	19.0	25.5	30.0	1.0	0.5

Table 3.2. Mineralogy by size class derived from SEM-EDS point-counts (n=125) on basal melt-out till sediments treated with sequential acetic acid leaches for carbonate dissolution. *See Table D.4 for data.*

Size Fraction:	*# Grains:*	*% K-Feldpsar:*	*% Quartz:*	*% Muscovite:*	*% Pyrite:*
>2 mm	*125*	40.5	36.7	0.6	0
0.5-2 mm	*125*	29.8	21.5	0.4	0
250-500 μm	*125*	18.3	17.4	0.6	0
125-250 μm	*125*	19.9	14.6	0.6	0
63-125 μm	*125*	24.9	21.2	0.4	0
<63 μm	*125*	28.2	30.6	0.5	0.8

Table 3.3. Mineralogy by size class derived from SEM-EDS point-counts (n=125) on reworked basal melt-out till sediments treated with sequential acetic acid leaches for carbonate dissolution. *See Table D.6 for data.*

Size Fraction:	# Grains:	% Quartz:	% K-Feldspar:	% Muscovite:
>2 mm	125	23.3	20.9	0
0.5-2 mm	125	19.4	18.2	0.3
250-500 μm	125	16.7	13.3	0.2
125-250 μm	125	21.4	16.2	0.6
63-125 μm	125	30.5	19.9	0.4
<63 μm	125	32.0	21.2	0.9

Table 3.4. Mineralogy by size class derived from SEM-EDS point-counts (n=125) on basal/supraglacial melt-out till sediments treated with sequential acetic acid leaches for carbonate dissolution. *See Table D.8 for data.*

Size Fraction:	# Grains:	% Quartz:	% K-Feldspar:	% Muscovite:
>2 mm	125	34.1	23.5	0
0.5-2 mm	125	31.5	18.6	0.4
250-500 µm	125	27.5	18.0	0.3
125-250 µm	125	27.9	15.9	0.3
63-125 µm	125	32.8	22.4	1.0
<63 µm	125	28.4	14.9	0

Table 3.5. Mineralogy by size class derived from SEM-EDS point-counts (n=125) on reworked melt-out till sediments treated with sequential acetic acid leaches for carbonate dissolution. *See Table D.7 for data.*

Size Fraction:	# Grains:	% Quartz:	% K-Feldspar:	% Muscovite:
>2 mm	125	36.4	32.5	0
0.5-2 mm	125	28.3	21.9	0.4
250-500 µm	125	20.8	16.8	0.7
125-250 µm	125	23.0	18.9	1.1
63-125 µm	125	31.3	27.9	0.9
<63 µm	125	35.1	29.8	0.3

Table 3.6. Calculated specific surface area of pyrite grains in native basal melt-out till. Sub-columns for 5/10/15 µm under specific surface area represent side length of assumed cube shape for pyrite. Pyrite oxidation rates were calculated using a linear first-order relationship between calculated pyrite specific surface area and pyrite oxidation rates from Nicholson et al (1988).

Size Fraction:	*% Pyrite (from SEM-EDS):*	*Specific Surface Area ($mm^2\ g^{-1}$)*		
		5 µm	*10 µm*	*15 µm*
>2 mm	0.4	958	479	319
0.5-2 mm	0	0	0	0
250-500 µm	0.2	479	240	160
125-250 µm	0.2	479	240	160
63-125 µm	0	0	0	0
<63 µm	0.1	240	120	80
Weighted Total % Pyrite:	0.27			
	Total Pyrite Specific Surface Area ($mm^2\ g^{-1}$)	2156	1078	719
	FeS_2 Oxidation Rate (µmol $SO_4^{2-}\ g^{-1}\ d^{-1}$)	2.2	1.1	0.7

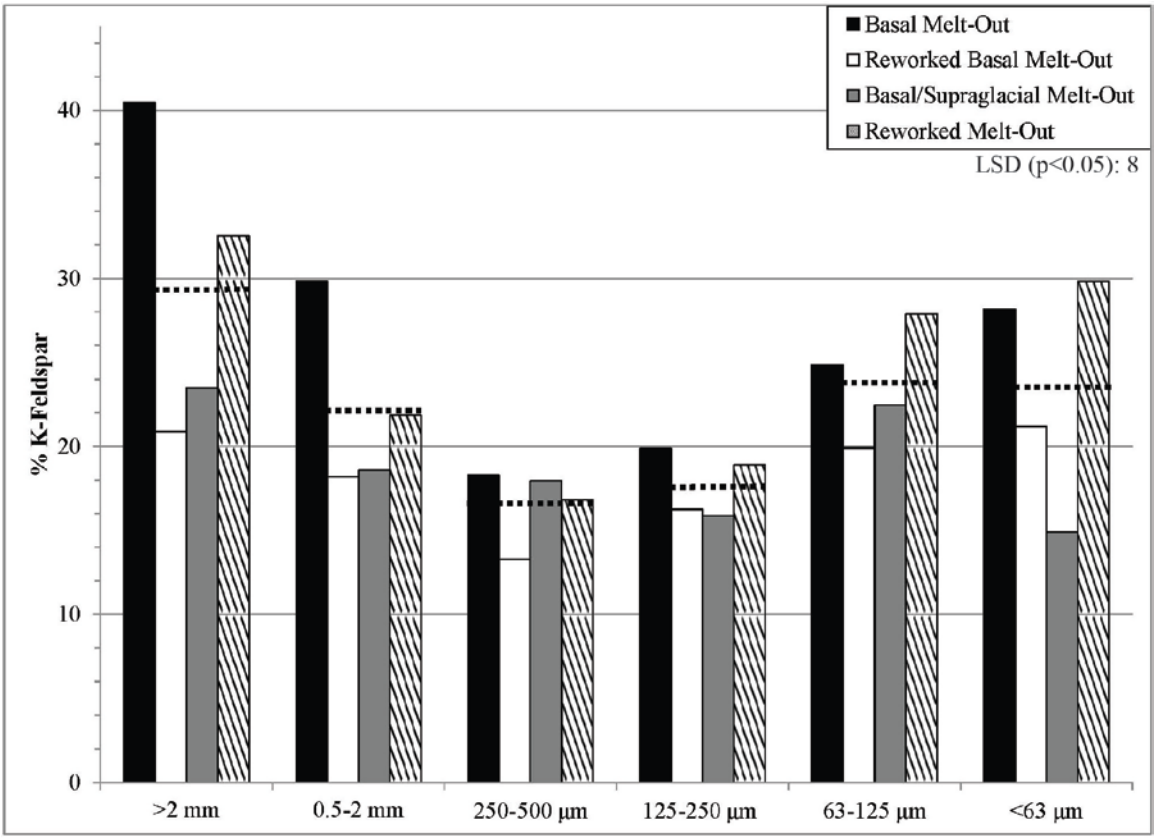

Figure 3.8. Comparison of K-feldspar content for all sediment samples across spectrum of grain size classes surveyed in this study. Black dotted lines represent average value for each grain size class. Least significant difference (LSD) value represents minimum difference between means to satisfy $p<0.05$ statistical probability of similarity. All means are within 10% of each other and are thus not statistically different.

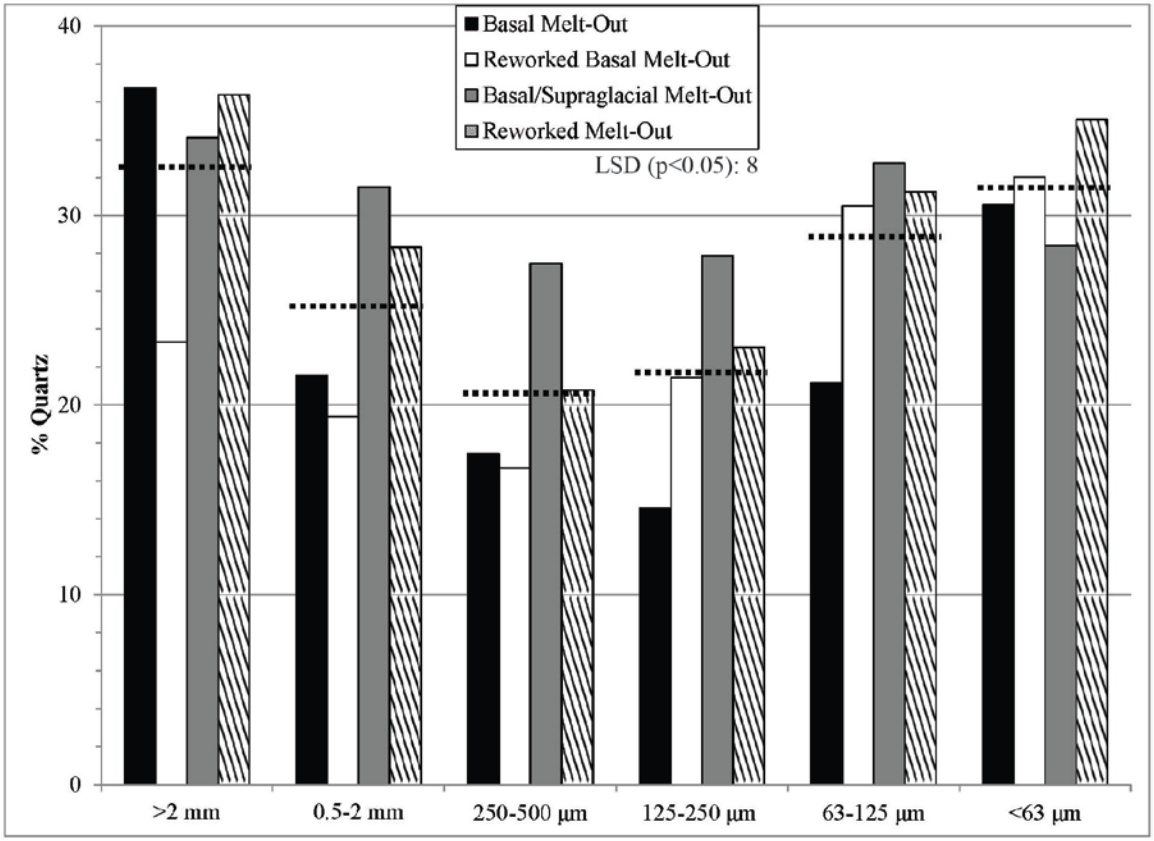

Figure 3.9. Comparison of quartz content for all sediment samples across spectrum of grain size classes surveyed in this study. Black dotted lines represent average value for each grain size class. Least significant difference (LSD) value represents minimum difference between means to satisfy $p<0.05$ statistical probability of similarity. All means are within 10% of each other and are thus not statistically different.

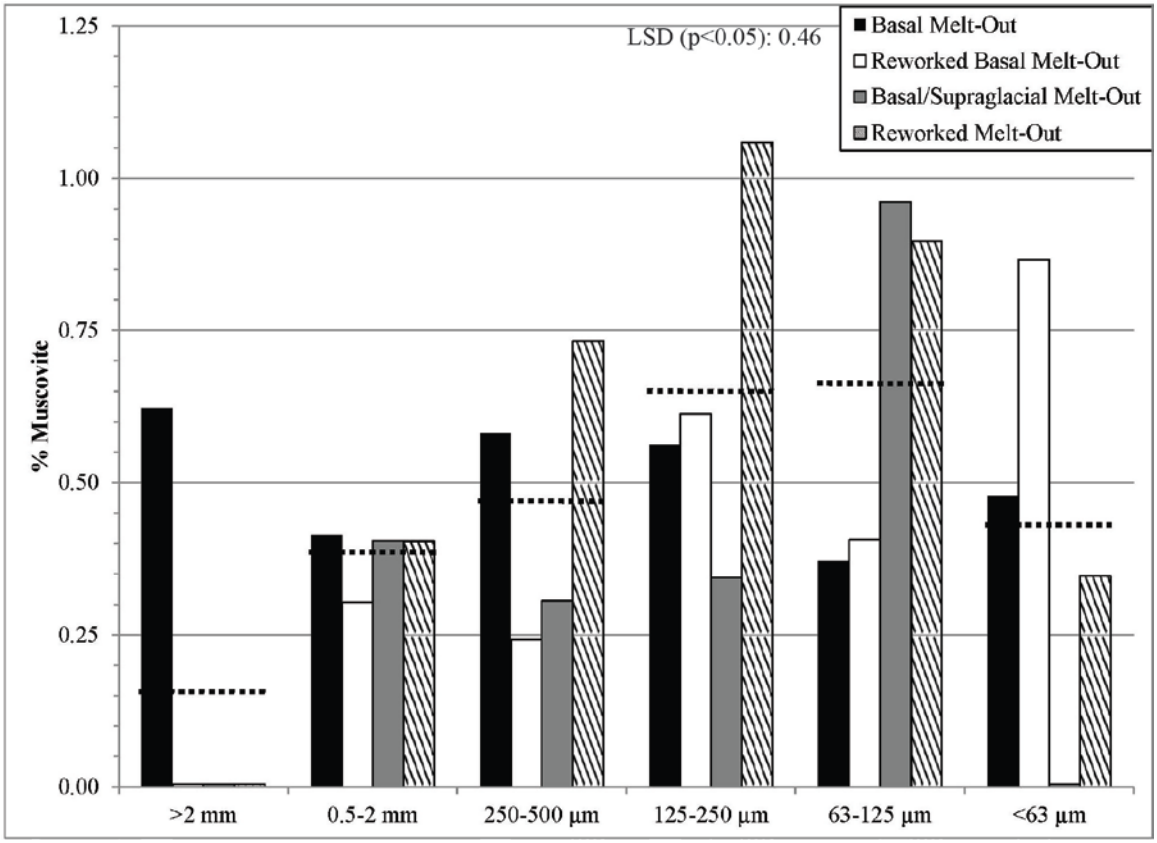

Figure 3.10. Comparison of muscovite content for all sediment samples across spectrum of grain size classes surveyed in this study. Black dotted lines represent average value for each grain size class. Significantly different means are >2 mm vs 125-250 and 63-125 µm size classes.

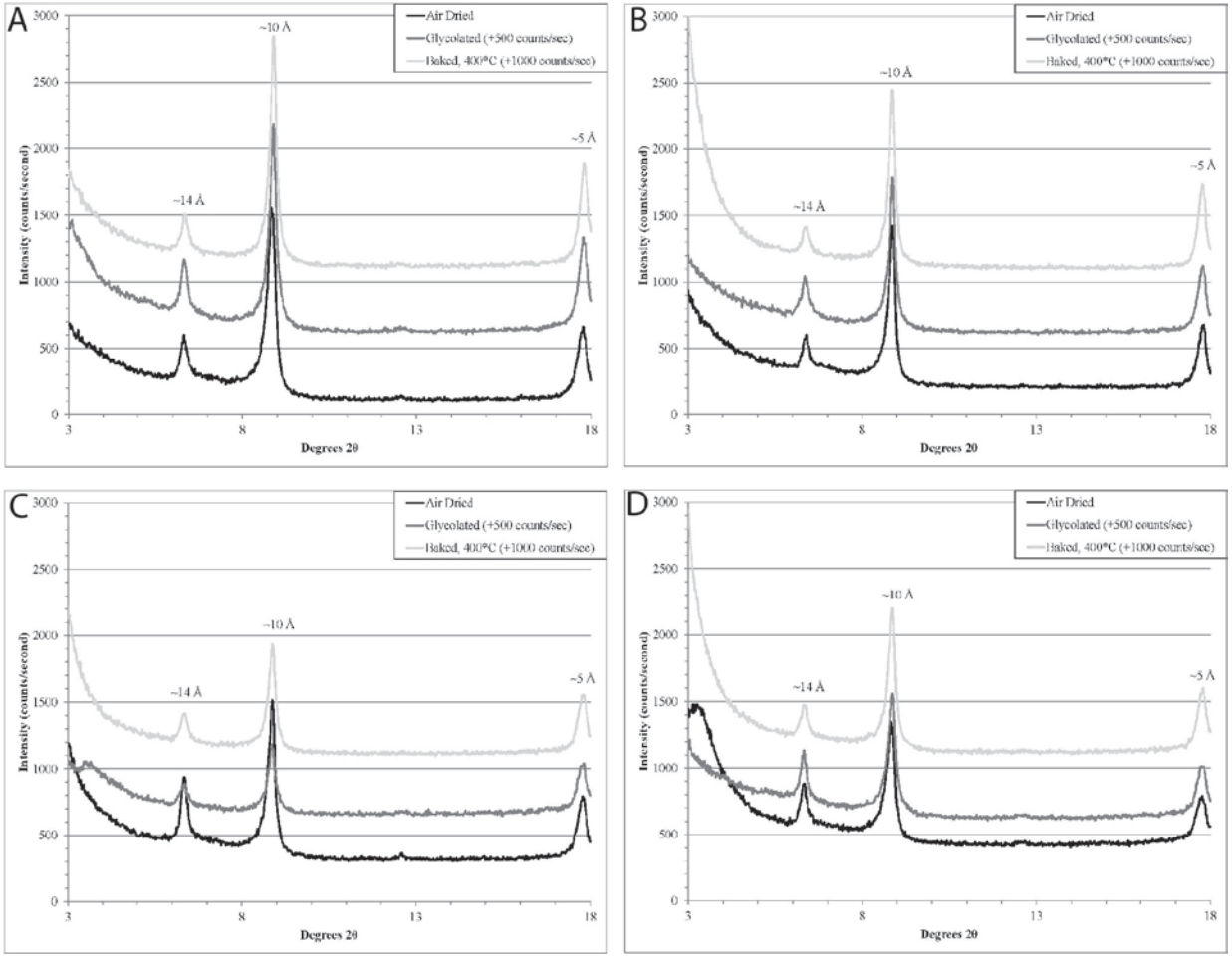

Figure 3.11. X-ray spectra for oriented mounts of basal melt-out till (*a)*, reworked basal melt-out till (*b*), basal/supraglacial melt-out till (*c*), and reworked melt-out till (*d*) sediments. Annotations represent approximate d-spacing of prominent peaks. 14 and 10 Å peaks were assigned to chlorite's [001] and muscovite's [002] crystal planes, respectively. The 5 Å peak was assigned to muscovite's [004] crystal plane. It is also possible that a portion of the 10 and 5 Å peak may correspond to illite, but peak width and associated illite crystallinity values suggest a predominance of muscovite.

CHAPTER 4: DISCUSSION

4.1. Grain Size

All four sediment samples exhibit a grain size distribution skewed toward medium to coarse sands (Figure 3.1). The positive correlation between grain size class frequency and grain size likely reflect the amount of glacial comminution that grains have undergone, suggesting that the majority (by weight) of the grains sampled have undergone limited physical weathering due to the short subglacial transport distance. Comparison of the % sand, silt, and clay from Robertson Glacier tills further supports this hypothesis, with a visible trend of fining (i.e., increased % clay/silt) for larger glacial systems (Figure 4.1). Furthermore, SEM imaging of grains supports the likelihood of limited physical weathering with the majority of grains presenting angular to sub-angular roundness (Figure 2.5).

It is important to note that the grain size distribution reported here represents only sediments sampled with a consistent experimental cutoff on the upper size of material due to the diameter of sampling containers. Grains larger than 4.5 cm for basal melt-out tills and 2.5 cm for basal/supraglacial melt-out and reworked melt-out tills were not collected and were not part of the analysis due to this sampling container diameter limit.

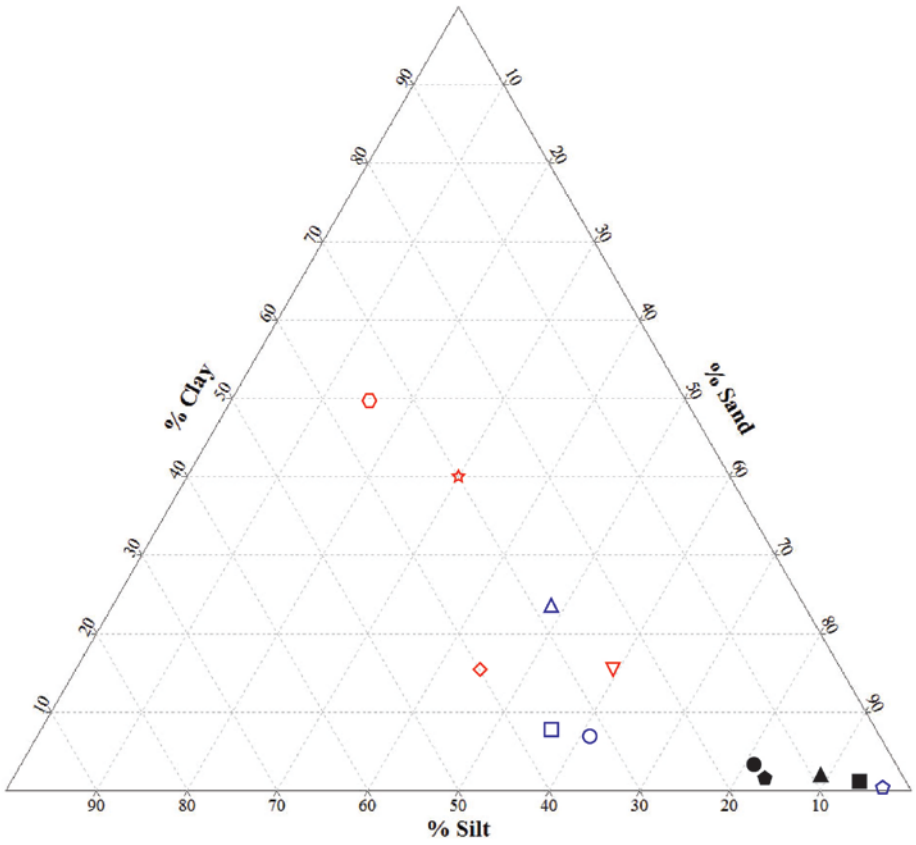

Sample:	*Data Source:*	*% Clay:*	*% Silt:*	*% Sand:*	*Bedrock Composition:*	*Length: (km)*	*Area: (km^2)*
Basal Melt-Out ■	Robertson Glacier	< 0.5	5	95	Impure limestone, dolostone, and dolomitic limestone, with shale/siltstone/sandstone interbeds	3	3
Reworked Basal Melt-Out ▲		1	9	90			
Basal/Supraglacial Melt-Out ●		2	16	82			
Reworked Melt-Out ⬟		1	15	84			
Other Glacial Environments *Valley-Scale*							
Slettsmarkbreen, Norway ○	Benn, 1994	6	32	62	Peridotite, pyroxene gneiss, amphibolite, and mylonite, with limited quartz-feldspar veins	2	3
Haut Glacier d'Arolla ⬠	Hubbard and Sharp, 1995	0	2	99	Schistose granite, amphibolite, greenschist, and gabbro	4	6
Athabasca Glacier, Alberta △	Mills, 1977	23	28	49	Limestone and dolostone, with lesser shale on walls and significant quartzite in bed	8	7
Burroughs Glacier, Alaska □	Ham and Mickelson, 1994	7	36	57	Metamorphosed calcareous shale and argillaceous limestone, with diorite/granodiorite intrusions	14	42
Continental-Scale							
Southeastern Manitoba	Fenton, 1974	15	40	45	Limestone and dolostone ◇	Continental	
Southern Ontario	Dreimanis, 1961	15	25	60	Limestone and dolostone ▽		
		40	30	30	Shale ☆		
		50	35	15	Stratified clay ⬡		

Figure 4.1. % clay, silt, and sand for tills from several glacial systems. Filled symbols represent Robertson Glacier data from this study, while outlined symbols represent data from other studies on glacial tills.

4.2. Particulate Organic Carbon

POC abundances reported here represent upper limits due to potential dehydration of clays during loss-on ignition. POC abundance is correlated with % calcite, especially when outlying data are removed (Figure 4.2-3). The correlation of POC and calcite abundances suggests that POC is primarily derived from bedrock in association with calcite. This correlation was analyzed for pooled size classes of >125 or <125 μm to determine whether the correlation varied with grain size, with the splitting point derived from the maximum of the observed normal distribution for % POC versus grain size. The positive correlation between POC and % calcite strengthens for the >125 μm size class, especially when outlying data points are removed (Figures 4.4 and 4.6). In contrast, the correlation between POC and % calcite weakens significantly for the <125 μm size class (Figures 4.5 and 4.7). There is no significant correlation between % dolomite and POC abundance when considered across all grain sizes (Figure 4.2). However, when this correlation is analyzed for the same size classes there is a potential weak correlation for the <125 μm size class when outlying data points are removed (Figures 4.4-7).

Furthermore, the observed negative correlation between grain size and % POC may be related to the increased surface area of smaller grains. Specifically, if POC was directly associating with grain surfaces via adsorption then POC content would scale with surface area and thus increase with decreasing grain size. Furthermore, the decrease in clay-sized particles observed in laser diffraction-based grain size analysis for sediments subjected to the loss-on-ignition protocol suggests that POC may primarily be <2 μm particles (Table A.5).

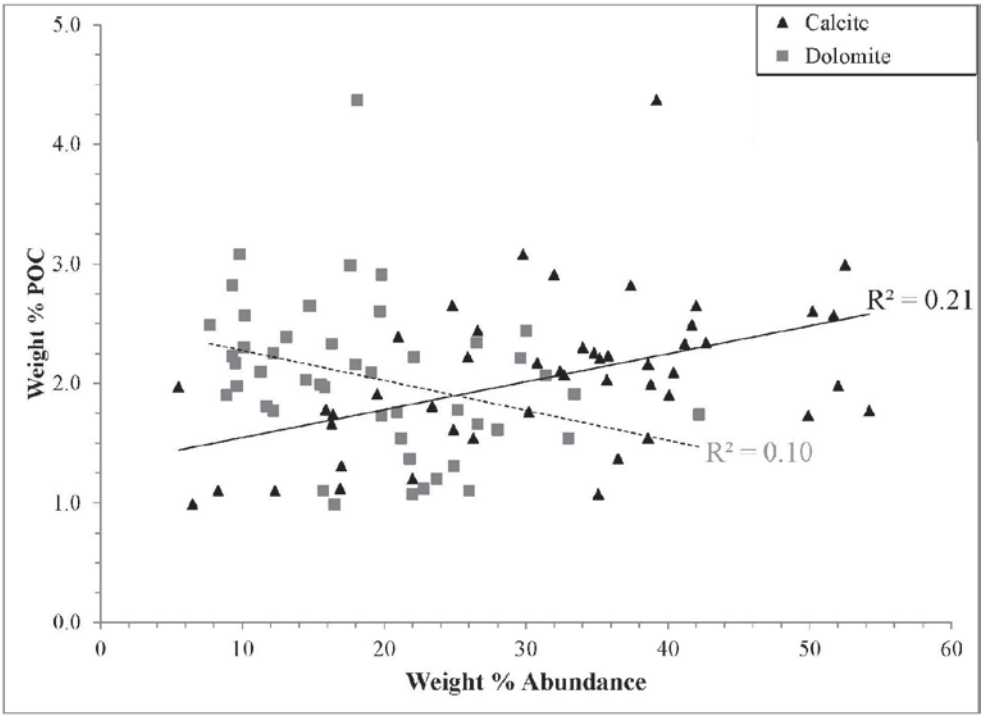

Figure 4.2. Relationships between % calcite/dolomite and POC abundance for all size classes.

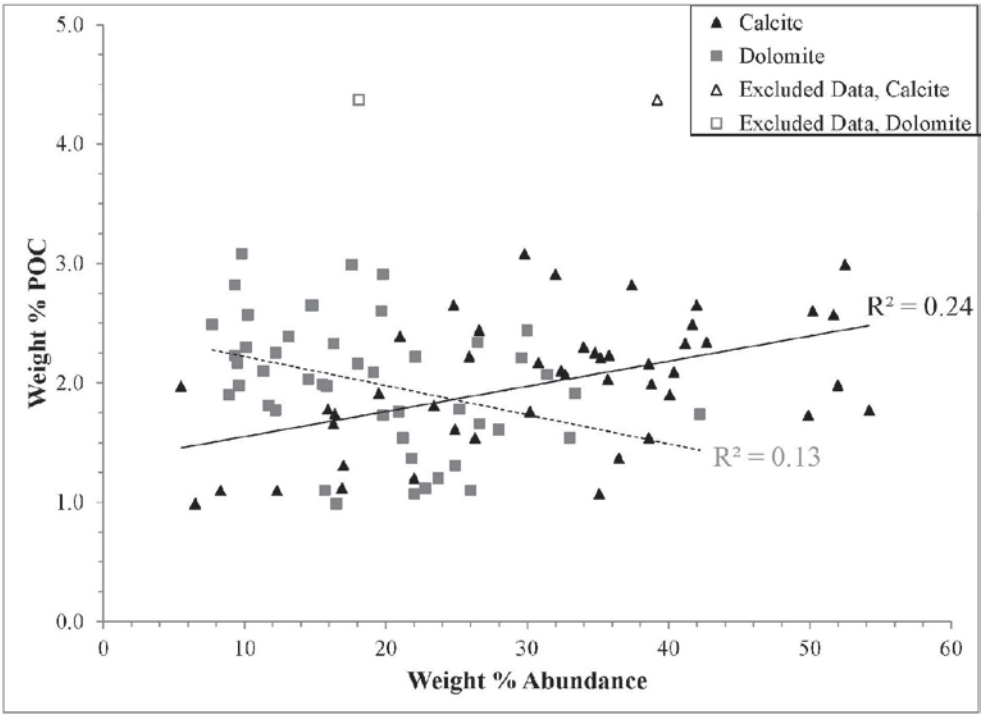

Figure 4.3. Relationships between % calcite/dolomite and POC abundance for all size classes, with outlying data excluded.

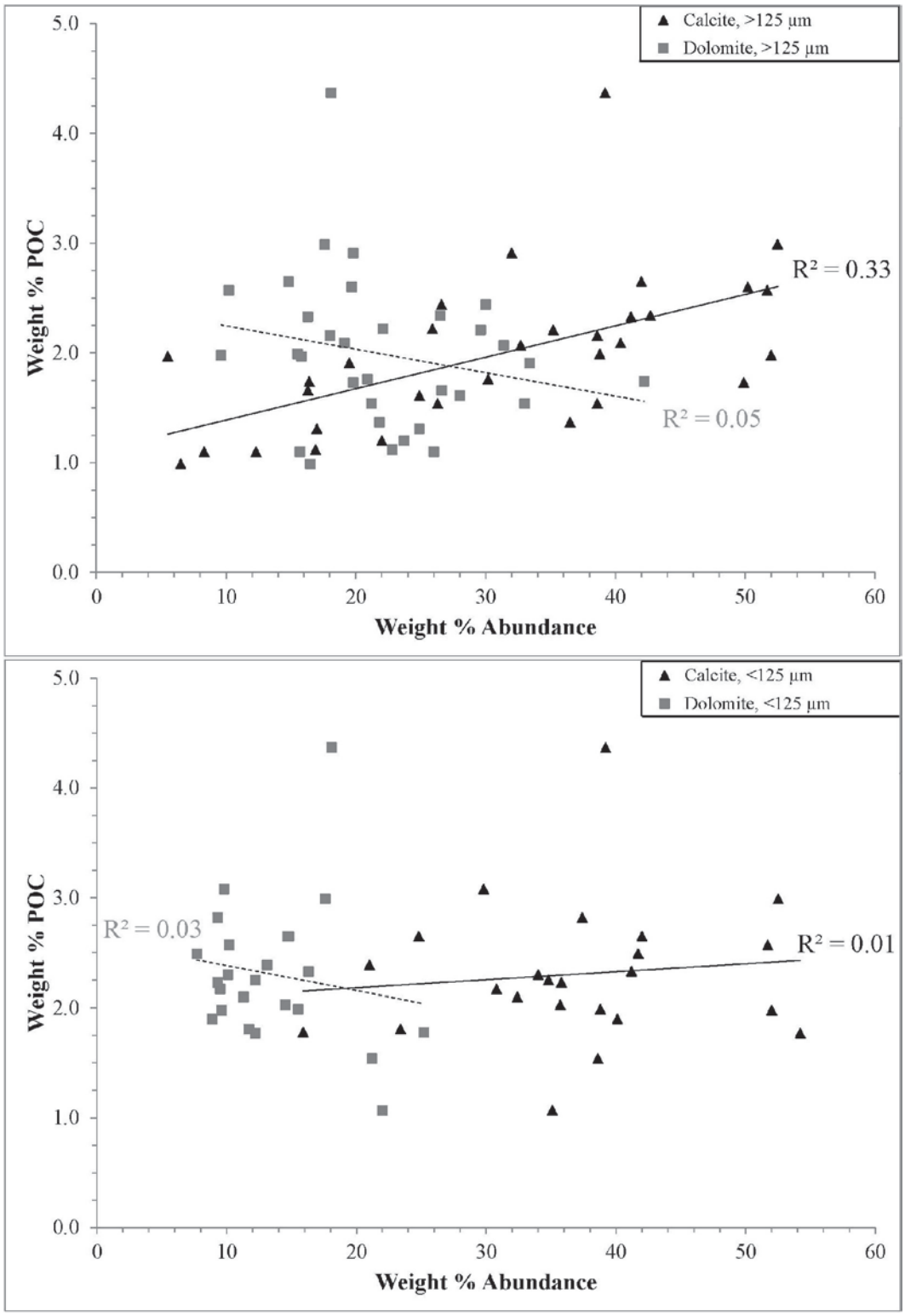

Figure 4.4-5. Relationships between % calcite/dolomite and POC abundance when grouped as >125 or <125 µm.

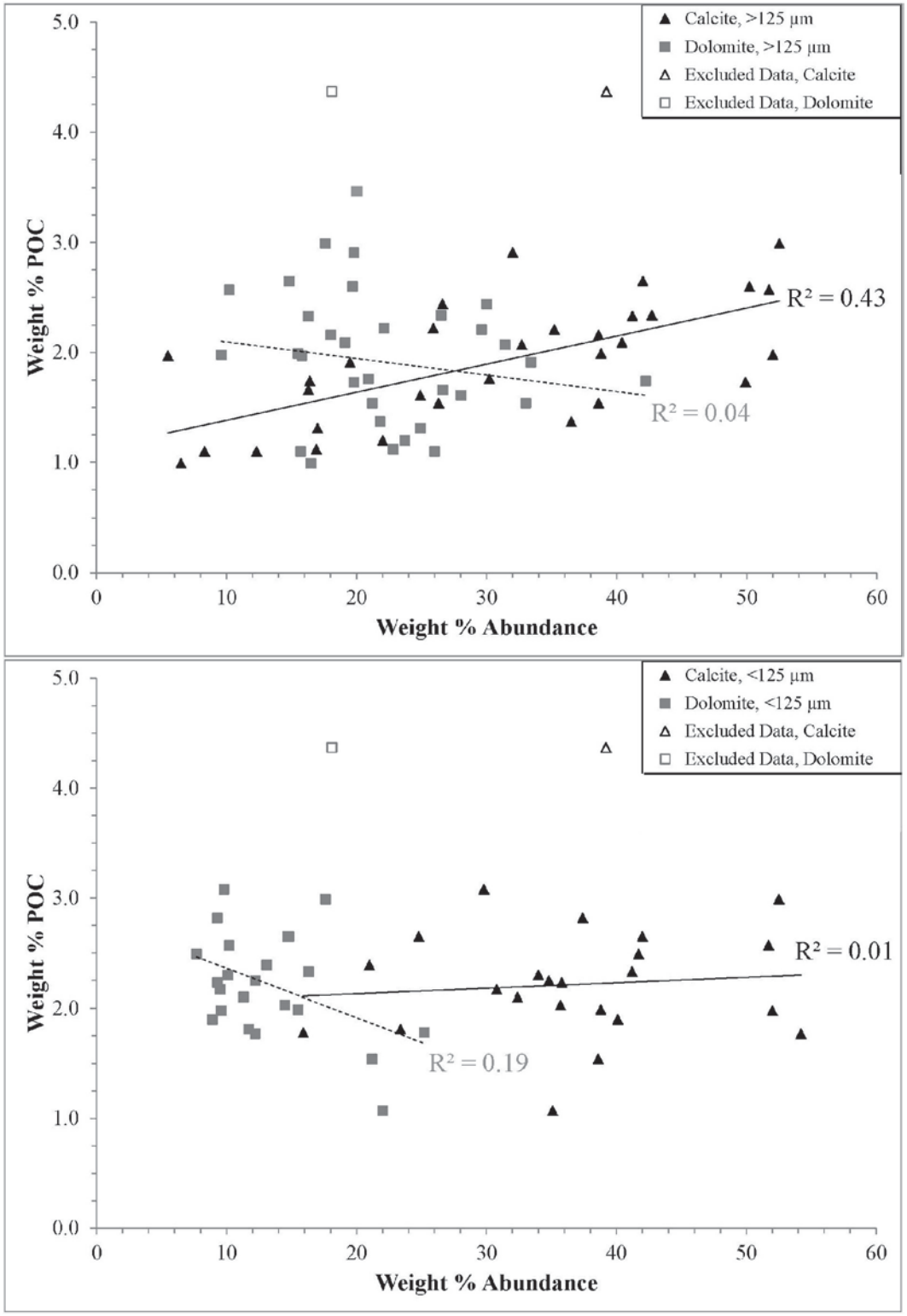

Figure 4.6-7. Relationships between % calcite/dolomite and POC abundance when grouped as >125 or <125 µm with outlying data excluded.

4.3. Mineralogy

The primary minerals in all sediment samples are calcite, dolomite, quartz, and K-feldspar. There are also much lower concentrations of muscovite (<2%), pyrite (< 1%), phlogopite (<~1%), and chlorite (< ~1%). Calcite and dolomite abundances, as derived from weight loss following acid dissolution, represent upper limits due to the complete dissolution of not just detrital carbonates, but also any carbonate cements or precipitates. Phlogopite abundance may be under-reported due to a systematic interpretation error. EDS spectra containing Si >> Al/K and near-background Mg were originally interpreted as K-feldspar with background Mg, but upon further analysis may actually represent phlogopite.

Pyrite was solely observed as secondary grain fragments ~5-15 µm diameter on the surface of basal melt-out till sediments. Although pyrite was not observed in mineralogical analyses of reworked basal melt-out till, basal/supraglacial melt-out till, or reworked melt-out till, its presence in the basal melt-out till suggests a potential bimodal distribution in the Robertson catchment as either large crystals in bedrock (as observed in Sharp et al, 2002) or very fine (< 15 µm) particles in till. The size of pyrite grains may support its observed presence solely in a primary till, due to preferential removal of small grains during aqueous reworking. The acid-dissolution protocol for removal of carbonates likely simulated this process in the laboratory, removing smaller grains from the surfaces of acid-washed sediments. Furthermore, calculation of theoretical specific surface area and rate of pyrite oxidation suggest that 5-15 µm cuboidal pyrite grains would provide sufficient surface area for significant pyrite oxidation greater than or equal

to that observed in laboratory sediment slurries of other glacial sediments (Table 4.1). However, these calculations assume similar reactivity of pyrite irrespective of bulk bedrock composition, which potentially skews values away from being fully representative of the natural environment. Additionally, the much lower calculated FeS_2 oxidation rate for sediments from Montross et al (2013) suggests that only a portion of the available pyrite would be oxidized in the natural environment, which supports the relatively high importance of pyrite oxidation as a subglacial weathering process despite its trace abundance. Although XRD analysis did not find any secondary minerals potentially derived from pyrite oxidation, observations of nanoparticles or surface coatings of Fe-oxyhydroxides in other glacial systems (Mitchell et al, 2001; Raiswell et al, 2009) suggests that Fe being liberated during pyrite oxidation is likely being sequestered as trace Fe-oxyhydroxides (Mitchell et al, in press).

Table 4.1. Comparison of calculated theoretical potential specific surface area and pyrite oxidation rates between Robertson Glacier tills and data from several laboratory experiments. Pyrite specific surface area for Ontario sands was calculated using pyrite grain size and abundance from Nicholson et al (1988). Pyrite oxidation rates for Robertson Glacier were calculated using a linear first-order relationship between calculated pyrite specific surface area and pyrite oxidation rates from Nicholson et al (1988). Note that substantially larger specific surface areas from Montross et al (2013) are due to inclusion of all minerals, not solely pyrite.

Experiment Type & Sediment Source	*Source:*	*Specific Surface Area: ($cm^2\ g^{-1}$)*	*FeS_2 Oxidation Rate: ($\mu mol\ SO_4^{2-}\ g^{-1}\ d^{-1}$)*
Theoretical Potential Calculations			
Robertson Glacier, Alberta	Theoretical 15 µm FeS_2 cubes	7 (pyrite)	0.7
	Theoretical 10 µm FeS_2 cubes	11 (pyrite)	1.1
	Theoretical 5 µm FeS_2 cubes	22 (pyrite)	2.2
Laboratory Experiments			
Haut Glacier d'Arolla, Switzerland	Montross et al., 2013	1,000-3,275 (all minerals)	0.003
Bodalsbreen, Jostedalsbreen, Norway		1,760 (all minerals)	0.1
Elliot Lake, Ontario sand, supplemented to 20% FeS_2 (215 µm)	Nicholson et al., 1988	11 (pyrite)	1.2
Elliot Lake, Ontario sand, supplemented to 20% FeS_2 (108 µm)		22 (pyrite)	2.3
Elliot Lake, Ontario sand, supplemented to 20% FeS_2 (54 µm)		44 (pyrite)	4.6

4.3.1. Mineralogy / Grain Size Associations

Grain size is positively correlated with % dolomite (R^2=0.38, p<0.01) (Figure 3.4). Muscovite is negatively correlated (R^2=0.37, p<0.01) with grain size down to 63 µm (Figure 3.10). Calcite and K-feldspar/quartz present differing correlations with grain size for large/small grains, switching at approximately 125 µm for normal and bimodal distributions, respectively. Calcite abundance is negatively correlated (R^2=0.83, p<0.01) with grain size for grains >125 µm (Figure 3.3), while K-feldspar (Figure 3.8) and quartz (Figure 3.9) are positively correlated (R^2=0.48, p=0.01; R^2=0.49, p=0.01). Further, calcite abundance is positively correlated (R^2=0.35, p<0.01) with grain size for grains <125 µm, while K-feldspar and quartz are negatively correlated (R^2=0.36, p=0.01; R^2=0.45, p<0.01). These observed correlations between grain size and specific mineral abundances are likely explained by the relative hardness of each mineral (Table 4.2), with larger grains containing higher abundances of harder minerals (i.e., positive correlation with grain size) and smaller grain size classes containing softer minerals with greater frequency (i.e., negative correlation with grain size). The inconsistent correlations between grain size and calcite, K-feldspar, and quartz abundances across all grain sizes suggests that another property or process is exerting greater influence than solely relative hardness.

Table 4.2. Mohs hardness of select minerals (Perkins, 2011).

Mineral:	*Mohs Hardness:*
Muscovite	2-2.5 (parallel to [001]) 4 (perpendicular to [001])
Calcite	3
Dolomite	3.5-4
K-Feldspar	6
Quartz	7

4.3.2. Potential Sources of Error in Mineralogy

The single XRD peak for acid-leached sediments (>0.5 mm size class for basal melt-out till, >2 mm size class for all other tills) that appeared to most closely correspond to a crystal plane of dolomite was likely produced by dolomite protected from acid dissolution by the smaller surface area of these larger sediments (Figures 3.6-3.7). The observed overestimate (relative to acid-leach values) of calcite and underestimate of dolomite by SEM-EDS in basal melt-out till sediments was likely due to counting errors, small sample size, and ambiguity in identifying overlapping grains during interpretation of the composite SEM-EDS spectra and misattribution of dolomite portions of the spectra as calcite due to low Mg content (Table D.3).

Similar to calcite/dolomite abundance data, there were also differences in quantitative results for K-feldspar, quartz, and muscovite content derived from SEM-EDS elemental analysis on native versus acid-leached unsorted basal melt-out till sediments (Table D.5). The divergence of these non-carbonate content values between analyses of the two sediment treatments may be related to the relatively small sample size of non-carbonate grains in the native sediments.

4.4. Comparison to Primary Literature

4.4.1. Grain Size Distribution

The grain size distribution of the tills examined here has two modes, one coarse sand-sized particles (>0.5 mm) and the other coarse silt-sized particles (31-63 μm). These findings are similar to the polymodal particle size distribution of till observed in other carbonate-dominated North American settings (e.g., Dreimanis and Vagners, 1971; Fenton, 1974; Taylor and Faure, 1979). However, due to differing mineral hardness/solubility and subglacial environmental conditions (e.g., pH), the grain size distribution of tills derived from glaciers overlying silicate-dominated bedrock would be expected to be slightly different. Specifically, the grain size distribution reported here for the melt-out tills sampled is very similar to the distribution of dolostone/dolomite grain sizes reported by Dreimanis and Vagners (1971) for Laurentide Ice Sheet (LIS)-derived tills having experienced 0-3 km of transport (Figure 4.8). The major difference, that of the larger mode being centered around ~0.5-2 mm instead of ~16 mm, between the grain size distribution reported here and that of Dreimanis and Vagners (1971) can be explained by the much larger size and transport capacity of the LIS compared to Robertson Glacier. Furthermore, the sediments sampled here exhibit a much lower silt/clay content than the 50-75% reported for LIS-derived tills from southeastern Manitoba (Fenton, 1974) or Ohio (Taylor and Faure, 1979), although this could just be due to the greater potential transport distance in the subglacial traction zone and thus greater potential comminution of larger particles.

The grain size distribution results presented here also contrasts with the results of a previous study at Robertson Glacier (those of Doxsey-Whitfield, 2012). Doxsey-Whitfield (2012) found significantly more clay-sized grains (~22-30%) in the tills sampled, although this increase may simply be a result of greater potential proglacial comminution due to the greater distance (15-1600 m) traveled in the subglacial traction zone prior to sampling.

4.4.2. Till Mineralogy

Till mineralogy based on XRD and SEM aligns closely with a previous study at Robertson Glacier by Doxsey-Whitfield (2012); however no plagioclase feldspar was observed in this study. There is also good agreement with previous results for Robertson Glacier bedrock mineralogy from Sharp et al (2002); however no bassanite was observed. Measured pyrite content of < 1% is also similar to the calculated 0.6/1.2 weight % for Robertson Glacier bedrock/sediment by Mitchell et al (in press). Sharp et al (2002) and Doxsey-Whitfield (2012) did not conduct quantitative mineralogical analyses, so there is no basis for comparison at Robertson Glacier.

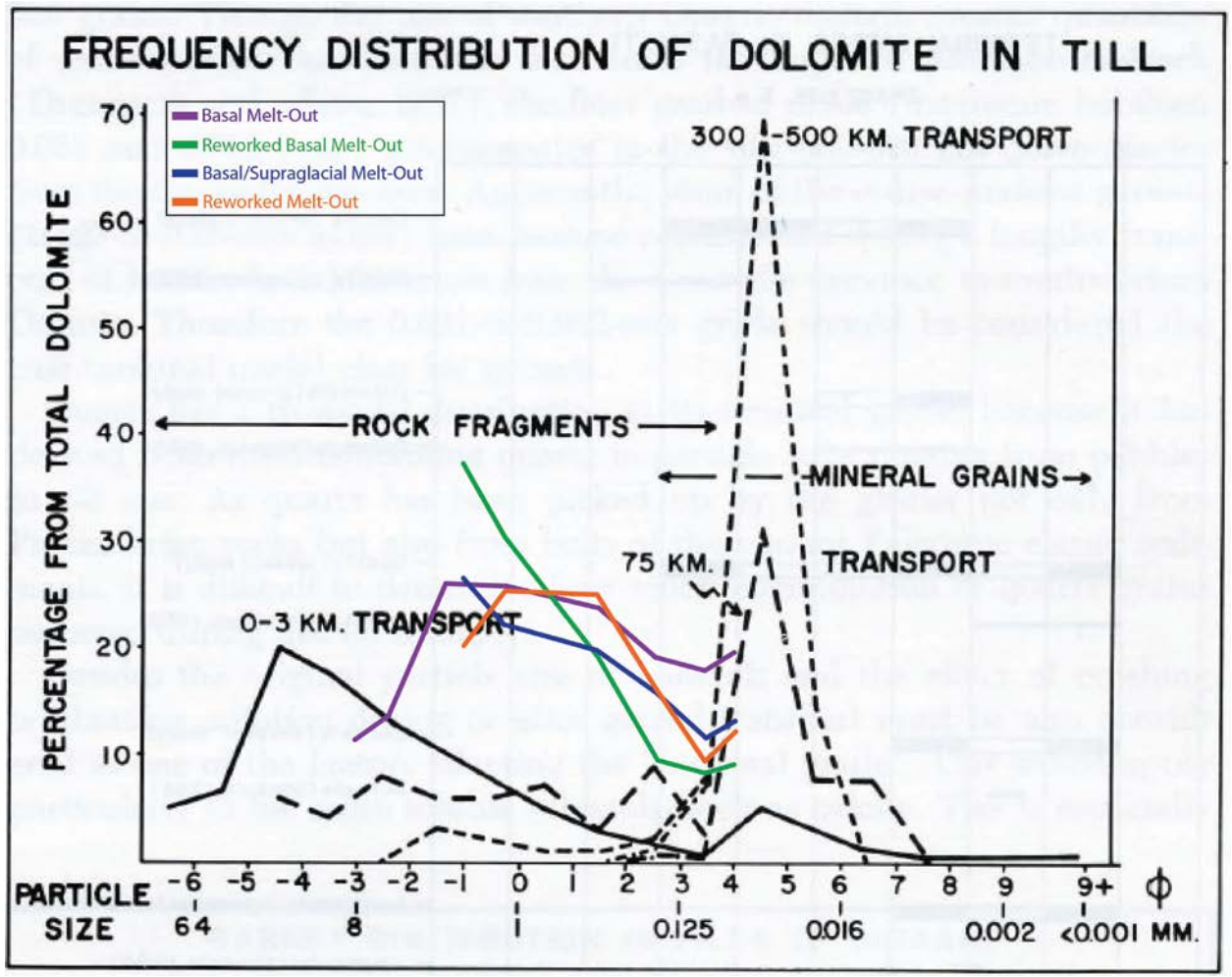

Figure 4.8. Comparison of dolomite/dolostone grain size distribution across three till samples representing differing distances (0-3, 75, or 300-500 km) of transport. Overlay of grain size distributions (bulk mineralogy) from this study.

Quantitative mineralogy values do match the magnitude observed in tills from other carbonate-dominated regions (e.g., Fenton, 1974; Taylor and Faure, 1979). In a similar range as the values reported by Fenton (1974) for Laurentide Ice Sheet (LIS)-derived tills from southeastern Manitoba, the coarse sand class is ~45% dolomite and calcite in a ~1.25:1 ratio, versus Fenton's results of 35-60% carbonate in a 1.3:1 ratio. Furthermore, the silt/clay class is ~40% carbonates, although in a 3:1 ratio of dolomite : calcite, versus the 30-50% carbonates and 2:1 ratio reported by Fenton. The carbonate grain size distribution reported here is also similar to that reported by Taylor and Faure (1979) for LIS-derived tills from Ohio, where carbonate content was highest for coarse sands and then decreased with decreasing grain size, in that the carbonate content reported here increases between coarse and medium sands and then decreases in fine sands and silts/clays. Distributions of feldspar abundance across grain size classes reported here are similar to the reported concentration in sand-sized grains by Taylor and Faure (1979), although feldspar is slightly more abundant in medium and coarse sands in the distribution reported here than the predominantly fine-sand mode found by Taylor and Faure. Furthermore, the distribution of quartz abundance by grain size class differs from that reported by Taylor and Faure (1979) in that quartz abundance is most abundant across the sand and silt/clay classes in the sediments sampled here while it was found to be most prominent in fine-medium sands by Taylor and Faure.

4.4.3. Particulate Organic Carbon

POC and calcite abundance have previously been linked in marine settings in relation to facilitation of POC sinking through the water column (Klaas and Archer, 2002; Sanders et al, 2010). However, such an association of POC with specific minerals has not previously been reported for terrestrial carbonate bedrock, especially from a glacial system. The range (1.1-3.5 weight %) of POC content in tills reported here is slightly greater than in previous studies (1.6-2.5 weight %) at Robertson Glacier (e.g., Boyd et al, 2010; Doxsey-Whitfield, 2012) but the arithmetic mean is similar within 22%. The range of POC content in tills in this study most closely matches values reported by Skidmore et al (2000) from John Evans Glacier of Ellesmere Island, Nunavut, Canada. This may be related to similar mineralogy of the underlying bedrock which is composed of an Ordovician/Silurian carbonate/evaporite sequence with a small clastic component (Kerr, 1972). However, a lack of quantitative mineralogy data for John Evans Glacier prevents further comparison, especially with regard to potential linkages with specific minerals. Furthermore, the POC present in RG melt-out till appears to exhibit very low bioavailability. If POC was readily bioavailable a significant decrease in POC abundance for small size classes would be expected due to their greater surface area and thus preferential use by microbes.

4.5. Major Findings of This Study

1) Dominant till mineralogy consists of calcite, dolomite, quartz, and K-feldspar with lesser muscovite, pyrite, phlogopite, and chlorite.
2) POC abundance, ranging from 1.1 to 3.5 weight %, is negatively correlated with grain size for grains >125 μm. POC abundance is also positively correlated with calcite abundance, especially for grains >125 μm.
3) The geochemically reactive trace mineral pyrite is present at < 1% bulk abundance. Pyrite abundance is not significantly correlated with grain size or abundance of other minerals. Calculated theoretical specific surface area and pyrite oxidation rates suggest that the amount of pyrite is sufficient for greater than or equal rates of pyrite oxidation than observed in laboratory sediment slurries of other glacial sediments and that potentially only a portion of the available pyrite is being oxidized in the natural system.
4) All sediment samples exhibited a grain size distribution strongly biased toward coarse (>0.5 mm) sand-sized grains and a positive correlation between grain size class frequency and grain size, which may be representative of limited physical weathering due to the short subglacial transport distance.

REFERENCES CITED

Akselsson, C., Holmqvist, J., Kurz, D., and Sverdrup, H. (2006). Relations between elemental content in till, mineralogy of till and bedrock mineralogy in the province of Småland, southern Sweden. *Geoderma* **136**, 643-659.

Anderson, S. P. (2007). Biogeochemistry of Glacial Landscape Systems. *Annual Reviews of Earth Planetary Science* **35**, 375-399.

Bayvel, L. P. and Jones, A. R. (1981). *Electromagnetic Scattering and its Applications*. Applied Science, London.

Benn, D. I. (1994). Fluted moraine formation and till genesis below a temperate valley glacier: Slettmarkbreen, Jotunheimen, southern Norway. *Sedimentology* **41**, 279-292.

Benn, D. I., and Evans, D. J. A. (1996).The interpretation and classification of subglacially-deformed materials. *Quaternary Science Reviews* **15**, 23-52.

Benn, D. I., and Evans, D. J. A. (2010). *Glaciers and Glaciation*. Hodder Education, 802 p.

Bottrell, S. H. and Tranter, M. (2002). Sulphide oxidation under partially anoxic conditions at the bed of the Haut Glacier d'Arolla, Switzerland. *Hydrological Processes* **16**, 2363-2368.

Boyd, E. S., Skidmore, M., Mitchell, A. C., Bakermans, C., and Peters, J. W. (2010). Methanogenesis in subglacial sediments. *Environmental Microbiology Reports* **2**, 685-692.

Crosby, W. O. (1892). Composition of the till or boulder-clay. *Proceedings of the Boston Society of Natural History* **25**, 115-140.

DMSNT (Diffraction Management System for NT), Version 1.37. 1999. Scintag.

Doxsey-Whitfield, E. L. (2012). Magnitude and controls of microbial nitrate production in the streams and till of a glaciated alpine catchment, Canadian Rocky Mountains, Alberta. M.Sc. thesis. Queen's University, Kingston, Ontario, Canada. 191 p.

Dreimanis, A. (1961). Tills of southern Ontario. *In:* Legget, R. F. (ed.), *Soils in Canada: Royal Society of Canada Special Publication 3*, p. 80-96.

Dreimanis, A. (1971). Procedures of till investigations in North America: a general review. *In:* Goldthwait, R. P. (ed.), *Till: A Symposium*. Ohio State University Press, Columbus, OH, p. 27-37.

Dreimanis, A. (1988). Tills: their genetic terminology and classification. *In:* Goldthwait, R. P. and Matsch, C. L. (eds.), *Genetic Classification of Glacigenic Deposits*. Balkema, Rotterdam, p. 17-84.

Dreimanis, A. and Vagners, U. J. (1971). Bimodal distribution of rock and mineral fragments in basal tills. *In:* Goldthwait, R. P. (ed.), *Till: A Symposium*. Ohio State University Press, Columbus, OH, p. 237-250.

Durand, B. (1980). Sedimentary organic matter and kerogen: definition and quantitative importance of kerogen. *In:* Durand, B., (ed.), *Kerogen. Insoluble Organic Material from Sedimentary Rocks*. Technips, Paris, p. 13-34.

Evans, D. J. A., Phillips, E. R., Hiemstra, J. F., and Auton, C. A. (2006). Subglacial till: Formation, sedimentary characteristics and classification. *Earth-Science Reviews* **78**, 115-176.

Fenn, C. R. and Gomez, B. (1989). Particle size analysis of the sediment suspended in a proglacial stream: Glacier de Tsijiore Nouve, Switzerland. *Hydrological Processes* **3**, 123-135.

Fenton, M. M. (1974). The Quaternary Stratigraphy of a Portion of Southeastern Manitoba. PhD thesis. University of Western Ontario, London, Ontario, Canada. 285 p.

Flint, R. F., Sanders, J. E., and Rodgers, J. (1960). Diamictite, a substitute term for symmictite. *Geological Society of America Bulletin* **71**, 1809-1810.

Foght, J., Aislabie, J., Turner, S., Brown, C. E., Ryburn, J., Saul, D. J., and Lawson, W. (2004). Culturable bacteria in subglacial sediments and ice from two southern hemisphere glaciers. *Microbial Ecology* **47**, 329-340.

Folk, R. L. and Ward, W. C. (1957). Brazos River Bar: A Study in the Significance of Grain Size Parameters. *Journal of Sedimentary Petrology* **27**, 3-26.

Geikie, A. (1863). On the Phenomena of the Glacial Drift of Scotland. Transactions of the Geological Society of Glasglow **1**, 190 p.

Gomi, T. and Sidle, R. (2003). Bed load transport in managed steep-gradient headwater streams of southeastern Alaska. *Water Resources Research* **39**, 1336.

Haldorsen, S. (1981). Grain-size distribution of subglacial till and its relation to glacial crushing and abrasion. *Boreas* **10**, 91-105.

Hallet, B. (1976). Deposits formed by subglacial precipitation of $CaCO_3$. *Geological Society of America Bulletin* **87**, 1003-1015.

Ham, N. R. and Mickelson, D. M. (1994). Basal till fabric and deposition at Burroughs Glacier, Glacier Bay, Alaska. *Geological Society of America Bulletin* **106**, 1552-1559.

Hamilton, T. L., Peters, J. W., Skidmore, M. L., and Boyd, E. S. (2013). Molecular evidence for an active endogenous microbiome beneath glacial ice. *ISME*, in press.

Harland, W. B., Herod, K. N., and Krinsley, D. H. (1966). The Definition and Identification of Tills and Tillites. *Earth Science Reviews* **2**, 225-256.

Heiri,, O., Lotter, A. F., and Lemcke, G. (2001). Loss on ignition as a method for estimating organic and carbonate content in sediments: reproducibility and comparability of results. *Journal of Paleolimnology* **25**, 101-110.

Hooke, R. LeB. and Iverson, N. R. (1995). Grain-size distribution in deforming subglacial tills: Role of grain fracture. *Geology* **23**, 57-60.

Hubbard, B. and Sharp, M. (1995). Basal Ice Facies and Their Formation in the Western Alps. *Arctic and Alpine Research* **27**, 301-310.

International Centre for Diffraction Data (ICDD), PDF-2 catalog. 2005.

Jackson, M. L. (1979). *Soil Chemical Analysis, Advanced Course (2nd edition).* Self-published, Madison, WI.

Kerr, J. W. (1972). Map 1358A Geology: Dobbin Bay, District of Franklin. Geological Survey of Canada, Ottawa, Ontario.

Kjær, K. H. (1997). Mode of subglacial transport deduced from till properties, Mýrdalsjökull, Iceland. *Sedimentary Geology* **128**, 271-292.

Klaas, C. and Archer, D. E. (2002). Association of sinking organic matter with various types of mineral ballast in the deep sea: Implications for the rain ratio. *Global Biogeochemical Cycles* **16**, 1116.

Kübler, B. and Jaboyedoff, M. (2000). Illite crystallinity. *Comptes Rendus de l'Académie des Sciences* **331**, 75-89.

Lawson, D. E. (1981). *Sedimentological Characteristics and Classification of Depositional Processes and Deposits in the Glacial Environment.* Cold Regions Research and Engineering Laboratory, Hanover, NH. Report 81-27.

Mao, L. and Lenzi, M. A. (2007). Sediment mobility and bedload transport conditions in an alpine stream. *Hydrological Processes* **21**, 1882-1891.

McMechan, M. E. (1988). *Geology of Peter Lougheed Provincial Park, Rocky Mountain Front Ranges, Alberta.* Open File Report 2057. Geological Survey of Canada.

Menzies, J., van der Meer, J. J.M., and Rose, J. (2006). Till as a glacial "tectomict", its internal architecture, and the development of a "typing" method for till differentiation. *Geomorphology* **75**, 172-200.

Mills, H. H. (1977). Differentiation of Glacier Environments by Sediment Characteristics: Athabasca Glacier, Alberta, Canada. *Journal of Sedimentary Petrology* **47**, 728-737.

Mitchell, A., Brown, G. H., and Fuge, R. (2001). Minor and trace element export from a glacierized Alpine headwater catchment (Haut Glacier d'Arolla, Switzerland). *Hydrological Processes* **15**, 3499-3524.

Mitchell, A. C., Lafrenière, M. J., Skidmore, M. L., and Boyd, E. S. (2013). Influence of bedrock mineral composition on microbial diversity in a subglacial environment. *Geology*, in press.

Montross, S. N. (2007). Geochemical Evidence for Microbially Mediated Subglacial Mineral Weathering. M.S. thesis, Department of Earth Sciences, Montana State University.

Montross, S. N., Skidmore, M., Tranter, M., Kivimäki, A.-L., and Parkes, R. J. (2013). A microbial driver of chemical weathering in glaciated systems. *Geology* **41**, 215-218.

Moore, D. M. and Reynolds, R. C. (1997*). X-ray diffraction and the identification and analysis of clay minerals, 2nd ed*. New York, Oxford University Press, 378 p.

Morse, J. W. and Arvidson, R. S. (2002). The dissolution kinetics of major sedimentary carbonate minerals. *Earth-Science Reviews* **58**, 51-84.

Nicholson, R. V., Gillham, R. W., and Reardon, E. J. (1988). Pyrite oxidation in carbonate-buffered solution: 1. Experimental kinetics. *Geochimica et Cosmochimica Acta* **52**, 1077-1085.

Owen, L. A., Derbyshire, E., and Scott, C. H. (2003). Contemporary sediment production and transfer in high-altitude glaciers. *Sedimentary Geology* **155**, 13-36.

Perkins, D. (2010). *Mineralogy, 3rd Edition.* Prentice Hall, Upper Saddle River, NJ.

Poppe, L. J., Paskevich, V. F., Hathaway, J. C., and Blackwood, D. S. (2001). *A Laboratory Manual for X-Ray Powder Diffraction*. USGS Open-File Report 01-041.

Raiswell, R., Benning, L. G., Davidson, L., Tranter, M., and Tulacyzk, S. (2009). Schertmannite in wet, acid, and oxic microenvironments beneath polar and polythermal glaciers. *Geology* **37**, 431-434.

Sanders, R., Morris, P. J., Poulton, A. J., Stinchcombe, M. C., Charalampopoulou, A., Lucas, M. I., and Thomalla, S. J. (2010). Does a ballast effect occur in the surface ocean? *Geophysical Research Letters* **37**, L08602.

Scherrer, P. (1918). Bestimmung der Grösse und der inneren Struktur von Kolloidteilchen mittels Röntgenstrahlen. *Nachrichten von der Gesellschaft der Wissenschaften zu Göttingen, Mathematisch-Physikalische Klasse* **26**, 98-100.

Sharp, M., Parkes, J., Cragg, B., Fairchild, I. J., Lamb, H., and Tranter, M. (1999). Widespread bacterial populations at glacier beds and their relationship to rock weathering and carbon cycling. *Geology* **27**, 107-110.

Sharp, M., Creaser, R. A., and Skidmore, M. (2002). Strontium isotope composition of runoff from a glaciated carbonate terrain. *Geochimica et Cosmochimica Acta* **66**, 595-614.

Sharp, M., Jouzel, J., Hubbard, B., and Lawson, W. (1994). The character, structure and origin of the basal ice layer of a surge-type glacier. *Journal of Glaciology* **40**, 327-340.

Singer, P. C. and Stumm, W. (1970). Acidic Mine Drainage: The Rate-Determining Step. *Science* **167**, 1121-1123.

Skidmore, M. L., Foght, J. A., and Sharp, M. J. (2000). Microbial Life beneath a High Arctic Glacier. *Applied and Environmental Microbiology* **66**, 3214-3220.

Skidmore, M., Anderson, S. P., Sharp, M., Foght, J., and Lanoil, B. D. (2005). Comparison of Microbial Community Compositions of Two Subglacial Environments Reveals a Possible Role for Microbes in Chemical Weathering Processes. *Applied and Environmental Microbiology* **71**, 6986-6997.

Sperazza, M., Moore, J. N., and Hendrix, M. S. (2004). High-Resolution Particle Size Analysis of Naturally Occurring Very Fine-Grained Sediment Through Laser Diffractometry. *Journal of Sedimentary Research* **74**, 736-743.

Szabo, J. P. (2006). Textural and Mineralogical Characteristics of Tills in Northeastern and North-Central Ohio. *Ohio Journal of Science* **106**, 9-16.

Taylor, K. S. and Faure, G. (1979). Mineral composition, $^{87}Sr/^{86}Sr$ ratios, and concentrations of strontium and rubidium in Late Wisconsin till of Ohio. *Ohio Journal of Science* **79**, 149-159.

Tarvainen, T. (1995). The geochemical correlation between coarse and fine fractions of till in southern Finland. *Journal of Geochemical Exploration* **54**, 187-198.

Tranter, M., Sharp, M. J., Lamb, H. R., Brown, G. H., Hubbard, B. P., and Willis, I. C. (2002). Geochemical weathering at the bed of Haut Glacier d'Arolla, Switzerland – a new model. *Hydrological Processes* **16**, 959-993.

Tranter, M. (2003). Geochemical weathering in glacial and proglacial environments. In *Treatise on Geochemistry, Vol. 5: Surface and Ground Water, Weathering, and Soils*, ed. J. I. Drever, p. 189–205.

Tranter, M., Skidmore, M., and Wadham, J. (2005). Hydrological controls on microbial communities in subglacial environments. *Hydrological Processes* **19**, 995-998.

Tulaczyk, S., Kamb, B., Scherer, R. P., and Engelhardt, H. F. (1998). Sedimentary Processes at the Base of a West Antarctic Ice Stream: Constraints from Textural and Compositional Properties of Subglacial Debris. *Journal of Sedimentary Research* **68**, 487-496.

van der Meer, J. J.M., Menzies, J., and Rose, J. (2003). Subglacial till: the deforming glacier bed. *Quaternary Science Reviews* **22**, 1659-85.

Verdel, C., Niemi, N., and van der Pluijm, B. A. (2011). Variations in the Illite to Muscovite Transition Related to Metamorphic Conditions and Detrital Muscovite Content: Insight from the Paleozoic Passive Margin of the Southwestern United States. *The Journal of Geology* **119**, 419-437.

White, A. F., Blum, A. E., Bullen, T. D., Vivit, D. V., Schulz, M., and Fitzpatrick, J. (1999). The effect of temperature on experimental and natural chemical weathering rates of granitoid rocks. *Geochimica et Cosmochimica Acta* **63**, 3277-3291.

Wilding, L. P., Drees, L. R., Smeck, N. E., and Hall, G. F. (1971). Mineral and Elemental Composition of Wisconsin-Age Till Deposits in West-Central Ohio. *In:* Goldthwait, R. P. (ed.), *Till: A Symposium*. Ohio State University Press, Columbus, OH, p. 290-317.

Williams, L. and Abdi, H. (2010). Fisher's Least Significant Difference (LSD) Test. *In:* Salkind, N. (ed.), *Encyclopedia of Research Design*. Sage: Thousand Oaks, CA.

APPENDICES

APPENDIX A

DATA FROM QUANTITATIVE PHYSICAL LITHOLOGICAL AND MINERALOGICAL ANALYSES

Table A.1. Summary of results from quantitative physical lithological and mineralogical analyses of basal melt-out till sediments.

Size Fraction:	*Weight Percent of Total:*	*Calculated Percent of Total Surface Area:*	*Percent Residual H_2O:*	*Percent Organic Carbon:*	*Percent Calcite:*	*Percent Dolomite:*
>8 mm	24.9	2.3	0.35	1.33 ± 0.62	3.0 ± 1.8	11.7 ± 6.4
4 - 8 mm	17.9	2.2	0.57	1.42 ± 0.34	5.6 ± 0.2	13.9 ± 1.1
2 - 4 mm	14.6	3.6	0.58	1.81 ± 0.44	11.6 ± 0.4	26.6 ± 7.7
2 - 0.5 mm	26.3	15.4	0.59	1.78 ± 0.66	21.8 ± 6.9	26.4 ± 5.1
500 - 250 µm	7.6	14.9	0.49	1.86 ± 0.48	39.6 ± 4.4	24.1 ± 3.3
250 - 125 µm	4.0	15.5	0.65	2.26 ± 0.73	45.6 ± 9.9	19.4 ± 2.5
125 - 63 µm	2.4	18.6	0.62	1.55 ± 0.48	35.4 ± 0.4	18.2 ± 5.3
<63 µm	2.4	27.5	0.72	2.21 ± 0.44	20.3 ± 6.3	20.0 ± 7.5

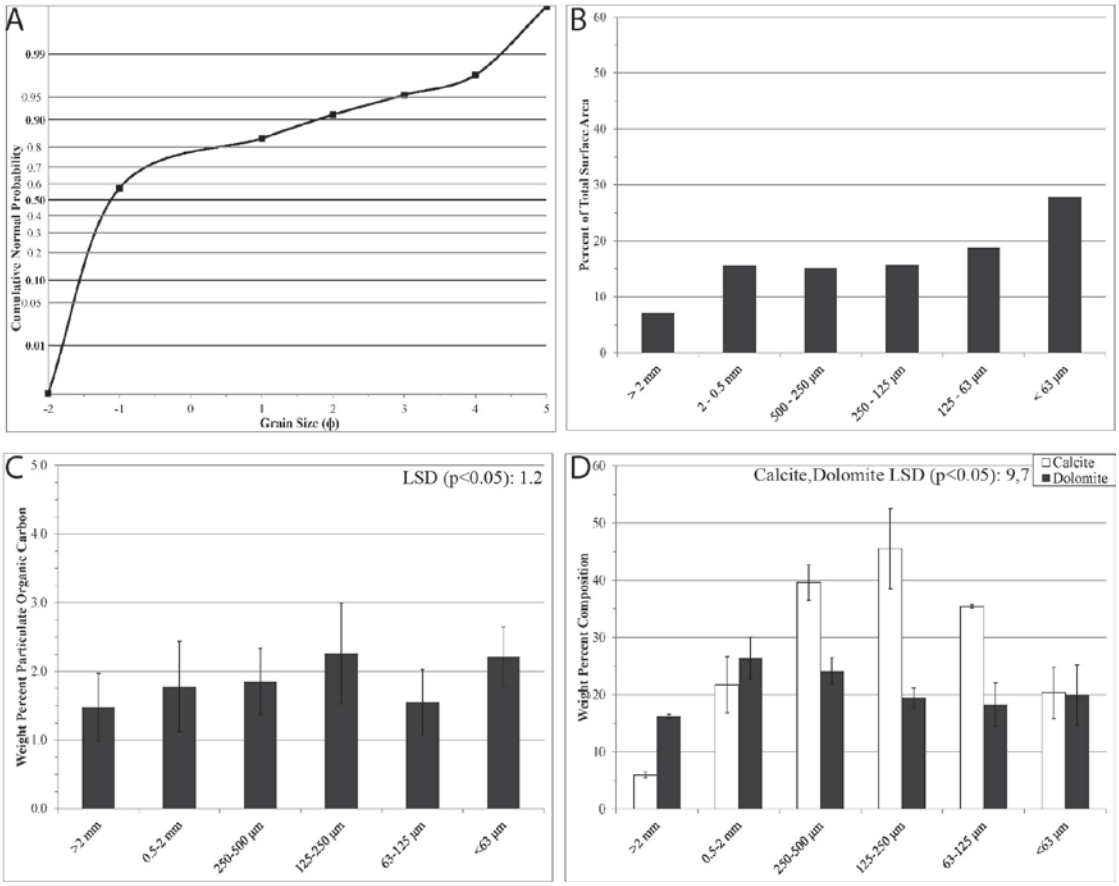

Figure A.1. Grain size distribution (*a*), calculated surface area distribution (*b*), POC content (*c*), and carbonate content (*d*) of Robertson Glacier basal melt-out till sediments. Error bars in *c* and *d* indicate standard deviation between duplicate samples. Least significant difference (LSD) values for panels *c* and *d* represent minimum difference between means to satisfy $p<0.05$ statistical probability of similarity.

Table A.2. Summary of results from quantitative physical lithological and mineralogical analyses of reworked basal melt-out till sediments.

Size Fraction:	*Weight Percent of Total:*	*Calculated Percent of Total Surface Area:*	*Percent Residual H_2O:*	*Percent Organic Carbon:*	*Percent Calcite:*	*Percent Dolomite:*
>2 mm	15.9	2.0	0.25 ± 0.22	1.82 ± 0.09	18.0 ± 2.2	37.8 ± 6.2
2 - 0.5 mm	30.9	6.2	0.37 ± 0.39	1.87 ± 0.33	30.8 ± 6.3	31.3 ± 2.4
500 - 250 µm	22.3	14.9	0.27 ± 0.24	2.16 ± 0.43	50.1 ± 0.2	19.7 ± 0.1
250 - 125 µm	12.8	17.0	0.47 ± 0.40	2.27 ± 0.30	51.8 ± 0.2	9.9 ± 0.4
125 - 63 µm	9.3	24.9	0.61 ± 0.05	2.20 ± 0.29	40.9 ± 1.1	8.3 ± 0.9
<63 µm	8.9	35.0	0.58 ± 0.17	2.52 ± 0.30	36.6 ± 1.1	9.3 ± 0.1

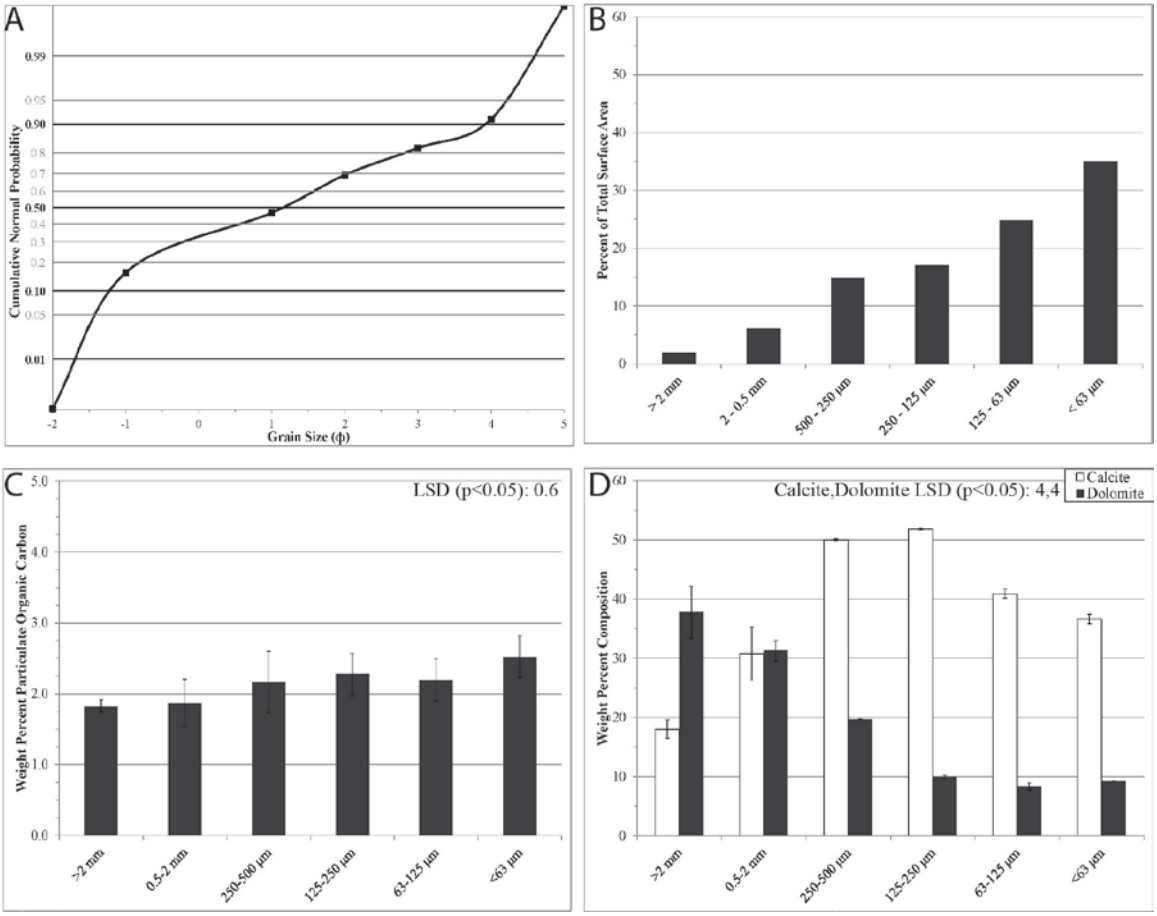

Figure A.2. Grain size distribution (*a*), calculated surface area distribution (*b*), POC content (*c*), and carbonate content (*d*) of Robertson Glacier reworked basal melt-out till sediments. Error bars in *c* and *d* indicate standard deviation between duplicate samples. Least significant difference (LSD) values for panels *c* and *d* represent minimum difference between means to satisfy $p<0.05$ statistical probability of similarity.

Table A.3. Summary of results from quantitative physical lithological and mineralogical analyses on RG basal/supraglacial melt-out till sediments.

Size Fraction:	*Weight Percent of Total:*	*Calculated Percent of Total Surface Area:*	*Percent Residual H_2O:*	*Percent Organic Carbon:*	*Percent Calcite:*	*Percent Dolomite:*
>2 mm	30.7	4.2	0.25 ± 0.06	1.48 ± 0.18	16.7 ± 0.5	25.7 ± 1.1
2 - 0.5 mm	35.9	7.9	0.35 ± 0.06	1.99 ± 0.23	28.0 ± 3.0	21.5 ± 0.8
500 - 250 µm	8.1	5.8	0.43 ± 0.10	2.53 ± 0.38	35.3 ± 4.6	18.9 ± 1.3
250 - 125 µm	5.6	8.1	0.50 ± 0.18	2.16 ± 0.17	40.0 ± 1.7	15.9 ± 0.6
125 - 63 µm	6.8	19.6	0.30 ± 0.01	2.20 ± 0.10	33.2 ± 1.1	10.7 ± 0.8
<63 µm	12.9	54.4	0.43 ± 0.13	2.01 ± 0.24	44.5 ± 13.8	12.2 ± 0.1

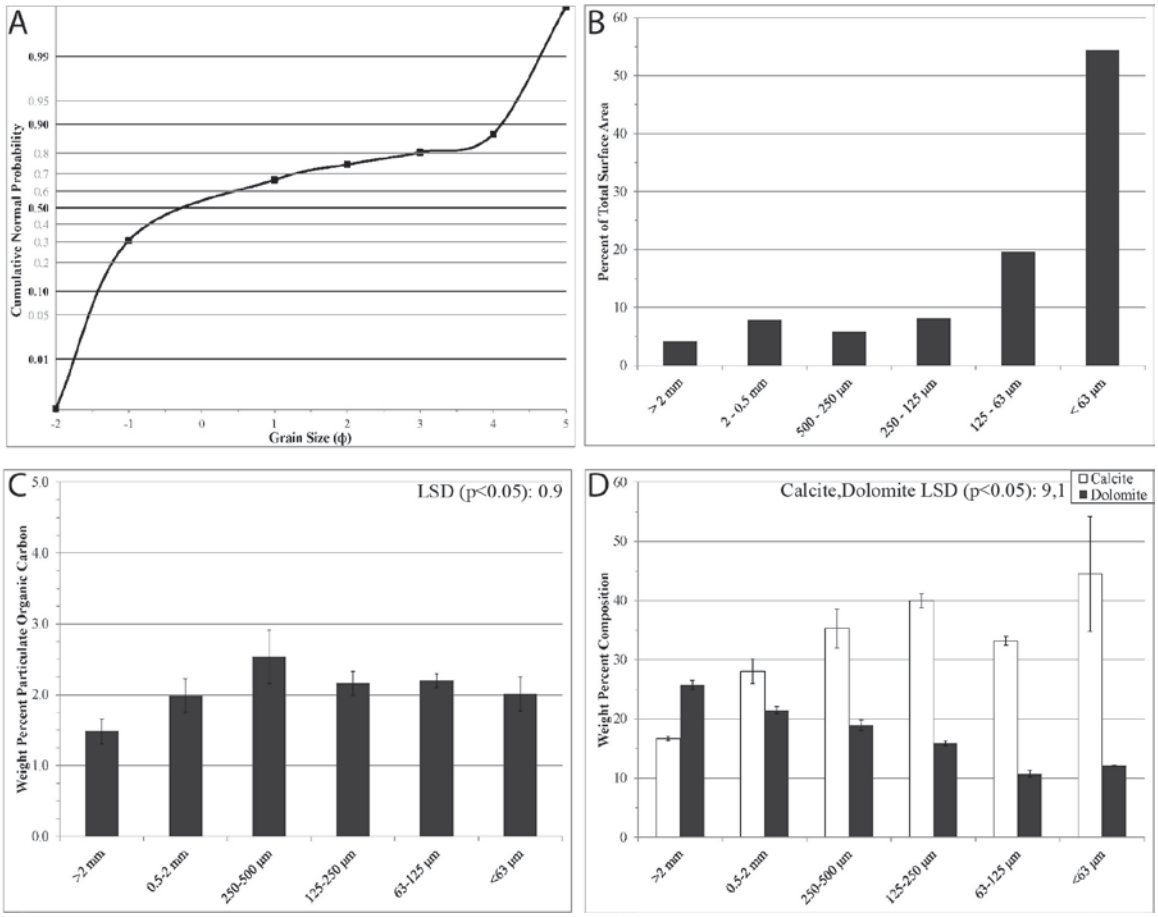

Figure A.3. Grain size distribution (*a*), calculated surface area distribution (*b*), POC content (*c*), and carbonate content (*d*) of Robertson Glacier basal/supraglacial melt-out till sediments. Error bars in *c* and *d* indicate standard deviation between duplicate samples. Least significant difference (LSD) values for panels *c* and *d* represent minimum difference between means to satisfy $p<0.05$ statistical probability of similarity.

Table A.4. Summary of results from quantitative physical lithological and mineralogical analyses on RG reworked melt-out till sediments.

Size Fraction:	*Weight Percent of Total:*	*Calculated Percent of Total Surface Area:*	*Percent Residual H_2O:*	*Percent Organic Carbon:*	*Percent Calcite:*	*Percent Dolomite:*
>2 mm	44.5	6.3	0.29 ± 0.06	1.10 ± 0.00	10.3 ± 2.8	20.8 ± 7.3
2 - 0.5 mm	22.0	5.0	0.23 ± 0.02	1.40 ± 0.21	23.5 ± 2.1	25.9 ± 3.0
500 - 250 µm	8.2	6.2	0.38 ± 0.11	2.08 ± 0.01	36.5 ± 5.5	25.3 ± 8.7
250 - 125 µm	6.5	9.9	0.23 ± 0.27	3.51 ± 0.86	40.6 ± 2.0	16.4 ± 2.3
125 - 63 µm	8.3	25.1	0.33 ± 0.09	2.63 ± 0.45	30.3 ± 0.7	9.6 ± 0.2
<63 µm	10.5	47.5	0.54 ± 0.16	2.10 ± 0.29	22.2 ± 1.7	12.4 ± 1.0

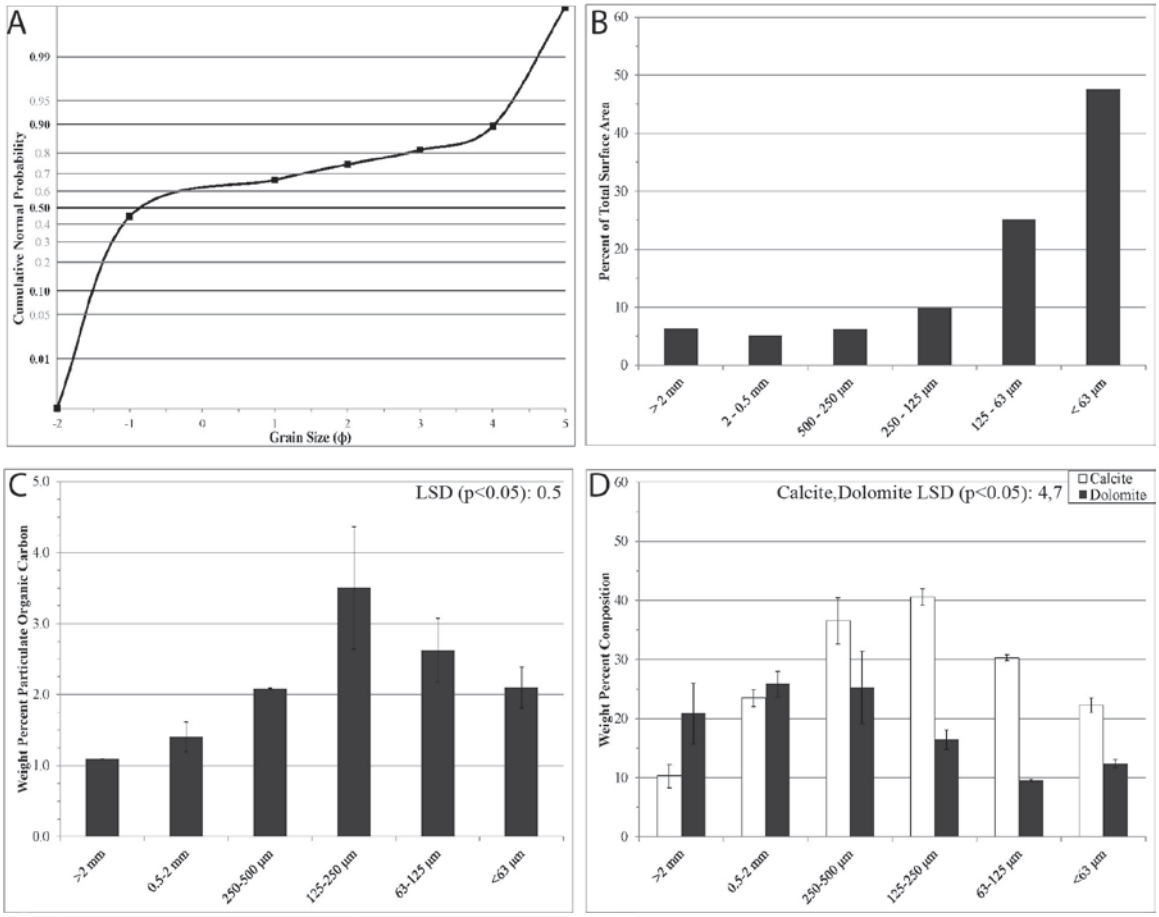

Figure A.4. Grain size distribution (*a*), calculated surface area distribution (*b*), POC content (*c*), and carbonate content (*d*) of Robertson Glacier reworked melt-out till sediments. Error bars in *c* and *d* indicate standard deviation between duplicate samples. Least significant difference (LSD) values for panels *c* and *d* represent minimum difference between means to satisfy $p<0.05$ statistical probability of similarity.

Table A.5. Grain size distribution data from laser diffractometry of <63 µm size class of all samples.

Sample:		*% Clay (0.1-2 µm):*	*% V. Fine Silt (2-8 µm)*	*% Fine Silt (8-16 µm)*	*% Medium Silt (16-31 µm)*	*% Coarse Silt (31-63 µm)*	*% V. Fine Sand (63-125 µm)*
Basal Melt-Out	Native	n/a					
	LOI	5.15	9.39	11.92	21.61	40.10	11.84
	Average	5.15	9.39	11.92	21.61	40.10	11.84
Reworked Basal Melt-Out	Native	13.84	18.35	15.00	23.27	25.06	4.48
	LOI	6.36	11.27	12.77	24.25	36.44	8.92
	Average	10.10	14.81	13.89	23.76	30.75	6.70
Basal/Supraglacial Melt-Out	Native	17.07	21.83	17.52	23.68	17.87	2.04
	LOI	9.60	16.72	17.54	27.59	25.53	3.02
	Average	13.34	19.28	17.53	25.64	21.70	2.53
Reworked Melt-Out	Native	4.86	8.19	7.71	20.28	43.78	15.17
	LOI	3.35	6.45	7.40	19.63	46.17	17.01
	Average	4.11	7.32	7.56	19.96	44.98	16.09

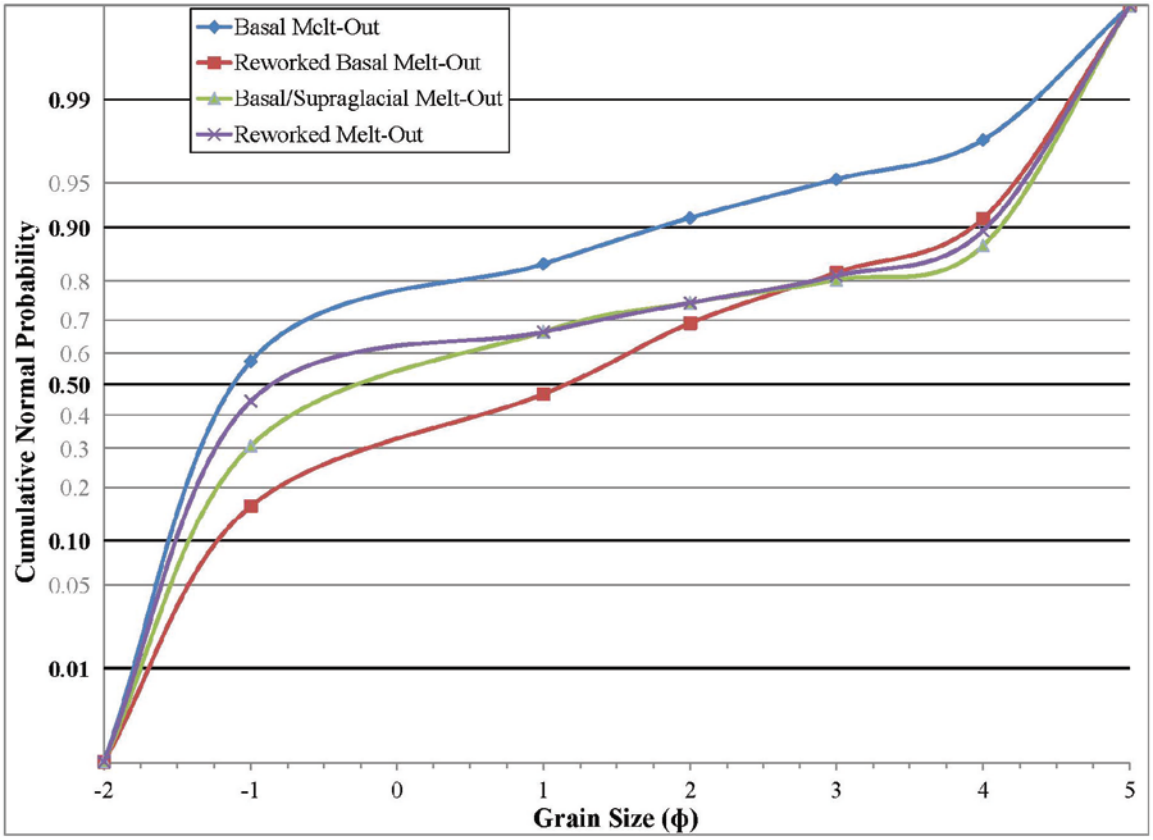

Sample:	*Mean, M (ϕ):*	*Standard Deviation, D (ϕ):*	*Skewness, S:*	*Kurtosis, K:*
Basal Melt-Out	-0.5	0.1	0.7	1.8
Reworked Basal Melt-Out	1.1	1.0	0.1	0.8
Basal/Supraglacial Melt-Out	0.7	1.0	0.6	0.8
Reworked Melt-Out	0.4	0.9	0.8	0.7

Figure A.5. Cumulative probability curves for all sediments, as analyzed via sieving. All samples have mean grain size centered on medium to very coarse sands ($-1 \leq M \leq 2$) and range from poorly ($1 \leq D \leq 2$) to moderately ($0.7 \leq D \leq 1$) or very well sorted ($D \leq 0.4$). Reworked basal melt-out till is nearly symmetrical ($-0.1 \leq S \leq 0.1$), while all other samples are strongly positively skewed toward negative-phi values ($0.3 \leq S \leq 1$). Basal melt-out till is highly leptokurtic ($1.5 \leq K \leq 3$), while all other samples are platykurtic ($0.7 \leq K \leq 0.9$).

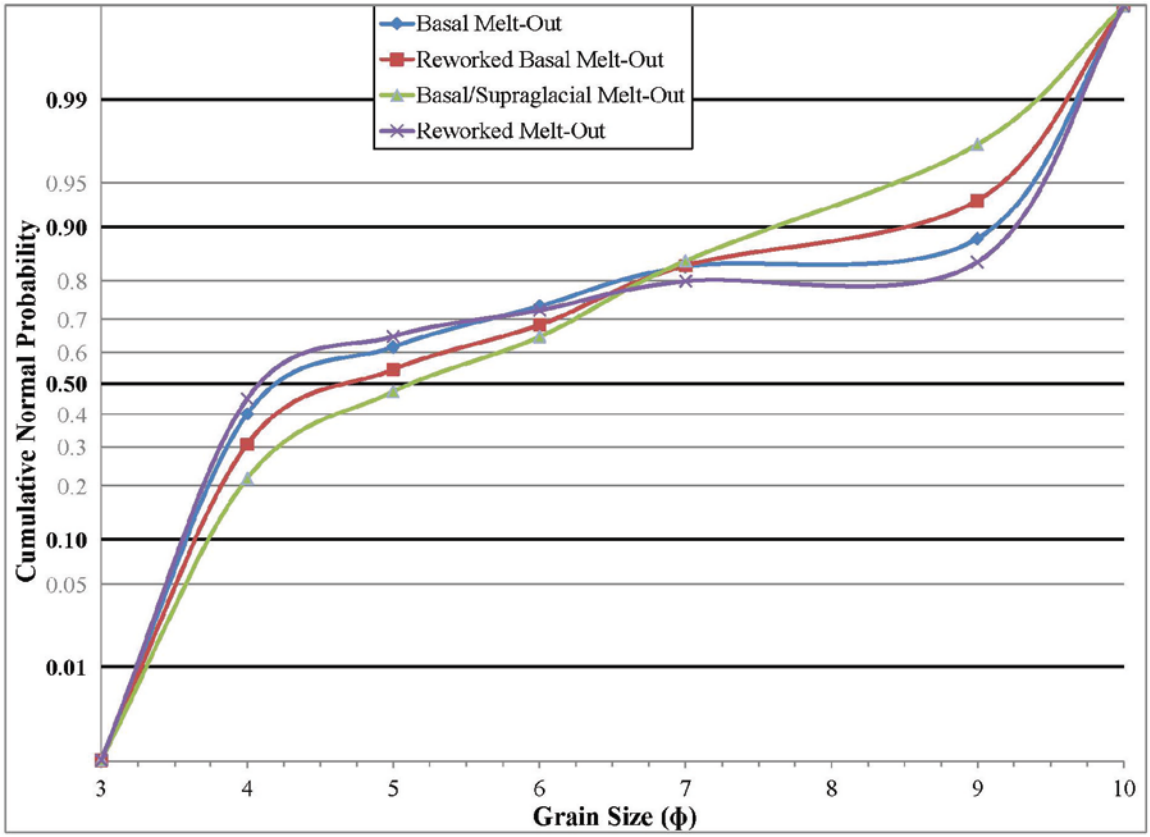

Sample:	*Mean, M (ϕ):*	*Standard Deviation, D (ϕ):*	*Skewness, S:*	*Kurtosis, K:*
Basal Melt-Out	5.4	5.0	0.8	1.0
Reworked Basal Melt-Out	5.1	4.6	0.5	0.9
Basal/Supraglacial Melt-Out	5.3	4.5	0.3	0.8
Reworked Melt-Out	5.6	5.1	0.8	1.0

Figure A.6. Cumulative probability curves for all sediment samples for <63 μm size class (from sieve analysis) as analyzed via laser diffractometry. All samples have mean grain size centered on silts ($4 \leq M \leq 8$) and are extremely poorly sorted ($D \geq 4$). All samples are positively skewed ($0.1 \leq S \leq 0.3$) toward smaller phi values and are mesokurtic ($0.9 \leq K \leq 1.1$).

APPENDIX B

XRD SPECTRA COMPOSITES FROM ALL SIZE CLASSES

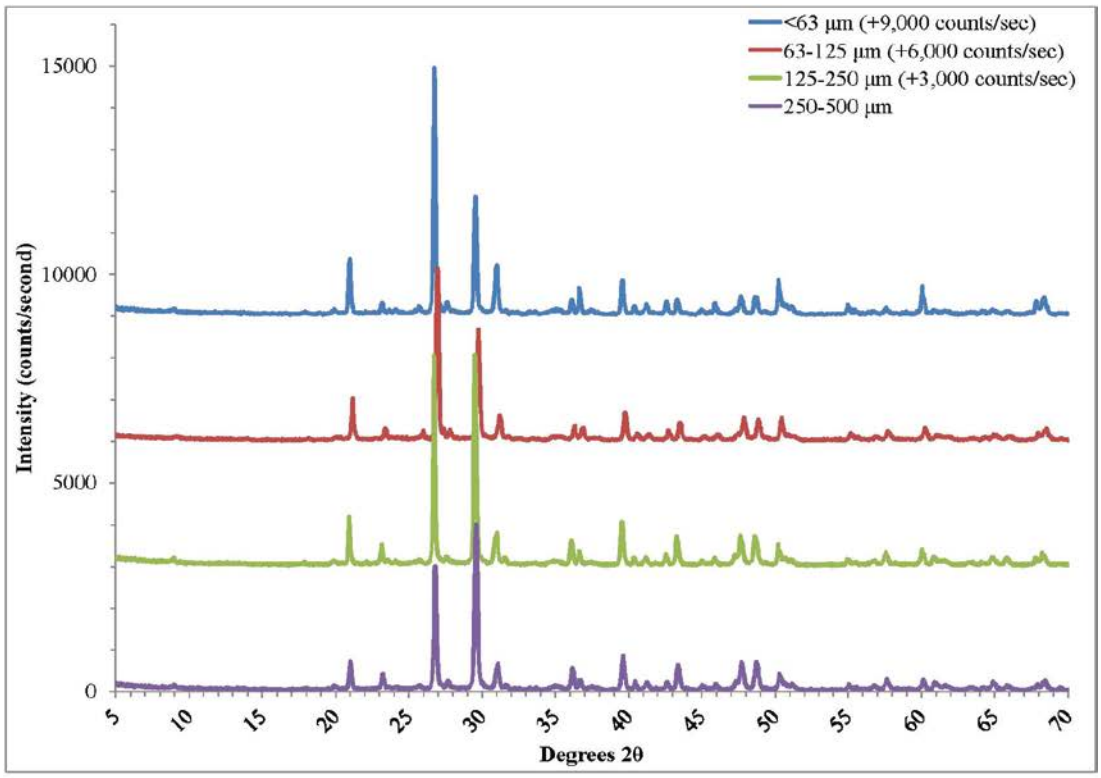

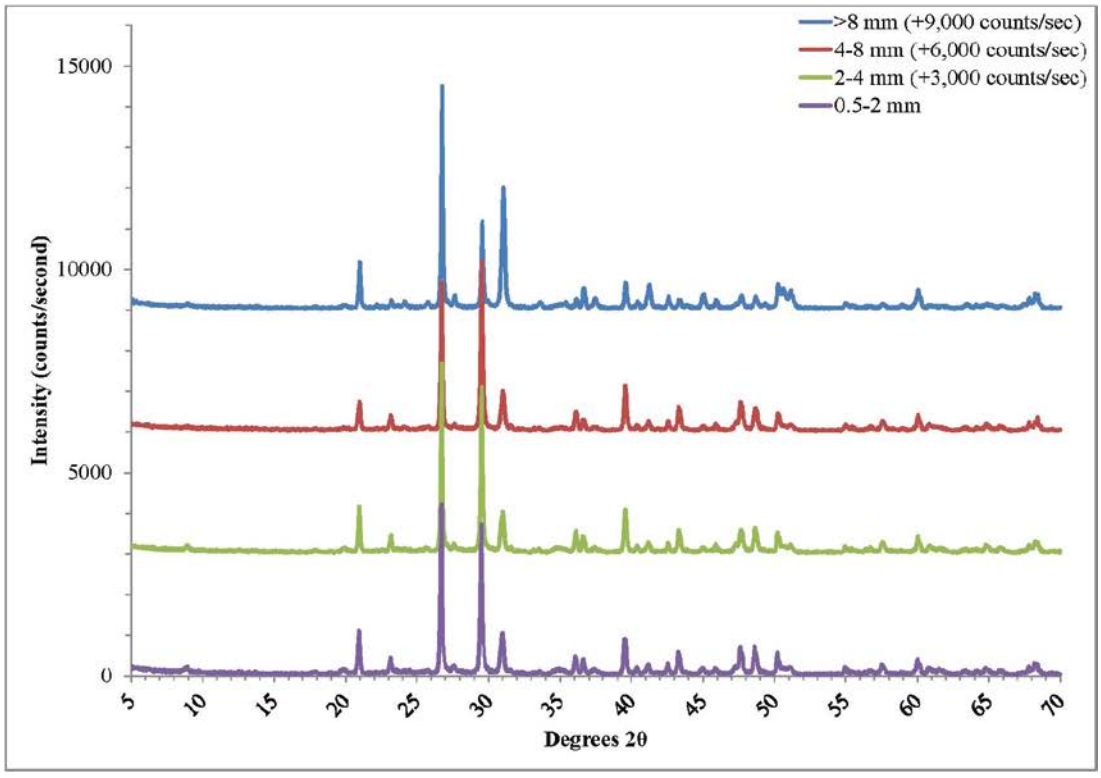

Figures B.1-B.2. Overlaid X-ray diffraction spectra from native grain size classes of basal melt-out till sediments.

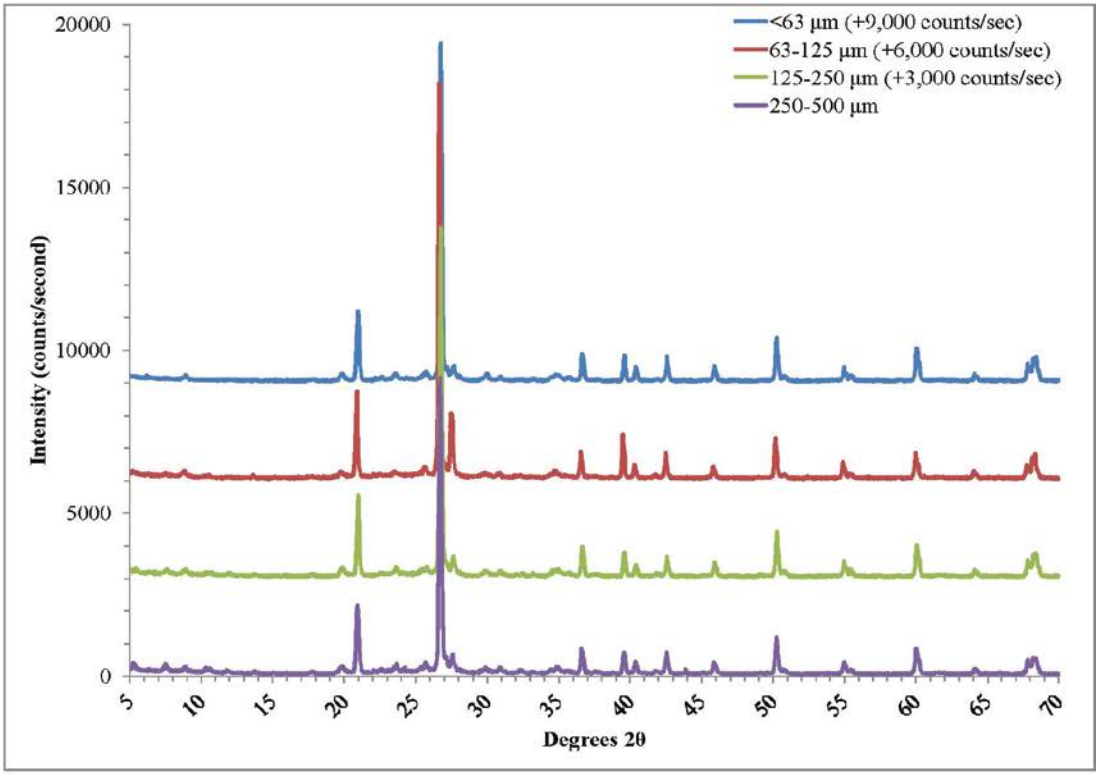

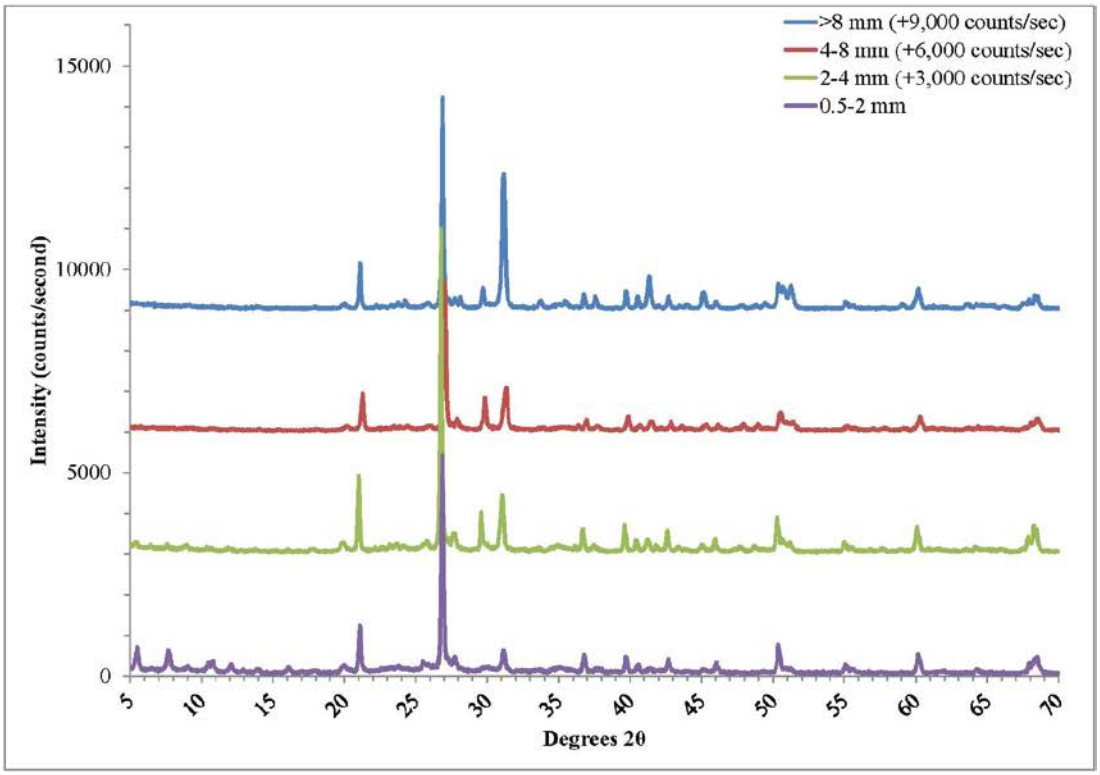

Figures B.3-B.4. Overlaid X-ray diffraction spectra from acetic-acid-leached grain size classes of basal melt-out till sediments.

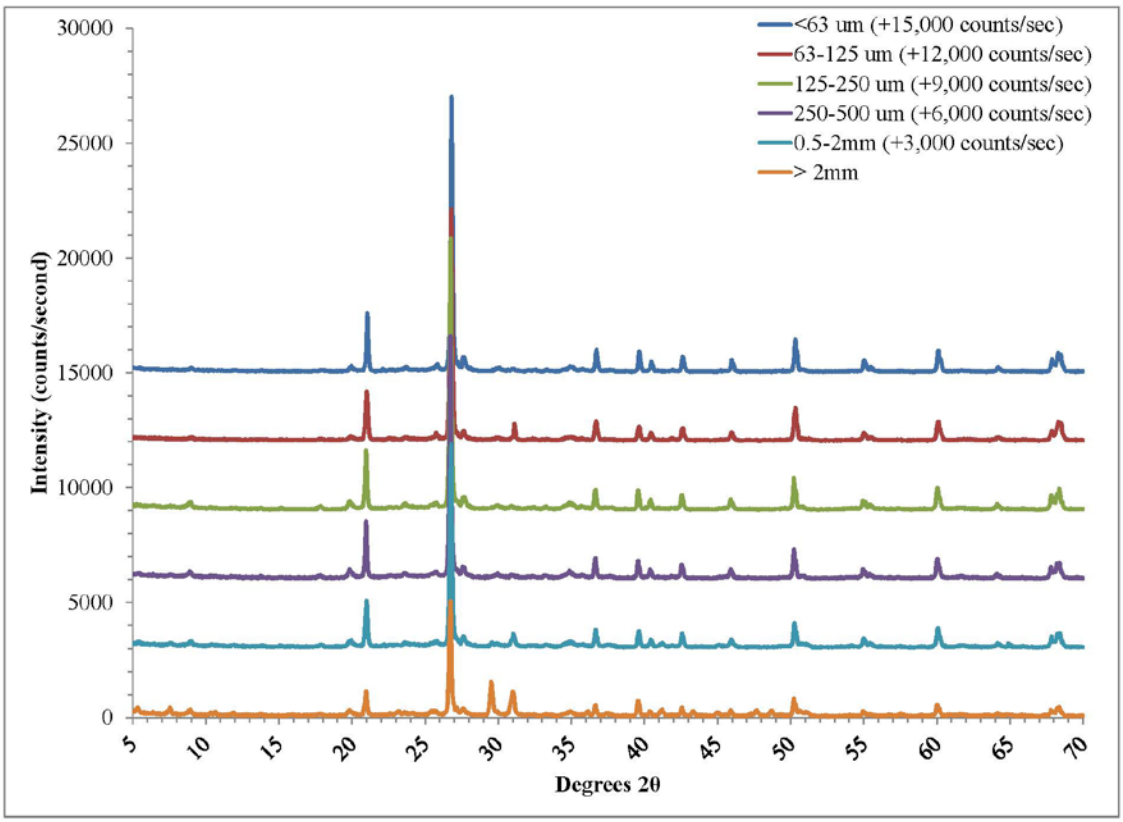

Figures B.5. Overlaid X-ray diffraction spectra from acetic-acid-leached grain size classes of reworked basal melt-out till sediments.

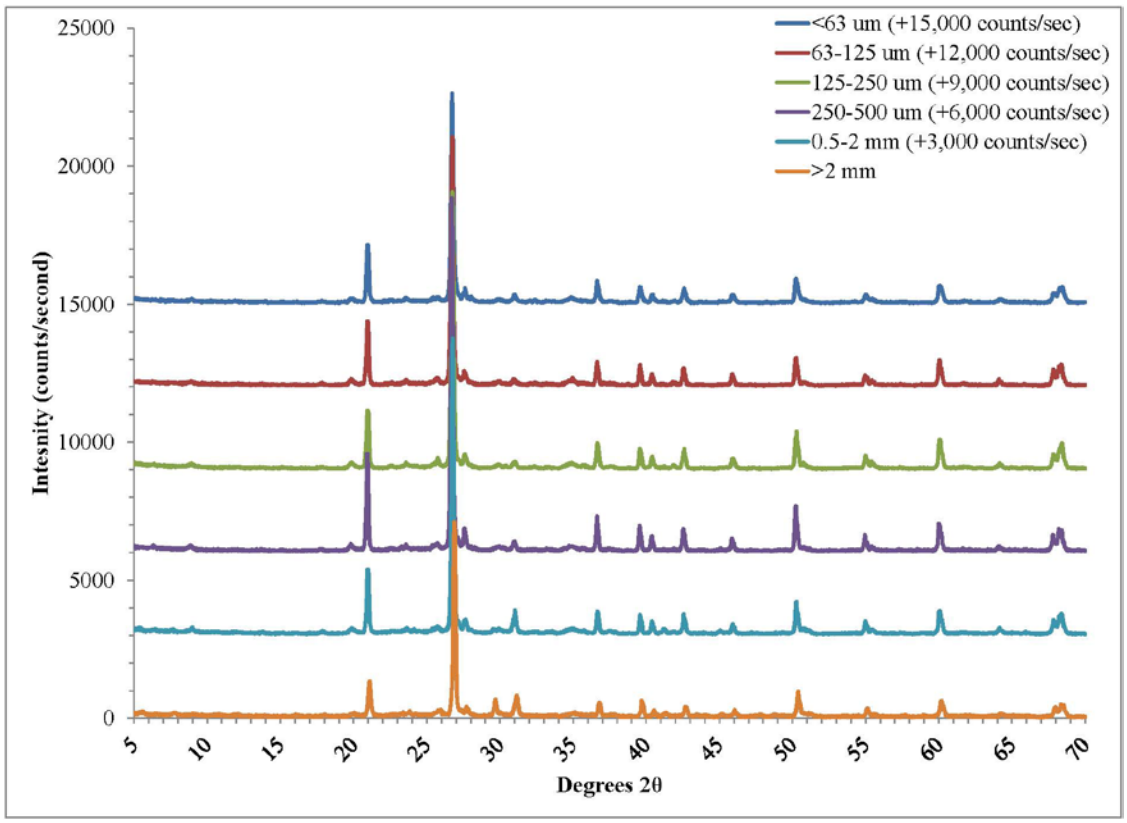

Figures B.6. Overlaid X-ray diffraction spectra from acetic-acid-leached grain size classes of RG basal/supraglacial melt-out till sediments.

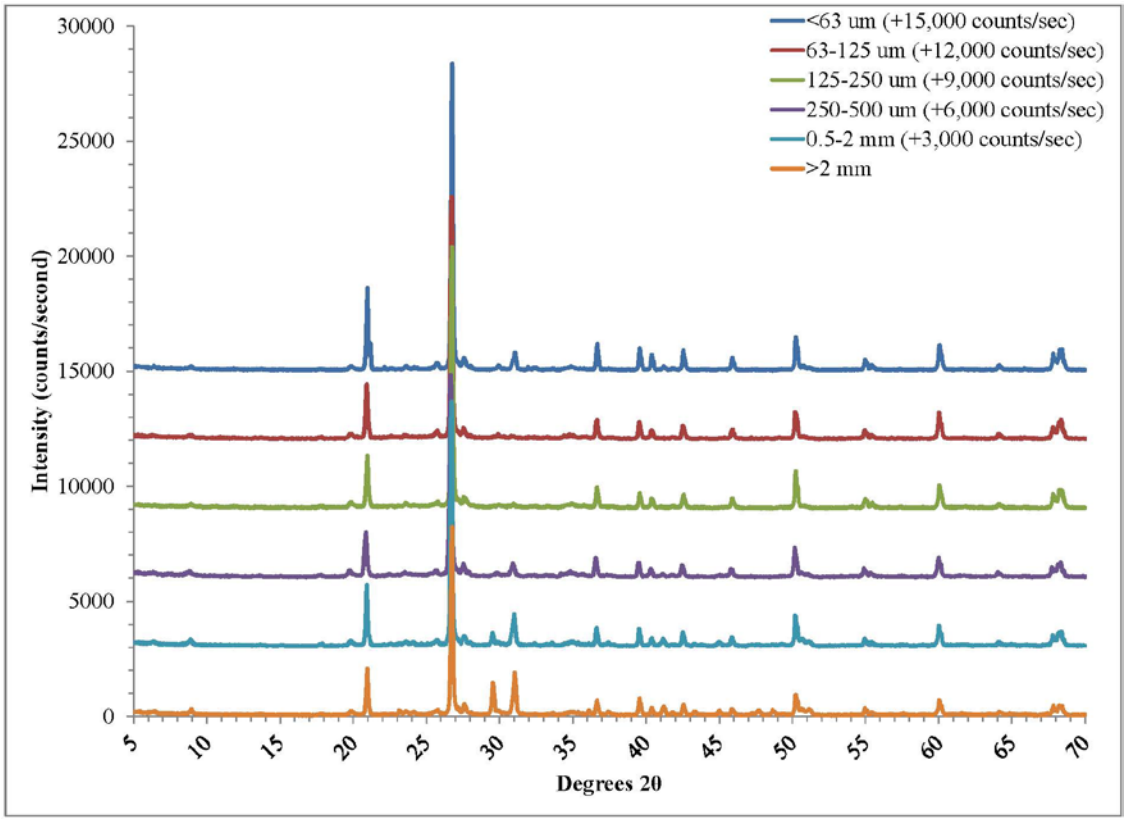

Figures B.7. Overlaid X-ray diffraction spectra from acetic-acid-leached grain size classes of RG reworked melt-out till sediments.

APPENDIX C

SEM IMAGES OF GRAIN SURFACES

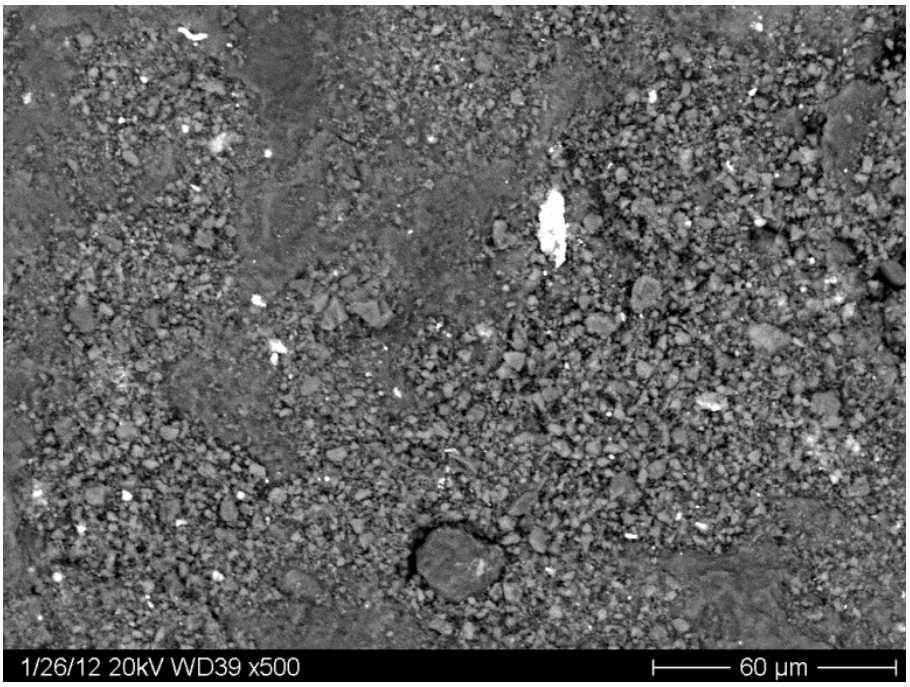

Figure C.1. Back-scattered electron image of surface of individual grain from the 2-4 mm size class of basal melt-out till sediments. Note coverage of significant portions of primary grain surface area with grain fragments.

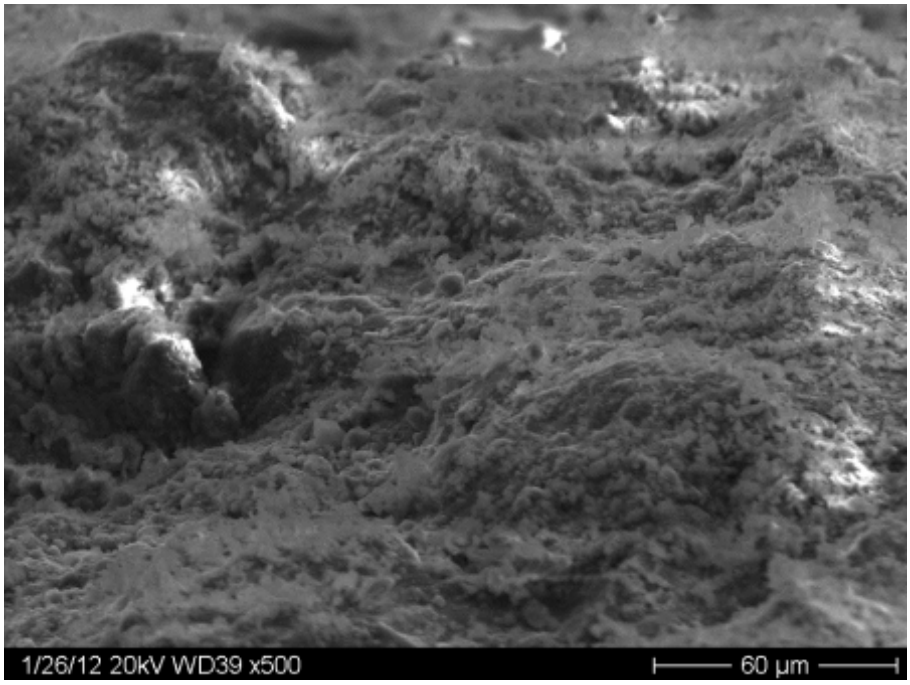

Figure C.2. Secondary electron image of surface of an individual grain from the >8 mm size class of basal melt-out till sediments. Note coverage of significant portions of primary grain surface area with grain fragments or possibly surficial $CaCO_3$ precipitates.

APPENDIX D

SEM-EDS DATA

Table D.1. SEM-EDS point-counts from native basal melt-out till sediments.

Size Fraction:	*# Grains:*	*Calcite:*	*Dolomite:*	*Quartz:*	*K-Feldspar:*	*Muscovite:*	*Pyrite:*
>8 mm	*200*	28	26	43	101	2	0
4-8 mm	*200*	23	20	54	101	2	0
2-4 mm	*200*	34	30	44	87	3	2
0.5-2 mm	*200*	41	33	44	81	1	0
250-500 µm	*200*	83	29	40	40	6	2
125-250 µm	*200*	76	26	35	58	3	2
63-125 µm	*200*	76	30	43	49	2	0
<63 µm	*200*	48	38	51	60	2	1

Table D.2. Mineralogy by size class of native basal melt-out till sediments, calculated from SEM-EDS point-counts.

Size Fraction:	*# Grains:*	*% Calcite:*	*% Dolomite:*	*% Quartz:*	*% K-Feldspar:*	*% Muscovite:*	*% Pyrite:*
>8 mm	*200*	14.0	13.0	21.5	50.5	1.0	0
4-8 mm	*200*	11.5	10.0	27.0	50.5	1.0	0
2-4 mm	*200*	17.0	15.0	22.0	43.5	1.5	1.0
0.5-2 mm	*200*	20.5	16.5	22.0	40.5	0.5	0
250-500 µm	*200*	41.5	14.5	20.0	20.0	3.0	1.0
125-250 µm	*200*	38.0	13.0	17.5	29.0	1.5	1.0
63-125 µm	*200*	38.0	15.0	21.5	24.5	1.0	0
<63 µm	*200*	24.0	19.0	25.5	30.0	1.0	0.5

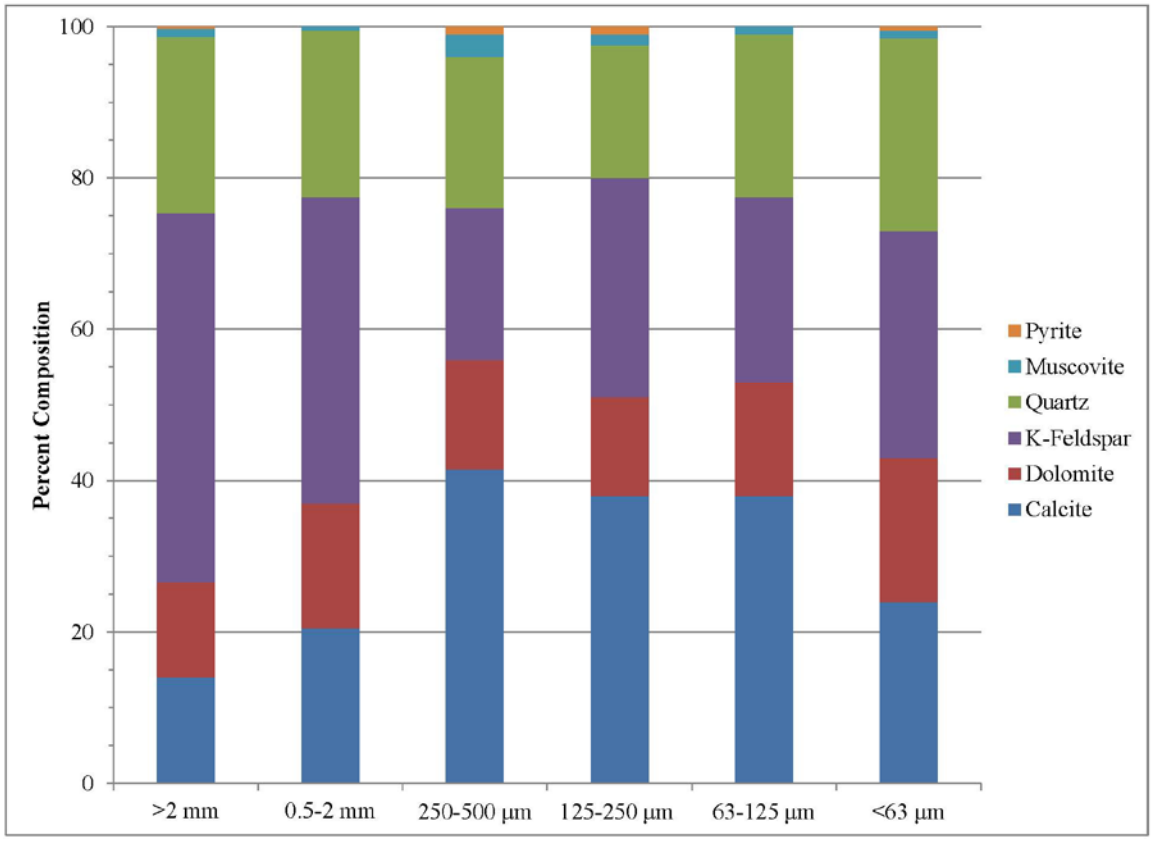

Figure D.1. Mineralogy by size class of native basal melt-out till sediments calculated from SEM-EDS point-counts. Size classes larger than 2 mm (>8 mm, 4-8 mm, and 2-4 mm) were pooled and pooled mineralogy recalculated based on weighting from weight percent composition of each grain size class relative to total sediment samples.

Table D.3. Comparison of calcite/dolomite contents from acid leaches and SEM-EDS for basal melt-out till sediment. Percent difference was calculated relative to acid-leach values.

Size Fraction:	*% Calcite*			*% Dolomite*		
	SEM-EDS:	*Acid Leaches:*	*% Difference:*	*SEM-EDS:*	*Acid Leaches:*	*% Difference:*
>8 mm	14.0	4.3	227.9	13.0	16.2	-19.8
4-8 mm	11.5	5.8	98.7	10.0	13.2	-24.1
2-4 mm	17.0	11.3	50.0	15.0	21.2	-29.3
0.5-2 mm	20.5	16.9	21.4	16.5	22.8	-27.6
250-500 µm	41.5	36.5	13.6	14.5	21.8	-33.4
125-250 µm	38.0	38.6	-1.5	13.0	21.2	-38.6
63-125 µm	38.0	35.1	8.1	15.0	22.0	-31.8
<63 µm	24.0	15.9	51.2	19.0	25.2	-24.7

Table D.4. SEM-EDS point-counts from acid-leached basal melt-out till sediments. All grains analyzed produced spectra representative of single minerals, not a composite of primary and secondary grain elemental composition.

Size Fraction:	*# Grains:*	*K-Feldspar*	*Quartz*	*Muscovite*	*Pyrite*
>2 mm	*125*	65	59	1	0
0.5-2 mm	*125*	52	72	1	0
250-500 µm	*125*	60	63	2	0
125-250 µm	*125*	52	71	2	0
63-125 µm	*125*	57	67	1	0
<63 µm	*125*	64	59	1	1

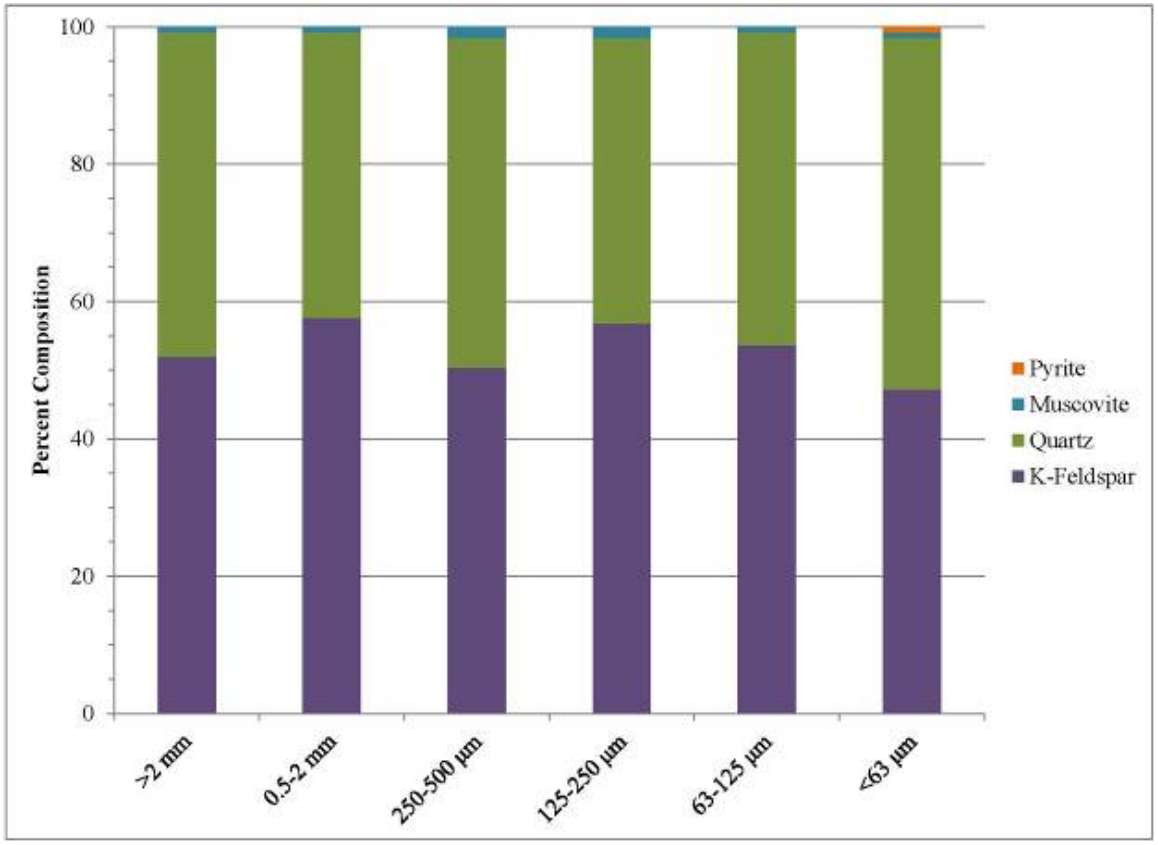

Figure D.2. Mineralogy by size class of acetic acid leached basal melt-out till sediments, calculated from SEM-EDS point-counts.

Table D.5. Comparison of K-feldspar, quartz, and muscovite content from SEM-EDS point-counts, pre and post acid-leaching for carbonate dissolution in basal melt-out till sediments. Percent content values for native sediments are calculated relative to total of non-carbonates. Percent difference calculated relative to acid-leach values.

Size	*% K-Feldspar*			*% Quartz*		
Fraction:	*Native:*	*Acid-Leached:*	*% Difference:*	*Native:*	*Acid-Leached:*	*% Difference:*
>2 mm	48.7	52	-6.3	23.3	47.2	-50.6
0.5-2 mm	40.5	57.6	-29.7	22.0	41.6	-47.1
250-500 µm	20.0	50.4	-60.3	20.0	48.0	-58.3
125-250 µm	29.0	56.8	-48.9	17.5	41.6	-57.9
63-125 µm	24.5	53.6	-54.3	21.5	45.6	-52.9
<63 µm	30.0	47.2	-36.4	25.5	51.2	-50.2

Size	*% Muscovite*		
Fraction:	*Native:*	*Acid-Leached:*	*% Difference:*
>2 mm	1.1	0.8	37.5
0.5-2 mm	0.5	0.8	-37.5
250-500 µm	3.0	1.6	87.5
125-250 µm	1.5	1.6	-6.3
63-125 µm	1.0	0.8	25.0
<63 µm	1.0	0.8	25.0

Table D.6. SEM-EDS point-counts from acid-leached reworked basal melt-out till sediments. All grains analyzed produced spectra representative of single minerals, not a composite of primary and secondary grain elemental composition.

Size Fraction:	*# Grains:*	*Quartz*	*K-Feldspar*	*Muscovite*
>2 mm	*125*	66	59	0
0.5-2 mm	*125*	64	60	1
250-500 µm	*125*	69	55	1
125-250 µm	*125*	70	53	2
63-125 µm	*125*	75	49	1
<63 µm	*125*	74	49	2

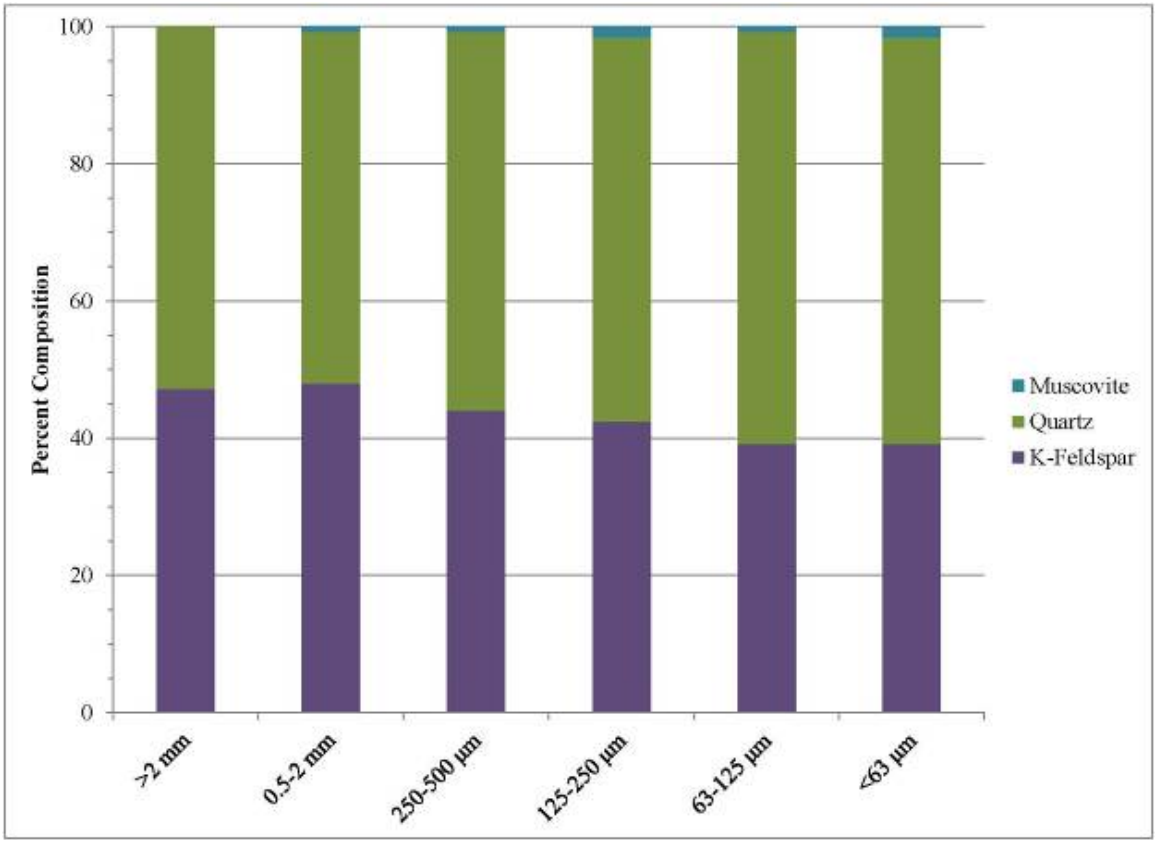

Figure D.3. Mineralogy by size class of acetic acid leached reworked basal melt-out till sediments, calculated from SEM-EDS point-counts.

Table D.7. SEM-EDS point-counts from acid-leached basal/supraglacial melt-out till sediments. All grains analyzed produced spectra representative of single minerals, not a composite of primary and secondary grain elemental composition.

Size Fraction:	*# Grains:*	*Quartz*	*K-Feldspar*	*Muscovite*
>2 mm	*125*	74	51	0
0.5-2 mm	*125*	78	46	1
250-500 µm	*125*	75	49	1
125-250 µm	*125*	79	45	1
63-125 µm	*125*	73	50	2
<63 µm	*125*	82	43	0

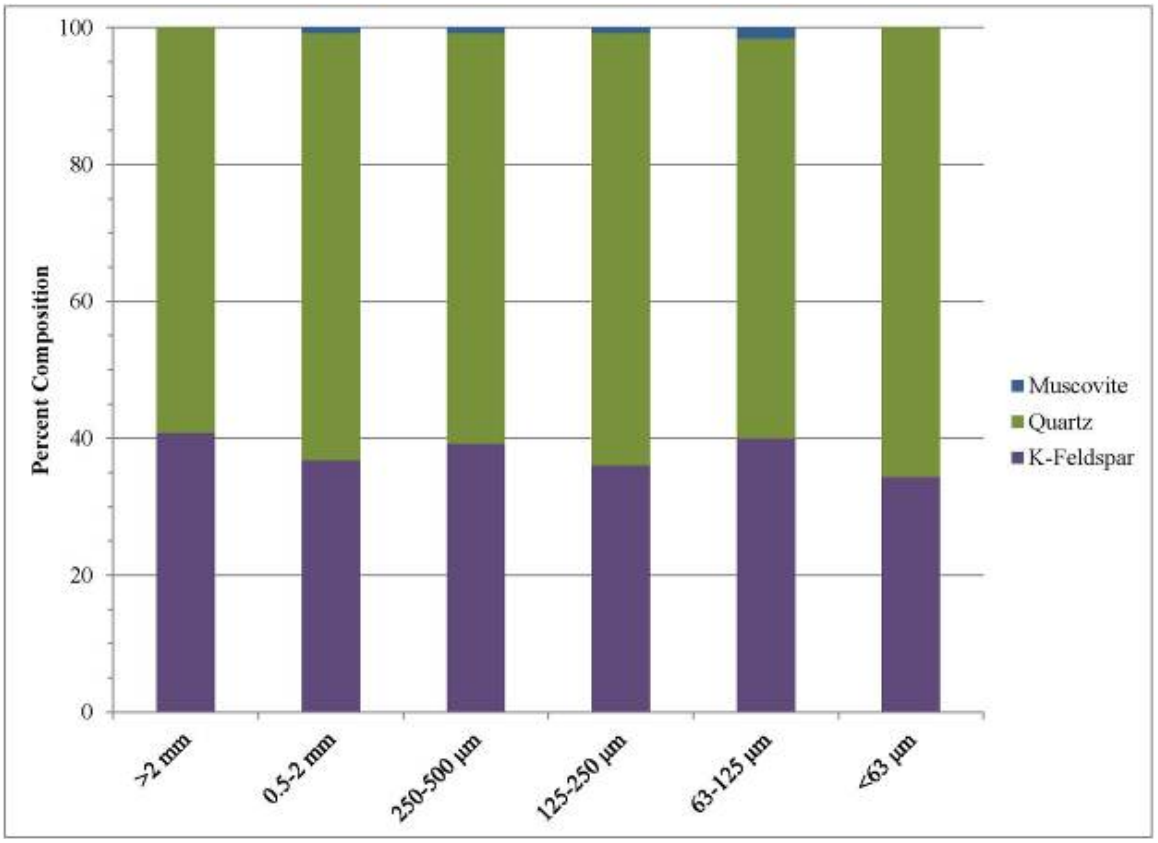

Figure D.4. Mineralogy by size class of acetic acid leached RG basal/supraglacial melt-out till sediments, calculated from SEM-EDS point-counts.

Table D.8. SEM-EDS point-counts from acid-leached reworked melt-out till sediments. All grains analyzed produced spectra representative of single minerals, not a composite of primary and secondary grain elemental composition.

Size Fraction:	*# Grains:*	*Quartz*	*K-Feldspar*	*Muscovite*
>2 mm	*125*	66	59	0
0.5-2 mm	*125*	70	54	1
250-500 µm	*125*	68	55	2
125-250 µm	*125*	67	55	3
63-125 µm	*125*	65	58	2
<63 µm	*125*	67	57	1

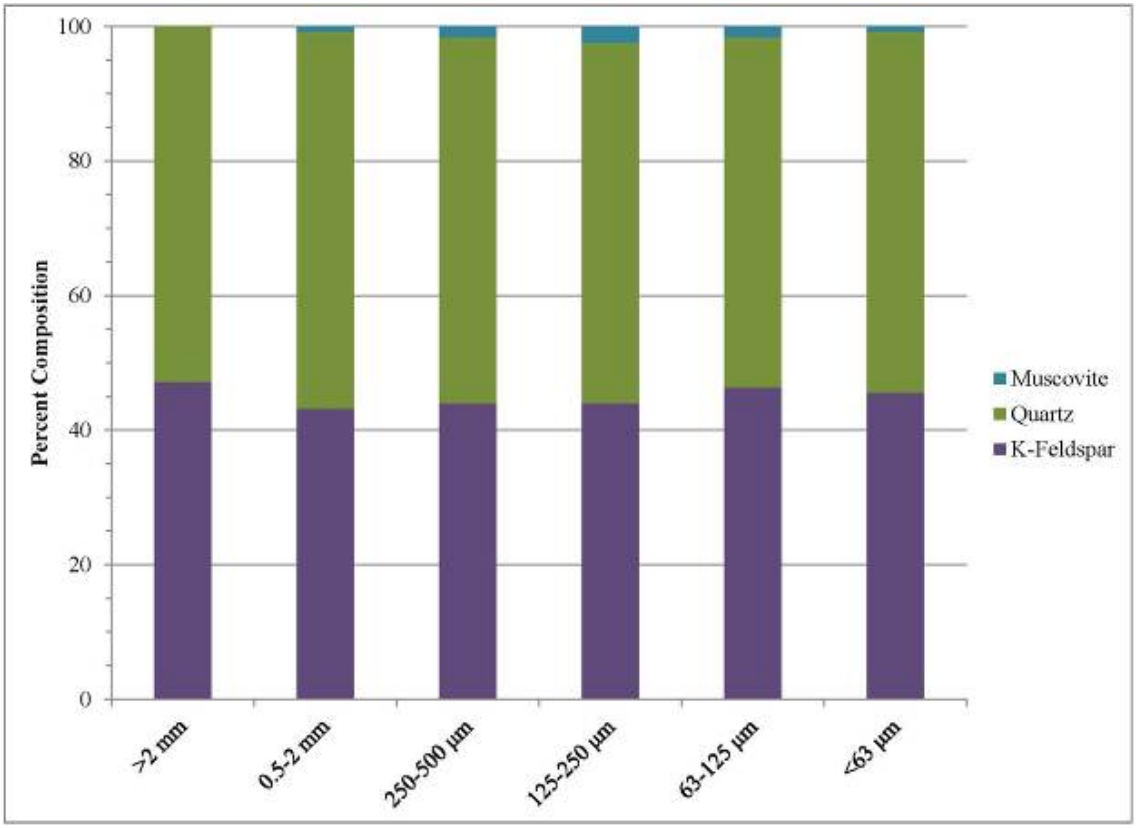

Figure D.5. Mineralogy by size class of acetic acid leached RG reworked melt-out till sediments, calculated from SEM-EDS point-counts.

APPENDIX E

SEM-EDS SPECTRA AND PROPOSED INTERPRETATIONS FROM BASAL MELT-OUT TILL

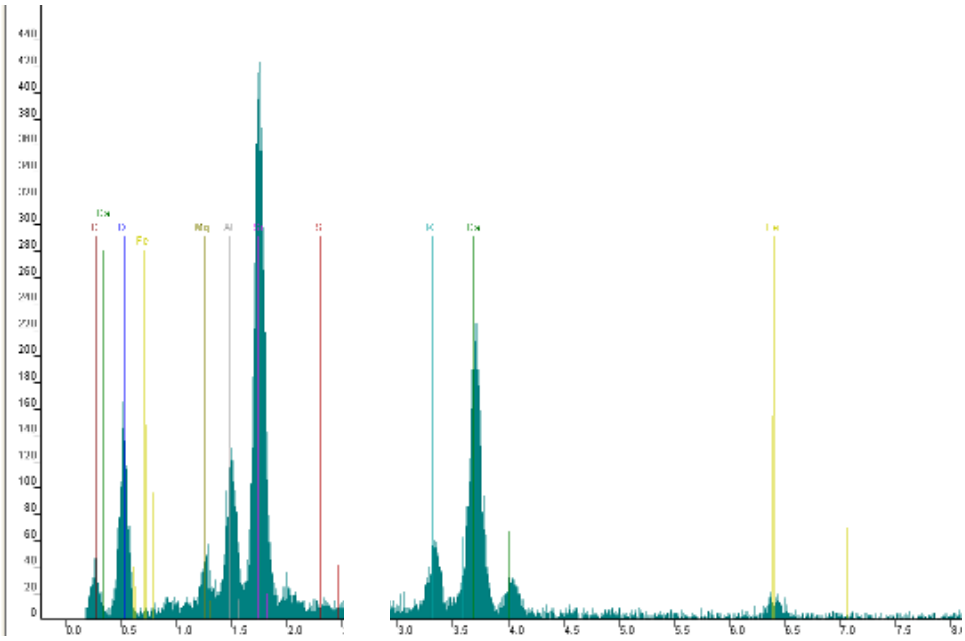

Figure E.1. SEM-EDS spectrum representing mixture of phlogopite and calcite from the native 125-250 µm size class of basal melt-out till sediments. Phlogopite identified due to presence of Si, Al, K, and Mg peaks, with calcite presence based on presence of Ca with lower Mg than would be expected for dolomite.

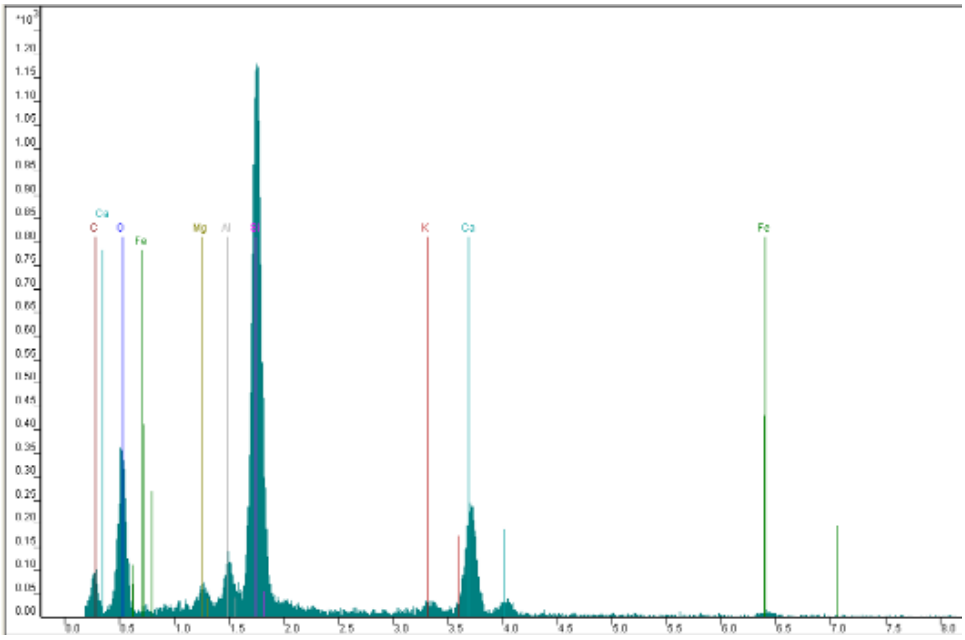

Figure E.2. SEM-EDS spectrum of quartz and calcite mixture from native <63 µm size class of basal melt-out till sediments. Quartz identified due to prominence of Si with lower K/Al than required for K-feldspar, with calcite presence based on Ca with lower Mg than would be expected for dolomite.

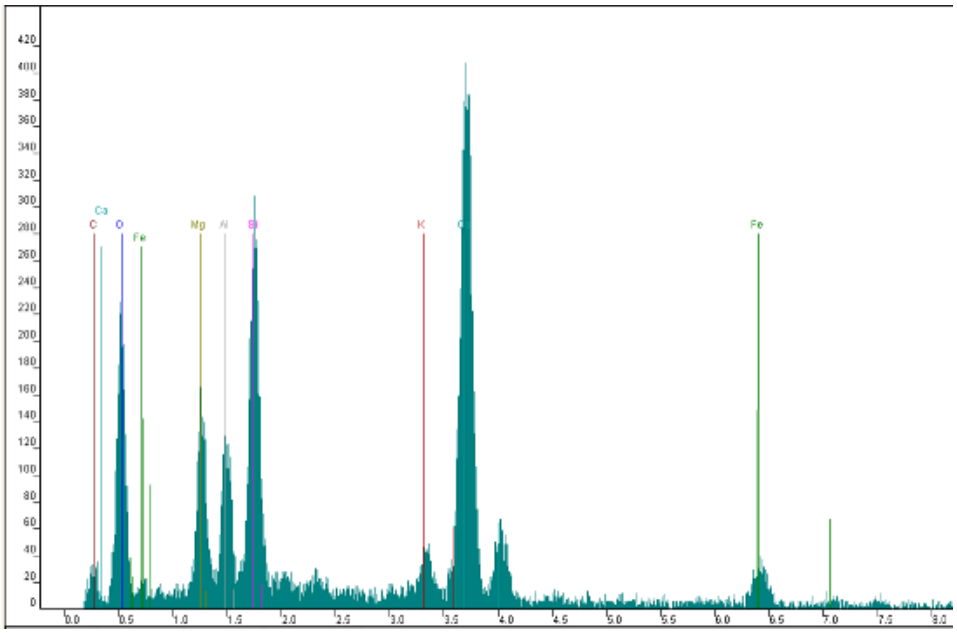

Figure E.3. SEM-EDS spectrum of dolomite and K-feldspar/phlogopite mixture from native <63 μm size class of basal melt-out till sediments. Dolomite identified due to relative height of Ca and Mg peaks compared to expectations for calcite. Second mineral identified as either K-feldspar or phlogopite based on presence of Si >> Al > K with possible attribution of portion of Mg peak to phlogopite.

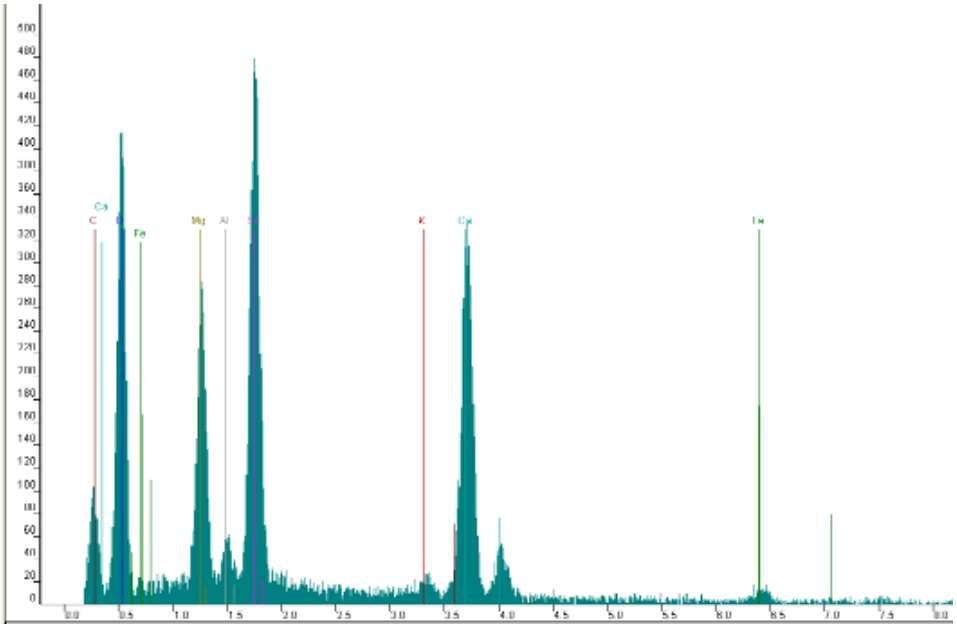

Figure E.4. SEM-EDS spectrum of quartz and dolomite from native <63 μm size class of basal melt-out till sediments. Quartz identified due to prominence of Si and lower Al than expected for K-feldspar. Second mineral identified as a dolomite based on relative heights of Ca and Mg peaks compared to expectations for calcite.

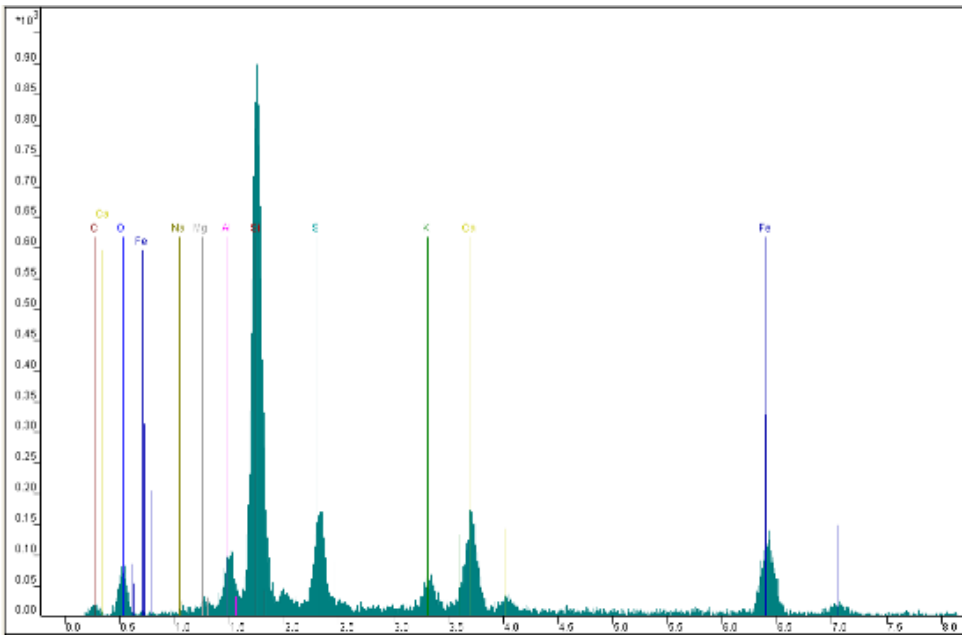

Figure E.5. SEM-EDS spectrum of K-feldspar, calcite, and pyrite from native 125-250 µm size class of basal melt-out till sediments. K-feldspar identified due to prominence of Si, Al, and K peaks. Other minerals identified as calcite and pyrite based on presence of Ca with lower Mg than observed in dolomite and presence of both S and Fe, respectively.

APPENDIX F

SEM-EDS SPECTRA FOR SELECT MINERAL STANDARDS

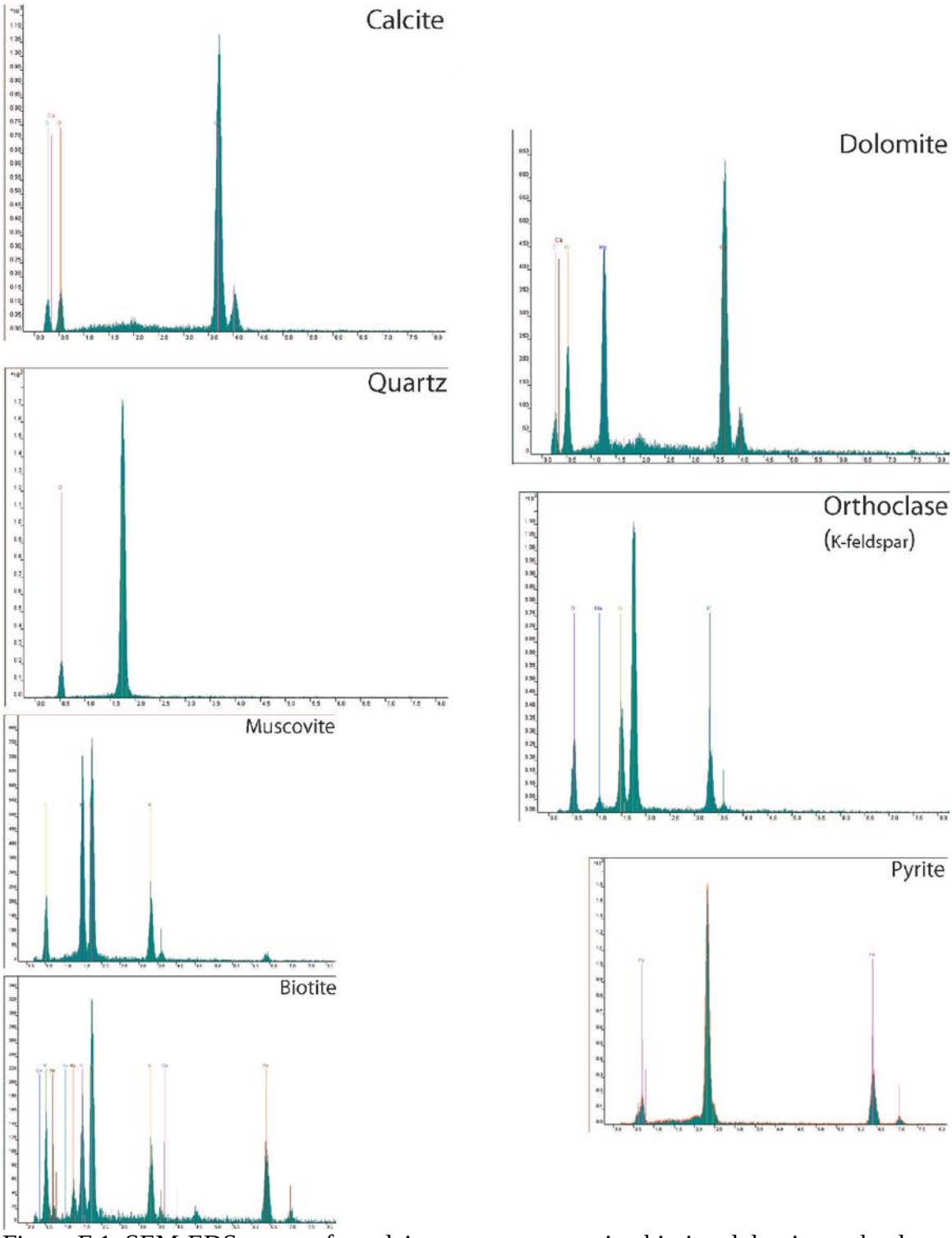

Figure F.1. SEM-EDS spectra for calcite, quartz, muscovite, biotite, dolomite, orthoclase K-feldspar, and pyrite mineral standards.